MODIFICATION OF THE ELECTRONIC PROPERTIES OF CONJUGATED POLYMERS

BY

DAVID JAMES IRVIN

A DISSERTATION PRESENTED TO THE GRADUATE SCHOOL
OF THE UNIVERSITY OF FLORIDA IN PARTIAL FULFILLMENT
OF THE REQUIREMENTS FOR THE DEGREE OF
DOCTOR OF PHILOSOPHY

UNIVERSITY OF FLORIDA

1998

To my wife and my parents

ACKNOWLEDGMENTS

First and foremost, this journey could not have begun or been completed without the loving support of my wife and parents

I wish to express my sincere gratitude to Professor John R. Reynolds for his guidance and patience, for allowing me to explore side projects, for teaching me the difference between data and junk, for teaching me the importance of presenting research in both written and oral forms, and for teaching me how to punt. For giving me the opportunity to present our work across the United States and France, I am grateful.

I would like to thank the faculty and staff at the University of Florida, especially the members of my committee, Dr. Ken Wagener, Dr. Randy Duran, Dr. Lisa McElwee-White, and Dr. Mark Meisel, for teaching me more than just chemistry and for reading this work. Special thanks to Lorraine Williams and Carol Lowe for keeping the Butler Polymer Laboratories running smoothly. I would be derelict in my duty if did not thank Donna Balkcom for always knowing how to fix any bureaucratic problem I had gotten myself into.

X-ray crystal structure analyses presented in this dissertation were performed by Dr. Peter Steel at the University of Canterbury, Christchurch, New Zealand, and Dr. Khalil Abboud at the University of Florida, whom I

thank for their expertise Special thanks to Dr Doug Dudis at Wright-Patterson Airforce Base, Dayton, OH, for his help, advice, and three months of his time working with me on the computational chemistry portion of this work

I thank the members of the Reynolds group, past and present, who have worked hard and played harder to help achieve the level of excellence found within our group The members of the Butler Polymer Laboratories have been instrumental in teaching me friendship, camaraderie, group dynamics, and leadership skills

TABLE OF CONTENTS

page

ACKNOWLEDGMENTS iii

LIST OF TABLES viii

LIST OF FIGURES ix

ABSTRACT xiii

CHAPTERS

1 INTRODUCTION 1

1.1 Electronic Band Structures of Polymers 1
1.2 Conjugated and Conductive Polymers 5
1.3 Derivatization of Thiophene 9
1.4 Methods and Mechanisms for Polymerization of Thiophenes 11
1.5 Extended Conjugation Monomers 13
1.6Thesis of this Work 19

2 ELECTRON-WITHDRAWING GROUPS PENDANT TO 1,4-BIS[2-(3,4-ETHYLENEDIOXY)THIENYL]BENZENES 22

2.1 Motivation 22
2.2 Results and Discussion 23
2.3 Conclusions 44
2.4 Synthesis 46
General Procedures 46
1,4-Bis[2-(3,4-ethylenedioxy)thienyl]-2,5-difluorobenzene 47
2,5-Dibromoterephthalic acid 48
1,4-Dibromo-2,5-dicyanobenzene 49
1,4-Bis[2-(3,4-ethylenedioxy)thienyl]-2,5-dicyanobenzene 49
1,4-Bis([2-(3 4-ethylenedioxy)thienyl]-5,5'-di(trimethylsilyl)[
-2,5-dicyanobenzene 50
1,4-Bis[2-(3,4-ethylenedioxy)thienyl]-2,5-dinitrobenzene 50
1,4-Bis[2-(3,4-ethylenedioxy)thienyl]-2-nitrobenzene 51
2.5 Computational Methods 52

2.6 X-ray Experimental ... 52

3 FLUORINATED 1,4-BIS[2 (3,4-ETHYLENEDIOXY)THIENYL] BENZENES ... 55

3 1 Motivation ... 55
3 2 Results and Discussion ... 56
3.3 Conclusions ... 70
3 4 Synthesis ... 70
General Procedures ... 70
1,4-Bis[2-(3,4-ethylenedioxy)thienyl]-2-fluorobenzene ... 71
1,4-Bis[2-(3,4 ethylenedioxy)thienyl]-2 3 5,6-tetrafluoro benzene ... 72
1,4-Bis[2-(3 4-ethylenedioxy)thienyl]-2,3,5,6-tetrafluoro-benzene ... 73
3 5 X-ray Crystal Structure ... 73

4 SULFUR TO OXYGEN INTERACTIONS IN 1,4-BIS[2-(3,4-ETHYLENEDIOXY)THIENYL]BENZENES ... 75

4 1 Motivation ... 75
4.2 Results and Discussion ... 76
4.3 Conclusions ... 97
4 4 Synthesis ... 98
General Procedures ... 98
1,4-Dibromo 2,5-diethoxybenzene ... 99
1,4-Bis[2-(3,4-ethylenedioxy)thienyl]-2,5-diethoxybenzene ... 100
1,4 Dibromo-2,5-di(methylthiomethoxy)benzene ... 100
1,4-Bis[2-(3,4-ethylenedioxy)thienyl]-2,5-di(methylthiomethoxy)benzene ... 101
1,4-Dibenzyloxy-2,5-dibromobenzene ... 101
1,4-Bis[2-(3,4-ethylenedioxy)thienyl] 2,5-dibenzyloxybenzene. ... 102
1,4-Dibromo-2,5-di(ethoxy-2-tetrahydropyranylether) benzene ... 102
1,4-Bis[2-(3,4-ethylenedioxy)thienyl] 2,5-di(ethoxy-2-tetrahydropyranylether)benzene ... 103
1,4-Bis[2-(3,4-ethylenedioxy)thienyl] 2,5 di(ethoxy-2-hydroxy) benzene ... 103
1,4-Diacyloxy-2,5-dibromobenzene ... 104
1,4-Bis[2-(3 4-ethylenedioxy)thienyl]-2,5-diacyloxybenzene ... 104
4 5 X-ray Experimental ... 104

5 BIS(EDOT)PYRIDINES N-DOPING AND ACID SENSITIVITY ... 113

5 1 Motivation ... 113
5 2 Results and Discussion ... 115
5 3 Conclusions ... 123
5 4 Synthesis ... 123
General Procedures ... 123

2,5-Bis[2-(3,4-ethylenedioxy)thienyl]pyridine 124
2,6-Bis[2-(3,4-ethylenedioxy)thienyl]pyridine 125
3,5-Bis[2-(3,4-ethylenedioxy)thienyl]pyridine 126

APPENDICES 127

TABLES OF BOND LENGTHS AND ANGLES 127
ATOM COORDINATES AND EQUIVALENT ISOTROPIC DISPLACEMENT PARAMETERS 144

REFERENCES 155

BIOGRAPHICAL SKETCH 163

LIST OF TABLES

page

1.1 Properties of Electrically Conductive Polymers ... 6

2.1 Electrochemical Results of EWG Monomers ... 30

2.2 Calculated Inter-ring Torsion Angles by Program Used ... 37

2.3 Percent Change in Bond Lengths Between Rings ... 41

2.4 Results of Band Gap Calculations by Method ... 43

3.1 Electrochemical Results of Fluorinated Monomers ... 63

4.1 X-ray Results and Calculated Charge Difference of S and O ... 78

4.2 Electrochemical Results of Dialkoxy Monomers ... 96

4.3 Crystal Data and Structure Refinement for **BEDOT-B-(OEt)$_2$** ... 107

4.4 Crystal Data and Structure Refinement for **BEDOT-B-(OEt)$_2$•THF** Solvate ... 108

4.5 Crystal Data and Structure Refinement for **BEDOT-B-(OHE)$_2$** ... 109

4.6 Crystal Data and Structure Refinement for **BEDOT-B-(OMTM)$_2$** ... 110

4.7 Crystal Data and Structure Refinement for **BEDOT-B-(OBz)$_2$** ... 111

4.8 Crystal Data and Structure Refinement for **BEDOT-B-(OAc)$_2$** ... 112

LIST OF FIGURES

page

1.1 Band Structure of Metals, Semiconductors, and Insulators 3

1.2 Transitions in Band Structure as a Function of Doping 4

1.3 Common Poly(heterocycle) Structures 8

1.4 Alkoxy Substituted Polythiophenes 10

1.5 Standard Three Electode Electrochemical Cell 11

1.6 Oxidation Potential vs 1/Monomer Units 14

1.7 Fused Bithiophene Monomers 14

1.8 Structural Variety in Bis(pyrrole)-vinylenes and -arenes 15

1.9 Design of Low Gap Systems with D-A Units 16

1.10 Monomers to Produce Soluble Conductive Polymers 17

1.11 33 Bis(EDOT) **ECM's** Synthesized by the Reynolds Group 18

2.1 Bis(EDOT)Benzenes with Pendant EWG's 24

2.2 Synthesis of 1,4-Dibromo-2,5-dicyanobenzene 24

2.3 Synthesis of **BEDOT-B-(NO$_2$)$_2$** 26

2.4 Repeated Potential Scan Electrochemical Polymerization of **BEDOT-B-F$_2$** 28

2.5 Cyclic Voltammetric Scan Rate Dependence of Poly(**BEDOT-B-F$_2$**) 29

2.6 Repeated Potential Scan Electrochemical Polymerization of **BEDOT-B-(CN)$_2$** 30

2.7 Cyclic Voltammetric Scan Rate Dependence of Poly(**BEDOT-B-(CN)$_2$**) 31
2.8 Spectroelectrochemical Analysis of Poly(**BEDOT-B-F$_2$**) 32
2.9 Perspective View and Atom Labeling of the X-ray Structure of **BEDOT-B-F$_2$** 34
2.10 Perspective View and Atom Labeling of the X-ray Structure of **BEDOT-B-(CN)$_2$-TMS$_2$** 34
2.11 Perspective View and Atom Labeling of the X-ray Structure of **BEDOT-B-NO$_2$** 35
2.12 Structures and Selected Bonds of Calculated Compounds 36
2.13 Calculated Rotation Barrier Potentials of BEDOT-B's 39
2.14 Interatomic Interactions for [**BEDOT-B-(NO$_2$)$_2$**]$^{++}$ 40
3.1 Fluorinated Bis(EDOT)Benzenes. 56
3.2 Attempted Syntheses of **BEDOT-B-F$_2$** by Hydrodefluorination 58
3.3 Attempted Synthesis of 1,4-Dibromo-2,3,5-trifluorobenzene 59
3.4 Perspective View and Atom Labeling of the X-ray Structure of **BEDOT-B-F$_4$** 60
3.5 ^{1}H NMR Spectra of the EDOT Bridges of **BEDOT-B-F$_2$** and **BEDOT-B-F$_4$** 62
3.6 Repeated Potential Scan Electrochemical Polymerization of **BEDOT-B-F$_2$** 64
3.7 Cyclic Voltammetric Scan Rate Dependence of Poly(**BEDOT-B-F$_2$**) 65
3.8 Repeated Potential Scan Electrochemical Polymerization of **BEDOT-B-F$_4$** 66
3.9 Cyclic Voltammetric Scan Rate Dependence of Poly(**BEDOT-B-F$_4$**) 67
3.10 UV-Vis Spectra of Neutral Polymers of **BEDOT-B**, **BEDOT-B-F$_2$**, **BEDOT-B-F$_2$**, and **BEDOT-B-F$_4$** 68
3.11 Spectroelectrochemical Analysis of Poly(**BEDOT-B-F$_4$**) 69

4.1 Dialkoxy BEDOT-ß Monomers 76

4.2 Perspective View and Atom Labeling of the X-ray Structure of **BEDOT-ß-(OEt)$_2$** 79

4.3 Perspective View and Atom Labeling of the X-ray Structure and Crystal Packing of **BEDOT-ß-(OEt)$_2$•THF Solvate** 80

4.4 Perspective View and Atom Labeling of the X-ray Structure of **BEDOT-ß-(OHE)$_2$** 81

4.5 Perspective View and Atom Labeling of the X-ray Structure of **BEDOT-ß-(OMTM)$_2$** 82

4.6 Perspective View, Atom Labeling, and Crystal Packing of **BEDOT-ß-(OBz)$_2$** 83

4.7 Crystal Packing of **BEDOT-ß-(OBz)$_2$** 84

4.8 Perspective View and Atom Labeling of the X-ray Structure of **BEDOT-ß-(OAc)$_2$** 85

4.9 ^{1}H NMR of the EDOT bridge of Selected **BEDOT-ß**s 87

4.10 Peak to Peak ^{1}H NMR Splitting of the BDOT Bridge verses the X-ray-Determined Torsion Angles 88

4.11 Repeated Potential Scan Electrochemical Polymerization of **BEDOT-ß-(OEt)$_2$** 89

4.12 Cyclic Voltammetric Scan Rate Dependence of Poly(**BEDOT-ß-(OEt)$_2$**) 90

4.13 Repeated Potential Scan Electrochemical Polymerization of **BEDOT-ß-(OMTM)$_2$** 91

4.14 Cyclic Voltammetric Scan Rate Dependence of Poly(**BEDOT-ß-(OMTM)$_2$**) 91

4.15 Repeated Potential Scan Electrochemical Polymerization of **BEDOT-ß-(OBz)$_2$** 92

4.16 Cyclic Voltammetric Scan Rate Dependence of Poly(**BEDOT-ß-(OBz)$_2$**) 93

4.17 Repeated Potential Scan Electrochemical Polymerization of **BEDOT-ß-(OHE)$_2$** 93

4.18 Cyclic Voltammetric Scan Rate Dependence of Poly(**BEDOT-B-(OHE)$_2$**) 94

4.19 Repeated Potential Scan Electrochemical Polymerization of **BEDOT-B-(OAc)$_2$** 95

4.20 Cyclic Voltammetric Scan Rate Dependence of Poly(**BEDOT-B-(OAc)$_2$**) 95

5.1 n-Dopable Polymers 114

5.2 Monomers Based on Bis(EDOT)Pyridines 116

5.3 Repeated Potential Scan Electrochemical Polymerization of **BEDOT-Pyr** 117

5.4 Cyclic Voltammetric Scan Rate Dependence of Poly(**BEDOT-Pyr**) 118

5.5 UV-VIS-NIR Spectra of Poly(**BEDOT-Pyr**) 119

5.6 Anodic and Cathodic Electrochemistry of Poly(**BEDOT-Pyr**) 120

5.7 UV-Vis-NIR Spectra of Poly(**BEDOT-Pyr**) as a Function of pH 122

5.8 Poly(**BEDOT-Pyr**) λ_{max} as a Function of pH 122

Abstract of Dissertation Presented to the Graduate School of the University of Florida in Partial Fulfillment of the Requirements for the Degree of Doctor of Philosophy

MODIFICATION OF THE ELECTRONIC PROPERTIES OF CONJUGATED POLYMERS

By

David James Irvin

December, 1998

Chairman: Professor John R. Reynolds
Major Department: Chemistry

The rational design of both low and high electronic bandgap (E_g) conjugated polymers can be accomplished by the incorporation of substituents onto the benzene ring of poly(1,4-bis[2-(3,4-ethylenedioxy)thienyl]benzene)s [poly(BEDOT-B)'s]. Fourteen new extended conjugation monomers based on BEDOT-B have been synthesized to investigate the effects of electron withdrawing groups (EWG), and intramolecular steric and electronic interactions, on these conjugated polymers. The monomers were analyzed by electrochemical, spectroscopic, computational, and X-ray crystallographic methods and polymerized electrochemically. The resultant polymers were analyzed by electrochemical and spectroscopic methods.

Of the BEDOT-B monomers with pendant EWG's, 1,4-bis[2-(3,4-ethylenedioxy)thienyl]-2,5-difluorobenzene (BEDOT-B-F_2) and 1,4-bis[2-(3,4-ethylenedioxy)thienyl]-2,5-dicyanobenzene (BEDOT-B-$(CN)_2$) were found to

electropolymerize at potentials 300 and 900mV higher than that of the parent monomer (BEDOT-B), respectively Similar monomers in the series containing 1 or 2 pendant nitro groups did not electropolymerize due to steric interactions, as observed using X-ray crystallography These interactions inhibit the three ring monomer from becoming planar as required to delocalize charge across more than one aromatic ring

In an effort to fine tune the electronic properties of the poly(BEDOT-B-F_n) system, mono-, di-, and tetrafluorinated poly(BEDOT-B)'s were synthesized With the incorporation of one or two fluorines, the E_g increased by 0.1eV relative to poly(BEDOT-B) The tetrafluoro analogue, on the other hand, exhibited a decrease in E_g by 0.3eV An electrostatic interaction between fluorine and sulfur in BEDOT-B-F_2 decreases the inter-ring torsion angle to 3° from 27° in the unsubstituted analogue, as probed using computational methods and measured using X-ray structural determination.

Five dialkoxy–substituted BEDOT-B's were synthesized to investigate the possibility of S-O electrostatic interactions analogous to the S-F interaction shown in BEDOT-B-F_2. The monomers were found to be coplanar unless steric interactions are present

A similar extended conjugation monomer containing pyridine has been synthesized to yield a polymer which both p- and n-dopes The peak monomer oxidation potential is the same as that of BEDOT-B, but the polymer half wave redox potential is 250mV higher due to the electron

accepting ability of the pyridine moiety The polymer can be quaternized with acid, and the resulting film exhibits acid sensitive behavior

CHAPTER 1
INTRODUCTION

1.1 Electronic Band Structures of Polymers

The study of electronic band structures of conjugated polymers reveals more about the nature of organic conduction than any other analysis. In the words of Roald Hoffmann of Cornell University, "To make sense of the marvelous electronic properties of the solid state, chemists must learn the language of solid-state physics, [and] of band structures."[1] From the chemist's point of view, the properties of solids begin at the molecular level. The properties can be illustrated by expanding molecular orbital theory beyond single molecules.

Two types of conduction in polymers are ionic conduction and electronic conduction. Ion-conductors, such as poly(ethylene oxide) containing lithium salts, act as a substrate for the diffusion of ions.[2] In electronic conduction, the polymer backbone acts as the transport medium for either electrons or electron holes (positive charges).[3] Only electronic conduction will be discussed in this work.

Within the categories of solid state electron transport types insulators, semiconductors, and metals are the most important and will be addressed here. One method for classifying these structures is by level of conductivity

(σ) of the material. Solids with a σ of below 10^{-7} S cm^{-1} are insulators and include glass, diamond, polyethylene, and most organic solids. Materials with a σ between 10^{-7} and 10^{2} S cm^{-1} are semiconductors, such as silicon, neutral trans(polyacetylene), and indium/tin alloys. Metals are the last group of conductors, which includes silver, copper, iron, some organic charge transfer complexes, graphite, and doped polyacetylene.[4] Along with conductivity, the three classes of conductors can be differentiated by the temperature dependence of conductivity. For metals, conductivity increases with decreasing temperature; conversely, in semiconductors and insulators, σ increases with increasing temperature.

To translate the above classes of conductors into molecular terms, we must examine the frontier orbitals, in particular, the highest occupied molecular orbital (HOMO) and the lowest unoccupied molecular orbital (LUMO). As the number of molecular orbitals increases in an infinite solid, the difference from orbital to orbital decreases;[5] thus a continuous band is formed. The proximity of the bands, and the extent to which they are filled, determine conductive properties.

As seen in **Figure 1.1**, the occupied or valence band is shaded and the unoccupied or conduction band is white. Electrical conduction is defined as the migration of electrons in a partially occupied band. In a metal, the occupied band is only partially filled; therefore there is no energy barrier to

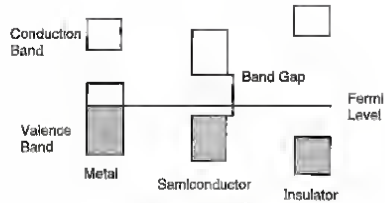

Figure 1 1 Band Structure of Metals, Semiconductors, and Insulators

excite electrons into the conduction band at room temperature This boundary is defined as the Fermi level, which is the HOMO at 0 K

In a semi-conductor, there is a gap (1 to 5 eV where 1 eV ≈ 1240 nm ≈ 96.5 kJ/mol ≈ 23 1 kcal/mol ≈ 8065 cm^{-1}) between the bands that requires thermal energy to excite electrons into the conduction band.[6] Once electrons have populated the conduction band, the valence band is now partially filled and can act as a medium for electron transport When the band gap increases until it can no longer be thermally populated, (>5 eV) the material is defined as an insulator

Organic conjugated polymers are semiconductors in the neutral state and become semimetals in highly doped states.[4] These polymers usually have a spectroscopically determined[7] band gap between 1 and 3 eV Unlike true metals, where the conduction electrons are delocalized throughout the entire solid, polymeric organic conductors have discrete mobile charge carriers that migrate as a function of applied potential To better understand

the phase transition from a semiconductor to a conductive polymer, we should inspect the effects of doping on the band structure (**Figure 1.2**) The fully dedoped or neutral polymer is a semiconductor

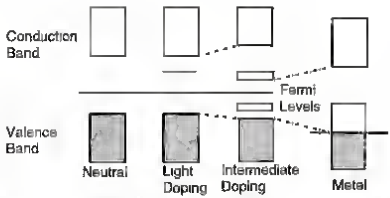

Figure 1.2 Transitions in Band Structure as a Function of Doping

As the polymer is doped, new intermediate energy bands are formed. These are the bipolaron bands. The lower energy band is labeled the bipolaron 1 band while the higher energy band is the bipolaron 2. With increased doping, the new bands expand until the valence and conduction bands meet; thus, with maximum doping, a semiconductive polymer becomes a metal, where the Fermi level has shifted to a lower energy due the removal of electrons from the system. There are pathways of conduction with light and intermediate doping due to the formation of partially filled bands, therefore, the polymer need not be fully doped to be conductive

1.2 Conjugated and Conductive Polymers

Conjugated polymers are highly desirable due to unique properties of light emission, transmission, and absorption that lead to electroluminescent,[8-10,11] electrochromic,[12,13,14] and light harvesting[15,16,17] devices. The conductive and capacitive properties of polymers lead to anti-static,[18,19,20] light weight electromagnetic field absorbing,[21,22,23] and charge storage[24,25,26] devices. The common thread that runs through organic conductive polymers is that they all contain a conjugated backbone in the oxidized state. A highly diverse range of polymer structures has been explored (**Table 1.1**).

Of the all carbon based fully conjugated polymers, polyacetylene, poly(*p*-phenylene) and poly(phenylene vinylene) are the most investigated. Of these three, polyacetylene (**PA**) has attracted the most attention as it is the simplest conjugated polymer.[27,28,29] **PA** has become the model for intrachain (down-the-chain) and interchain (chain hopping) conduction. **PA** films were first synthesized in 1974[30] and first doped in 1977.[31,32] With these first reports, the race to improve organic conductors had begun.

PA has a band gap of 1.4-1.5 eV and can be n- and p-doped, although neither form is stable to air.[33] Poly(*p*-phenylene) (**PPP**) is the simplest aromatic polymer to be introduced. With a band gap of 2.9-3.2 eV and a high oxidation potential, **PPP** is used in blue light emitting diodes (LEDs) in its

Table 1.1 Properties of Electrically Conductive Polymers

Polymer	Structure	Color Change w/doping	Band Gap (eV)	Common Synthetic Methods
Polyacetylene	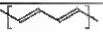	varies with method	1.4-1.5	Mostly Ziegler-Natta initiation and precursor routes
Poly(p-phenylene)		colorless to black	2.9-3.2	Aryl coupling in neutral state
Poly(phenylene-vinylene)	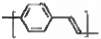	yellow to black	2.3-2.5	Soluble precursor followed by thermal elimination
Polyaniline		yellow to green to dark blue to black	2.5-3.0	Radical oxidative polymerization
Poly(phenylene sulfide)		white to brown/black	3.3	Condensation of arylhalide and arylthiolate
Polythiophene		red to blue-black	2.1-2.3	Electrochemical or chemical oxidative polymerization
Poly(3-alkylthiophene)		red to blue-black	1.9-2.0	Electrochemical or chemical oxidative polymerization, aryl coupling in neutral state
Poly(3,4-ethylenedioxy-thiophene)		blue to pale blue	1.6	Electrochemical or chemical oxidative polymerization

neutral form, enabling it to withstand high temperatures. Soluble **PPP**s can be synthesized with the introduction of solubilizing side-chains.[34] Poly(phenylene vinylene) (**PPV**) can be viewed as the alternating copolymer of **PA** and **PPP**, and likewise has a band gap between both homopolymers at around 2.5 eV. **PPV** is also thermally stable in its neutral form and is used in LEDs.

In an effort to increase the stability of the doped state, heteroatoms can be introduced in to the main chain of the **PPP** to yield polymers such as polyaniline[35,36] and poly(phenylene sulfide).[37,38] One of the immediate benefits of these systems is that they are conjugated only in the doped or partially doped states. This leads to increased solubility and allows the polymers to be processed before doping. With introduction of the electron donating heteroatoms, the environmental stability of the doped state increased dramatically. Polyaniline[39] (**PANI**) can be doped in a variety of structural states, determined by the level of protonation and oxidation, and it has high environmental stability.[35] Poly(phenylene sulfide) (**PPS**) forms a conductive state when highly doped with AsF_5.[37] **PPS** is solution and melt processable, but due to its high band gap and its instability in the doped form, **PPS** is not widely used as a conductive polymer.

A method of incorporating a heteroatom into the polymer while maintaining a fully carbon based conjugated backbone is to use heterocycles. Polyheterocycles, including polyfurans,[40,41] polypyrroles,[42] and

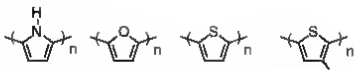

Polypyrrole Polyfuran Polythiophene Poly(3-alkylthiophene)

Figure 1.3 Common Poly(heterocycle) Structures

polythiophenes,[43] (**Figure 1.3**) have received much attention in the literature.[44] Each of the polyheterocycles has its own unique benefit such as polypyrrole's low oxidation potential and polythiophene's relatively high environmental stability.

The electrochemical synthesis of polyfuran (**PF**) from furan is difficult due to the high monomer oxidation potential (1.8 - 2.5 V).[45] At this potential, extensive defect sites, including diones caused by the incorporation of water,[46] are produced. These diones, in conjunction with other defects, cause the band gap to be elevated to 2.7 eV[47] compared with the more recently reported polymers produced from terfuran which have a band gap of 2.3 eV.[41]

Polypyrrole (**PP**) forms highly stable electrochemically deposited films[48] with a band gap of 2.5 eV.[49] With a relatively low polymer oxidation potential ($E_{1/2}$ = -0.2 V vs SCE[50]), **PP** is stable in the doped form. The polymer is not melt or solution processable.[51] Functionalization of pyrrole with N-, 3-, or 3, 4- substituents can cause adverse effects due to twisting adjacent rings out of plane[52,53] which decreases the π-overlap. **PP** has been found to be a good material for bio-applications[54] due to aqueous compatibility and microelectronics[55] due to low monomer and polymer oxidation potentials.

Polythiophene (**PT**) has good environmental stability but is insoluble, infusable and unprocessable.[56,57] The electrochemical polymerization of thiophene is anomalous since the polymer decomposes at a lower potential than the monomer oxidizes. The kinetics of the decomposition are much slower than that of the polymerization, and therefore **PT** can be synthesized electrochemically. High stability and ease of derivatization have made a wide range of **PT** structures and properties possible.

1.3 Derivatization of Thiophene

Two of the motivations for the derivatization of thiophene polymers include altering the electronic properties and increasing solubility. The addition of electron donating or withdrawing groups in direct electronic communication with the polymer backbone maximizes modification of the electronic properties. The solubility of **PT**s can be increased by the addition of alkyl and alkoxy side chains.

A great deal of work has been done on the 3-alkyl derivatives to enhance the solubility and electronic properties of **PT**. The monomer oxidation potential is lowered and the band gap is also lowered from 2.20 to 1.90 eV.[58] Thiophenes with alkyl chains of larger than four carbons produce soluble polymers.[59] A problem associated with the 3,4-dialkyl substitution is that steric bulk of the two groups twists the thiophene rings out of plane, and the benefits of the second group are diminished by the decrease in π-overlap of the backbone.[60]

In the search for a method to increase solubility and lower monomer oxidation potential, thiophene monomers with alkoxy substituents in the 3 or 3,4- positions have been explored. The simplest of these (**Figure 1 4**), 3-alkoxythiophene, has increased stability in the conductive state.[61,62]

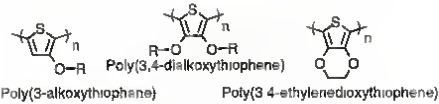

Figure 1 4 Alkoxy Substituted Polythiophenes

The incorporation of an electron donating group increases the electron density, such as the alkoxy group on the thiophene, and increases the energy of the HOMO and LUMO. The LUMO is increased to a lesser extent compared to that of the HOMO, and as a result, the band gap is decreased. If an additional alkoxy group is placed on thiophene, the steric interaction between adjacent rings forces them out of plane and decreases conjugation.[63] To overcome this problem, 3,4-ethylenedioxythiophene (EDOT)[64] was synthesized with the purpose of "pinning back" the alkoxy groups to limit the steric interactions.[13] As a result of the above benefits, poly(EDOT) (**PEDOT**) is highly conductive and has a comparatively low band gap of 1.6 eV.[64]

1.4 Methods and Mechanisms for Polymerization of Thiophenes

PT can be synthesized either electrochemically or chemically. In potentiostatic polymer deposition, an electrochemical cell (**Figure 1.5**) containing solvent, supporting electrolyte, and working, reference, and

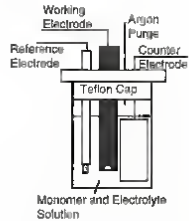

Figure 1.5 Standard Three Electrode Electrochemical Cell

counter electrodes, is maintained at or slightly below the peak monomer oxidation potential and polymer is deposited on the electrode in its doped and insoluble form. The polymer on the electrode is in the conductive state and becomes the new electrode surface.

In the repeated scan deposition, the electrochemical cell is cycled between the monomer oxidation potential and the polymer reduction potential. Monomer oxidizes to radical cations, which combine to form oligomers that deposit on the electrode. Then, the polymer is reduced to its

neutral form. When the polymer is re-oxidized, it becomes the new electrode surface, and a new layer is deposited on the electrode.

As alluded to previously, the accepted mechanism for the electropolymerization/deposition of thiophene is as follows: the monomer diffuses to the electrode surface and is oxidized to form the radical cation. The radical cation reacts with a second radical cation to form a dimer dication. The dicationic dimer can eliminate two protons to form the neutral dimer, which oxidizes at a lower potential than the monomer. The dimer can then be oxidized to form the radical cation which reacts further, until the oligomers precipitate onto the electrode or the monomer/oligomer concentration is depleted.

Two methods employed for the chemical polymerization of thiophene are oxidative and non-oxidative coupling. In oxidative coupling, the monomer is oxidized with any of a variety of oxidants, including nitronium and nitrosonium salts,[65] AsF_5,[66] and $FeCl_3$,[67] in a mechanism similar to electrochemical polymerization. The oxidant also serves to dope the newly formed polymer, and it precipitates in its conductive state. The major drawback of oxidative polymerization is that side reactions occur including cross-linking at the 3- or 4- (β-) positions,[68] which can produce insoluble polymers.

In non-oxidative coupling,[69] the polymer is synthesized in its neutral, non-conductive state by means of aryl coupling. Most commonly a 2-halothiophene or 2,5-dihalothiophene is reacted with a low valent transition

metal by oxidative insertion followed by reductive elimination of the oligomer[70,71] In the case of monoalkyl substituted thiophenes, high molecular weight, regioregular polymers are produced.

1.5 Extended Conjugation Monomers

A variety of monomers with extended conjugation have been synthesized including fused heterocycles, biheterocycles, terheterocycles, and bis(heterocycle)arylenes, with the motivation of altering the band gap and lowering monomer oxidation potential[72] The influence of the extended conjugation is demonstrated in the series of oligothiophenes (**Figure 1.6**), as the number of thienyl rings (from 1 to 5) in the monomer increases, the peak monomer oxidation potential decreases from 2.1 to 0.8 V.[50]

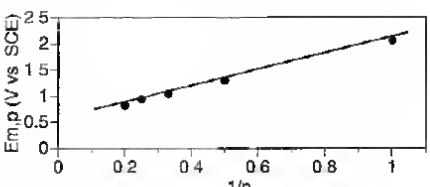

Figure 1.6 Oxidation Potential vs 1/Monomer Units

In addition to extending the conjugation, there is also the possibility for the modification of electronic properties by the addition of electron donating or withdrawing groups (**Figure 1 7**) By altering the substitution at the β,β' position of bithiophene, a family of polymers with varied band gaps and oxidation potentials have been prepared. In this series, the polymer band gaps were found to be highly dependent upon the substitution pattern The potential exists for symmetrical monomers which lead to regioregularity and more ordered chains As stated by Heeger and coworkers,[8] as conductive polymers become more "perfectly" ordered they become more like true metals

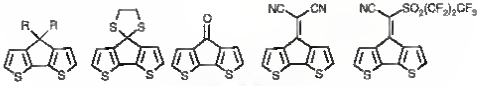

Figure 1 7 Fused Bithiophene Monomers

Extended conjugation monomers (**ECMs**) are not limited to homologues, property modification can be attained by designing systems with various conjugated linkers, including vinylenes, phenylenes, and heterocycles Since the only restriction as to the number of rings/functional groups is solubility, **ECMs** can be structurally and electronically modified by design using different conjugated units

With the work of Reynolds, Zotti, and others[73], heterocycles have been incorporated with vinylenes and arylenes to form ECMs. Zotti and coworkers[74] produced an extensive series of bis(pyrrole) monomers (**Figure 1.8**) varying the electron density and symmetry of the spacer to produce

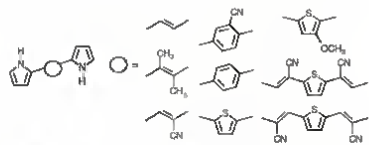

Figure 1.8 Structural Variety in Bis(pyrrole)-vinylenes and -arenes

polymers with spectra showing band gaps ranging from 1.6 to 2.9 eV. In addition to steric factors, an electronic "push-pull" design aided the range of band gaps attained. In a "push-pull" system, electron donating (D) and electron accepting (withdrawing) groups (A) are placed in conjugation on the same polymer chain. The D-A design is successful in lowering the band gap. One model of explaining this interaction is to examine the bands of the donor and acceptor segments. The HOMO of the donor segment is higher in energy than that of the acceptor segment due to increased electron density, and the LUMO of the acceptor is lower than that of the donor. The transition between the HOMO of the donor and the LUMO of the acceptor must be lower energy than that of band gap of either the donor or acceptor.

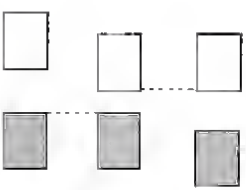

Figure 1-9 Design of Low Gap Systems with D-A Units

The mixing of donors and acceptors is also effective in changing ground state structure of the polymer from aromatic to quinoidal.[75]

Within the Reynolds group we have synthesized a plethora of ECMs with a majority based on bis(heterocycle) benzenes but also encompassing bis(heterocycle) vinylenes, arenes, and heterocycles.[12,76,77,78,79] The major focus of this work has been to enhance solubility and functionality, but more recently, the purpose has shifted to designing electroactive materials with variable transmission windows. These materials have use in electroactive windows and shutters for UV, IR and visible light in scientific, display, telecommunication, and military applications. The preliminary work (**Figure 1-10**) concentrated on synthesizing and characterizing soluble conductive polymers utilizing bis(thienyl) and bis(furanyl) benzenes.[80,81,82] With these soluble fully characterized polymers, in-depth studies of spin states, molecular weight, conductivity, mass and charge transport, and optical properties were presented with definitive evidence.

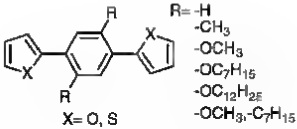

Figure 1.10 Monomers to Produce Soluble Conductive Polymers

The next goal was to rationally design systems with different optical properties. To do this, the optical band gap must be fine tuned such that the polymer absorbs in various segments of the electromagnetic spectrum. For example, if the polymer is to appear blue by transmission, the polymer should have a high absorptivity in the red to yellow region (~600 to 720 nm) with minimal absorbance in the blue region (~530 to 450 nm). This can be attained by producing a conjugated polymer with a λ_{max} around 620 nm or 2 eV, as found in EDOT.

The rational design of both low and high gap polymers required the incorporation of many different conjugated linkers into bis(EDOT)systems (**Figure 1.11**).[83,84,85] The purpose for the use of EDOT was to lower the monomer oxidation potential to decrease detrimental side reactions discussed above in Sections 1.2 and 1.4. Each linker was chosen for its donor (EDOT, dialkoxybenzene, etc.) or acceptor (difluorobenzene, pyridine, etc.) properties, or for its ability to solubilize the resultant polymers (di(oxyethylhexyl) benzene, 9,9 didecylfluorene, etc.)

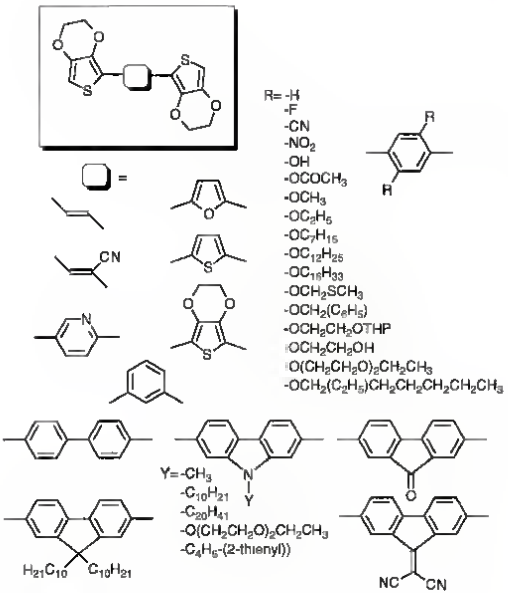

Figure 1.11 33 Bis(EDOT) **ECM**s Synthesized by the Reynolds Group

A more recent endeavor within the Reynolds group is to produce high gap, low oxidation potential polymers. The high oxidation potentials of most of the high gap polymers (see **Table 1.1**) lead to oxidation of common environmental impurities and some electrolytes which could have deleterious effects on the lifetime of any electrochemical cell employing these polymers. The synthesis of new high gap, low oxidation potential materials based on bis(heterocycle)fluorenones is ongoing. The net result of the structural and electronic manipulation is a closely related series of monomers and polymers with optical band gaps ranging from 1.1 to >2.6 eV with polymer colors across the entire visible spectrum.

1.6 Thesis of this Work

The overall theme of this research is to investigate the effects of electron withdrawing groups and intramolecular interactions on conjugated polymers. To help identify and illuminate these effects, a cohesive series of monomers was synthesized and studied. An investigation of this nature is facilitated by the use of bis(EDOT)benzenes for the following reasons: the unsubstituted monomer can be used as a baseline, the extended conjugation lowers monomer oxidation potential, the use of EDOT lowers the monomer oxidation potential further, the monomers can be symmetrical thus leading to isoregic polymers. In this work, we are extending the current range of utility of BEDOT-benzene based monomers by the inclusion of electron withdrawing groups and with other functional groups for use as electroactive

coatings. Due to the nature of the chemistry and variation of the projects presented here, conclusions will be given at the end of each chapter.

Computational chemistry is used as a tool to aid in the design of new monomers. The ground state structure and the electronic properties of conductive polymers starting with discrete monomers, dimers and trimers and extrapolating to higher molecular weights are investigated. GAMESS, HyperChem, and GAUSSIAN92 are used to implement semiemperical AM1 calculations, and the results of the various programs are compared. The band gaps, torsion angles, and inter-ring bond lengths are calculated, and neutral and dicationic species are compared. The band gaps are calculated using HOMO-LUMO and S_0-T_1 transitions.

Structure determination of the monomers by x-ray crystallography is used to validate the above calculations of the ground state of the monomers. It is also used to investigate subtle electronic and steric effects in alkoxy substituted bis(EDOT)benzenes. Although the solid state structure is not necessarily the same as in solution and the torsion angles can vary, ^{1}H NMR has been found to be a unique probe of the major solution conformation.

Electrochemistry is used extensively as a method of polymerization as well as an analytical tool. The oxidation potentials of the monomers and the oxidation/reduction (redox) properties of the resultant polymers is investigated using linear sweep cyclic voltammetry. Constant potential or potentiostatic methods are used in the electrodeposition of some monomers.

Electrochemistry is used in conjunction with spectroscopy in order to determine the electrochromic properties of the polymers

UV-Vis-NIR spectroscopy is used in conjunction with electrochemistry in order to determine the electrochromic properties of the polymers Spectroscopy is also used to determine the band gap, which is defined as the onset of the π–π^* band of the conjugated polymer The band gap is of ultimate importance in determining the electrochromic changes of the polymer

CHAPTER 2
ELECTRON-WITHDRAWING GROUPS PENDANT TO 1,4-BIS[2-(3,4-ETHYLENEDIOXY)THIENYL]BENZENES

2.1 Motivation

A determining factor in the color change of an electrochromic polymer is the optical band gap. The absorption of the π–π^* band in the visible region dictates its ground state color. With this in mind, it is advantageous to produce a range of electroactive polymers with varying band gaps, thus allowing a rainbow of colors. Low band gap materials, such as poly(**EDOT**), have π–π^* absorbances which are observed in the red portion or NIR of the visible region of the spectrum. As poly(**EDOT**) is oxidized the π–π^* absorbance diminishes, and new bipolaron bands exhibit increasing absorbance in the infrared, in theory giving colorless films. Another way of approaching colored to colorless films is to produce polymers with the π–π^* band in the ultraviolet. In this system, the polymer is colorless in the neutral, undoped state, and as the polymer is oxidized, bipolaron absorbances are induced in the visible region of the spectrum.

It is also necessary for the electroactive polymer to have its oxidation and reduction processes occur within 1V to -1V vs Ag/Ag^+. Redox processes much outside this range require strenuous exclusion of oxygen and water in

order to eliminate deleterious side reactions which would lead to polymer decomposition. The use of extended conjugation monomers containing EDOT lends itself well to this requirement since EDOT-based polymers have been shown to have low oxidation potentials and excellent stability

Electron withdrawing groups (**EWG**) are incorporated into conjugated polymers to raise the band gap. As the high gap polymer is oxidized, new lower energy bands appear in the visible region, thus making it an anodically coloring material. In addition to the obvious applications in the field of display technologies, electrochromic polymers can be used in IR shutters for telecommunications and military applications. Therefore, materials that can be tuned to absorb UV, visible, and/or IR light on demand are crucial.

In this work, the synthesis and subsequent electropolymerization of new monomers with pendant **EWG**'s are discussed. The techniques used include electropolymerization/deposition, cyclic voltammetry, UV-Vis-NIR spectroscopy, single crystal x-ray diffraction, and computational chemistry.

2.2 Results and Discussion

A series of EWG containing monomers (**Figure 2.1**) were synthesized using Pd catalyzed cross-coupling reactions. 1,4-Bis[2-(3,4-ethylenedioxy)thienyl]-2,5-difluorobenzene (**BEDOT-B-F_2**) was synthesized under Negishi type reaction conditions in good yield (85%).[85] 1,4-Dibromo-2,5-dicyanobenzene, needed for the synthesis of the dicyano analogues, was synthesized as shown in **Figure 2.2**.

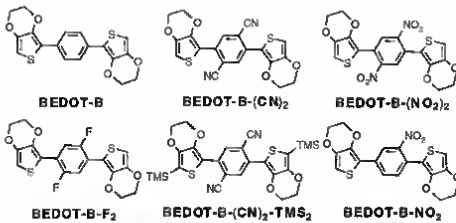

Figure 2.1 Bis(EDOT)Benzenes with Pendant EWG's

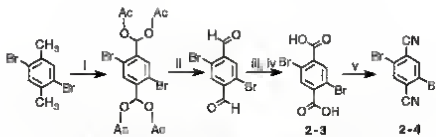

Figure 2.2 Synthesis of 1,4-Dibromo-2,5-dicyanobenzene (**2-4**)
i) CrO_3/acetic anhydride, ii) H^+/H_2O iii) Ag_2O/aq NaOH,
iv) H^+/H_2O, v) $TsNH_2/PCl_5$ heat

Attempted reproduction of the literature synthesis[87,88] of 2,5-dibromoterephthalic acid did not produce the product in the reported overall yield of 75 %, but proceeded in a much lower yield of ~10% In that synthesis, two steps in the oxidation of 2,5-dibromoxylene used water as the solvent As the xylene is sparingly soluble in water thus might account for the poor yield, therefore a non-aqueous medium was used for this oxidation CrO_3 in acetic anhydride was used to oxidize 2,5-dibromoxylene producing a tetra-acetate

derivative of terephthaldehyde 2,5-Dibromoxylyl-α,α,α',α'-tetra-ol tetra-acetate was hydrolyzed to 2,5-dibromoterephthaldehyde, which was not isolated since one of the side products of the reaction was the carboxylic acid [89] The crude product was used in the subsequent oxidation with silver oxide[90] in base followed by acidification for an overall yield of **2-3** of 50% The nitrile was subsequently synthesized in a 41% yield by a tandem amidization/dehydration reaction with tosylamide and phosphorous pentachloride [91]

The Stille cross-coupling reaction was used for the synthesis of the cyano analogues of the bis(EDOT)benzene series, since the cyano functionality is not stable to the lithio or the organozinc adducts used in the Negishi reactions outlined above 1,4-Bis[2-(3,4-ethylenedioxy)thienyl]-2,5-dicyanobenzene (**BEDOT-B-(CN)$_2$**) was synthesized in 62% yield and was recrystallized from nitrobenzene to yield yellow crystals The compound was very poorly soluble making purification and subsequent electrochemical analysis difficult 1,4-Bis[[2-(3,4-ethylenedioxy)thienyl]-5,5'-di(trimethylsilyl)]-2,5-dicyanobenzene (**BEDOT-B-(CN)$_2$-TMS$_2$**) was synthesized in high yield (90%) with improved solubility in hopes to improve the electropolymerization since other studies[92] have shown that TMS analogues polymerize more readily yet at the same oxidation potential The cyano derivatives reported exhibit a low carbon content by elemental analysis but both hydrogen and nitrogen content were within acceptable limits indicating unoptimized combustion conditions

1,4-Bis[2-(3,4-ethylenedioxy)thienyl]-2,5-dinitrobenzene (**BEDOT-B-(NO_2)$_2$**) was also synthesized by a Stille cross coupling using 1,4-dibromo-2,5-dinitrobenzene (**Figure 2.3**) in a 14% yield. 1,4-Dibromo-2,5-dinitrobenzene was first synthesized in an 11% yield,[93] by the direct nitration of 1,4-dibromobenzene, followed by separation of the isomers by solvent partition. The low yield for **BEDOT-B-(NO_2)$_2$** is probably due to the use of toluene as the reaction solvent since the monosubstituted derivative (1-bromo-4-[2-(3,4-ethylenedioxy)thienyl]-2,5-dinitrobenzene) was isolated in 50% yield based on

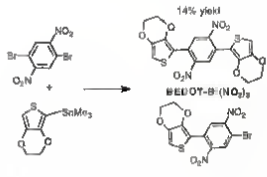

Figure 2.3 Synthesis of **BEDOT-B-(NO_2)$_2$**

1,4-dibromo-2,5-dinitrobenzene. The monosubstituted derivative [mp 145-148 °C] was poorly soluble in toluene and was identified by ^{1}H NMR, ^{13}C NMR and HRMS. Attempts at using DMF as the reaction solvent failed, possibly due to charge transfer complexes between 1,4-dinitrobenzene and DMF. The solution turned blood red upon addition of the dinitro compound, instead of the characteristic yellow-brown observed in successful reactions. **BEDOT-B-(NO_2)$_2$** was also poorly soluble, and a strategy for increasing

solubility was to synthesize the unsymmetrical mononitro derivative 1,4-Bis[2-(3,4-ethylenedioxy)thienyl]-2-nitrobenzene (**BEDOT-B-NO$_2$**) was synthesized by a Stille reaction in 84% yield from DMF and was soluble in acetone, chloroform and acetonitrile

Oxidative electrodeposition *via* repeated potential scanning in a standard three-electrode cell under inert atmosphere was used to polymerize the monomers to determine the electronic properties of the resultant polymers In a repeated potential scanning experiment, the cell is held at a reducing potential such that there is no electrochemical response from the monomer or polymer This initial potential is different for each monomer/polymer system but usually between 0 0 and -1 0 V vs. Ag/Ag^+ for the bis(EDOT) series. After an equilibration time, 0 to 30 s, the potential is linearly increased anodically The upper potential limit best set to just beyond the monomer oxidation peak, such that subsequent oxidations do not occur At the switching point, the potential is cathodically ramped back to the starting potential, thus forming one complete cycle This is repeated as necessary until the desired film thickness, number of cycles, or current response is attained

Figure 2.4 shows the repeated potential scan polymerization for **BEDOT-B-F$_2$** The onset of monomer oxidation ($E_{onset,m}$) begins at 0.83 V with a peak monomer oxidation potential ($E_{p,m}$) at 0 91 V On the reverse scan, the polymer reduces to its neutral state in two reductions with peaks at 0 5 and -0 1 V In second and subsequent scans the polymer oxidizes first at *ca* -0.2 V

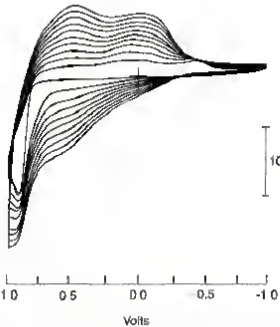

Figure 2.4 Repeated Potential Scan Electrochemical Polymerization of (10 mM) **BEDOT-B-F_2** (on a Pt Button in 0 1 M TBAP/CH_2Cl_2 at a Scan Rate of 100 mV/s)

as indicated by the increased current response The repeated scans result in more monomer oxidizing/depositing on the electrode as polymer **Figure 2.5** shows the cyclic voltammetry of poly(**BEDOT-B-F_2**) in monomer-free electrolyte solution (0.1 M TBAP/CH_3CN) as the scan rate is increased from 50 to 300mV/s in order to determine if the polymer is well-adhered to the electrode surface Note that in **Figure 2.5**, the anodic and cathodic polymer redox processes increase linearly with increasing scan rate, this is indicative of a well-adhered polymer film [74] It is also important to note that there is a minimal shift in the redox peaks of the polymer with increasing scan rate indicative of fast influx of charge compensating ions

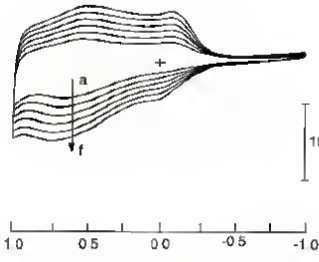

Figure 2.5 Cyclic Voltammetric Scan Rate Dependence of Poly(**BEDOT-B-F$_2$**) on a Pt Button in 0.1 M TBAP/CH_3CN at a Scan Rates of (a) 50 (b) 100 (c) 150 (d) 200 (e) 250 (f) 300 mV/s)

The redox processes for poly(**BEDOT-B-F$_2$**) include two oxidation waves peaking at 0.0 and 0.7 V and two reduction waves at 0.5 and -0.1 V, thus giving polymer redox half potentials ($E_{1/2}$) of 0.05 and 0.6 V. A summary of the electrochemical results for the series of monomers is found in **Table 2.1**.

BEDOT-B-(CN)$_2$ was poorly soluble and not electroactive at room temperature in nitrobenzene or benzonitrile, but at 135 °C in nitrobenzene, the monomer did begin to oxidize at ~1.45 V vs. a Ag° wire quasi-reference electrode (**Figure 2.6**). The polymer redox (**Figure 2.7**) shows that the polymer is electroactive but is not electrochromic, possibly indicating that the desired 5,5'- coupling was not the only product of the oxidation.

Table 2.1 Electrochemical Results of EWG Monomers

Monomer	$E_{onset,m}$	$E_{c,p}$	$E_{a,p}$	$E_{1/2}$	E_g
BEDOT-B[12]	0.6	–	–	0.23	1.8
BEDOT-B-F$_2$	0.8	0.5/-0.1	0.7/0.0	0.6/0.0	1.9
BEDOT-B-(CN)$_2$	1.5	1.0	0.8	0.9	n/a
BEDOT-B-(CN)$_2$**-TMS**$_2$	1.1	np	np	np	np
BEDOT-B-(NO$_2$**)**$_2$	2.2	np	np	np	np
BEDOT-B-NO$_2$	1.2	np	np	np	np

np = no polymer deposited on the electrode

BEDOT-B-(CN)$_2$**-TMS**$_2$ was synthesized in hopes that improved solubility would improve the electropolymerization behavior In this instance, although there was an oxidation peak by electrochemistry, no solids precipitated onto the electrode In fact, neither **BEDOT-B-(NO**$_2$**)**$_2$ nor

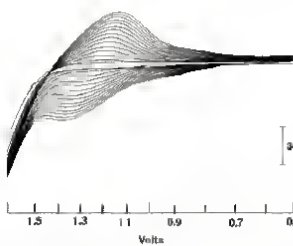

Figure 2.6 Repeated Potential Scan Electrochemical Polymerization of (10 mM) **BEDOT-B-(CN)**$_2$ (on a Pt Button in 0.1 M TBAP/nitrobenzene at a Scan Rate of 100 mV/s at 135 °C)

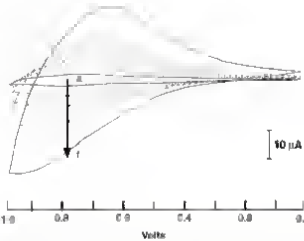

Figure 2.7 Cyclic Voltammetric Scan Rate Dependence of Poly(**BEDOT-B-$(CN)_2$**) (on a Pt Button in 0.1 M TBAP/Nitrobenzene at a Scan Rates of (a) 100 (b) 200 (c) 300 (d) 400 (e) 500 (f) 1000 mV/s)

BEDOT-B-NO_2 yielded electroactive polymer films although there were oxidative processes observed. We believe that the monomers with pendant cyano and nitro groups failed to polymerize due to steric constraints. This was substantiated using x-ray structures of the monomers and rotational energy barrier calculations as described below.

The x-ray structure determined ring to ring torsion angles for **BEDOT-B-$(CN)_2$-TMS_2** and **BEDOT-B-NO_2** are 46.4° and 42.9°, respectively indicating that there is little conjugation across the three ring system. Rotational energy barriers were calculated and found to be high for the cyano and nitro monomers relative to the unsubstituted and difluorinated derivatives. One of the reasons that **ECM**'s have lower oxidation potentials is that the radical

cation formed in the oxidative process can be delocalized over more than one ring. This delocalization is achieved only if the unit can attain a somewhat planar conformation for better π overlap. When steric interactions affect the formation of the planar state, the polymerization is obstructed.

In order to determine the band gap and electrochromic properties of electrochemically produced polymer film, spectroelectrochemical experiments were performed on thin films of each polymer. In this experiment, a polymer film was electrodeposited on indium tin oxide (ITO) coated glass, then the sample was incorporated into an electrochemical cell containing monomer-free electrolyte assembled in the path of a UV-Vis-NIR spectrophotometer. The film was oxidized and reduced in 0.1 V steps and a spectrum was collected at each potential. A set of spectra for **BEDOT-B-F$_2$** equilibrated at potentials between 0.0 and 1.2 V vs. Ag/Ag$^+$ is shown in **Figure 2.8**. The onset of the π–π^* transition of electrochemically neutral polymer (a)

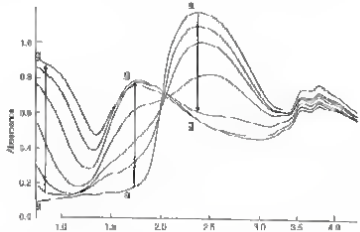

Figure 2.8 Spectroelectrochemical Analysis of Poly(**BEDOT-B-F$_2$**) (on a ITO in 0.1 M TBAP/CH_3CN at (a) 0.0 (b) 0.2 (c) 0.4 (d) 0.6 (e) 0.8 (f) 1.0 (g) 1.2 V)

can be extrapolated to the background absorbance to yield a band gap of 1 85 eV. This is the accepted method for determining the optical band gap of conjugated polymers. As the polymer is electrochemically oxidized, the π–π^* band decreases in intensity, and two lower energy bands develop. The lower energy bands are the bipolaron 1 and bipolaron 2 bands, corresponding to the two intermediate bands shown in **Figure 1.2**. In the fully reversible electrochemically oxidized state (1.2 V vs Ag/Ag^+), the π–π^* band is reduced to a shoulder of the bipolaron 2 band. It is important to note that in **Figure 2.8**, spectra e, f, and g show an increase in the bipolaron 1 band, but no increase in the bipolaron 2 band. In other studies in our group,[77] this phenomenon was also seen and was attributed to the transition of the polymer from the doped state to a semi-metallic state, which has lower energy transitions. The thin films of poly(**BEDOT-B-F_2**) are electrochromic. In the neutral state (0 0 V), the polymer film is transmissive red, then as the polymer is fully oxidized (1.0V), the polymer becomes blue.

Of the monomers synthesized above, we were able to obtain x-ray crystal structures for **BEDOT-B-F_2**, **BEDOT-B-$(CN)_2$-TMS_2**, and **BEDOT-B-NO_2**, and compare these to the structure of **BEDOT-B** determined previously.[12] In all of structures presented below, the central benzene is held in the plane of the page. **Figure 2.9** shows a perspective view and atom labeling of **BEDOT-B-F_2**, which is close to planar. The plane of the thiophene ring of the EDOT group makes an angle of only 3.4° to the plane of the benzene ring. **Figure 2.10** shows a perspective view and atom labeling of **BEDOT-B-$(CN)_2$-TMS_2**,

which deviates significantly from planarity. Specifically, the plane of the thiophene ring of the EDOT group makes an angle of 46.4° to the plane of the attached benzene ring. **Figure 2.11** shows a perspective view and atom

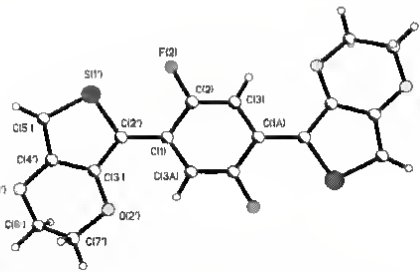

Figure 2.9. Perspective View and Atom Labeling of the X-ray Structure of **BEDOT-B-F_2**

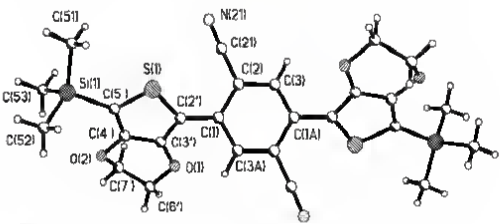

Figure 2.10. Perspective View and Atom Labeling of the X-ray Structure of **BEDOT-B-$(CN)_2$-TMS_2**

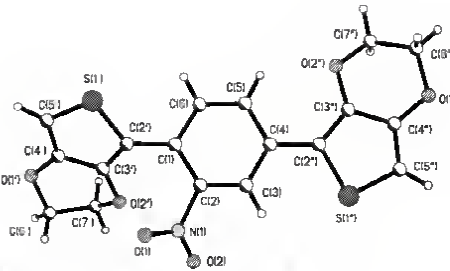

Figure 2.11 Perspective View and Atom Labeling of the X-ray Structure of **BEDOT-B-NO_2**

labeling of **BEDOT-B-NO_2**, which exists in a conformation with the thiophene ring of the EDOT substituent adjacent to the nitro group significantly twisted out of the plane of the benzene ring (angle between the meanplanes = 42.9°). In contrast, the plane of the other EDOT thienyl ring is almost coplanar with the benzene ring (angle between the meanplanes = 5.4°). The plane of the nitro group is twisted 43.3° out of the plane of the benzene ring and in the opposite direction to the twist of the adjacent EDOT group.

In an effort to determine if molecular modeling can predict the structure and electronic properties of this set of EWG containing poly(BEDOT-B)'s, discrete monomers, dimers and trimers (three, six, and nine rings respectively) were studied (**Figure 2.12**). Computational analyses include the structural conformation of the ground and dicationic states. The electronic

properties of each molecule were then determined and extrapolation to higher molecular weights was used to approximate the electronic properties of the polymers. The calculated structures are denoted as bracketed acronyms of the related compounds, with the dimers and trimers similarly identified.

The first step was to determine the ground state geometry of the compounds. Comparison of the calculated ground state geometries of the four monomeric compounds ([**BEDOT-B**], [**BEDOT-B-F$_2$**], [**BEDOT-B-(CN)$_2$**], [**BEDOT-B-(NO$_2$)$_2$**] and [**BEDOT-B-(NO$_2$)$_2$]$_2$**) with the crystal structures of the related compounds (**BEDOT-B**, **BEDOT-B-F$_2$**, **BEDOT-B-(CN)$_2$-TMS$_2$**, and **BEDOT-B-NO$_2$**), yields a good correlation. The calculated bond lengths and angles (excluding the ring

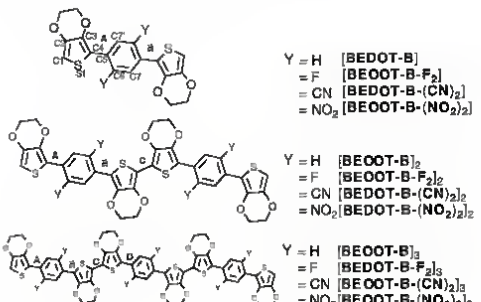

Figure 2.12. Structures and Selected Bonds of Calculated Compounds

to ring torsion angles) were within 1% of experimentally determined values for all monomer structures

Subsequent calculations of torsion angles were carried out for the four monomers at the AM1 level within GAMESS[92] and HyperChem[93] in both neutral (z=0) and the dicationic (z=2) states as shown in **Table 2.2** It should be noted that, even though both programs use AM1, the model is implemented in slightly different ways and the results are program dependent. GAMESS and HyperChem yield torsion angles that are similar in most cases (**Table 2.2**) All further calculations were done using GAMESS for consistency

Table 2.2. Calculated Inter-ring Torsion Angles (°) by Program Used[a]

Compound	GAMESS		Hyper Chem	
	z=0	z=2	z=0	z=2
[BEDOT-B]	17.1	1 0	17 2	0 5
[BEDOT-B-F_4]	43.8	1 4	45 8	1 4
[BEDOT-B-$(CN)_2$]	23.2	1 2	26.3	0 9
[BEDOT-B-$(NO_2)_2$]	86 6	0/30	46 9	14.3

[a]all calculations carried out using AM1

The crystal structure determined torsion angle of **BEDOT-B**[92] is 27.5°, while the calculated value for **[BEDOT-B]** is 17° More interestingly, the energy difference between the 27.5° and 17° structures was calculated to be <1 kcal/mol (a more in-depth discussion of the rotational barrier calculations is found below) Since the optimized geometry was calculated in vacuum, there

is some variance due to crystal lattice packing energy. The crystal structure of **BEDOT-B-F_2** determined an inter ring torsion angle of 3.4°, which is much lower than the predicted value 43.8° for **[BEDOT-B-F_2]**, although once again the energy difference was calculated to be <1 kcal/mol. **BEDOT-B-$(CN)_2$-TMS_2** was determined to have a 46.4° torsion angle, significantly higher than the calculated value of 23.2° for **[BEDOT-B-$(CN)_2$]**. In this case, there is over 1.5 kcal/mol difference in the 46° and 23° torsion angle structures. This may be due to a difference in electron density of the EDOT rings caused by the presence of the solubilizing TMS groups. The crystal structure of **BEDOT-B-NO_2** shows a torsion angle of 42.9°. The value calculated within the GAMESS program was 86.6° for **[BEDOT-B-$(NO_2)_2$]**, twice that found by x-ray (note that the HyperChem value of 46.9° is very close).

In order to more fully understand the rotational energy barriers in these molecules, the energy differences were calculated as a function of torsion angle for the monomers using a matrix containing two dummy atoms. The AM1 calculations were implemented within GAUSSIAN92[87]. The calculated values were normalized to show the energy barriers per EDOT ring. The results are shown in **Figure 2.13**. Both **[BEDOT-B]** and **[BEDOT-B-F_2]** have a low potential barrier as the molecule becomes planar, demonstrating the small steric interactions imposed by hydrogen and fluorine. The steric bulk of the cyano and nitro groups greatly increases the potential barrier and twists the molecule out of planarity.

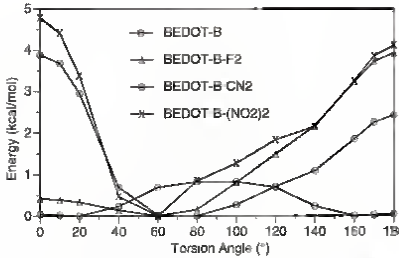

Figure 2.13 Calculated Rotation Barrier Potentials of BEDOT-B's

One of the opportunities afforded by the analysis of the structures of the neutral and dicationic compounds is to predict the structure of the charge carrier in oxidatively doped systems, the bipolaron. By investigating torsion angle and inter-ring bond distances, the bipolaronic structure was determined by comparing the optimized geometry of the dicationic species to the optimized geometry of the neutral compound.

All modeled compounds exhibited a marked decrease in torsion angles as dicationic species. [**BEDOT-B**], [**BEDOT-B-F**$_2$], and [**BEDOT-B-(CN)**$_2$] were found to be coplanar as dications. In [**BEDOT-B-(NO**$_2$**)**$_2$], one of the thienyl rings was coplanar, while the other maintained an angle of 30° out of plane. Thus demonstrates that the steric energy barriers can be overcome in the charged states. In an effort to determine why [**BEDOT-B-(NO**$_2$**)**$_2$] is unsymmetrical, the interatomic distances reported by GAMESS were

examined. One of the nitro oxygens was found to be a very short 1.80Å from the thienyl sulfur in the dication. This gave credence to the structure proposed in **Figure 2.14**, in which a six member heterocycle was formed on one side of the molecule. The bond distances of the other oxygens were larger (4.2Å and 2.4Å) indicating weaker interactions. In addition, the oxygen-nitrogen bond length for the non-sulfur bonded oxygen was 1.17Å, while the interacting oxygen had a bond length of 1.30Å, suggesting that the non-sulfur bonded oxygen has more double bond character. On the other nitro group, the nitrogen to oxygen bond distances were both 1.20Å, as in a normal, non-interacting nitro group.

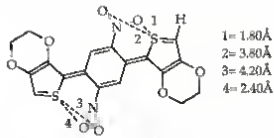

Figure 2.14 Interatomic Interactions for $[\mathbf{BEDOT\text{-}B\text{-}(NO_2)_2}]^{++}$

The dicationic dimers coalesced to a coplanar configuration over the entire six ring system, with exception of the nitro compound, $[\mathbf{BEDOT\text{-}B\text{-}(NO_2)_2}]_2^{++}$. In the trimers, all showed a coplanar structure for the five internal rings and varying degrees of rotation, from 4° for $[\mathbf{BEDOT\text{-}B}]_3^{++}$ to 20°, for $[\mathbf{BEDOT\text{-}B\text{-}F_2}]_3^{++}$, and $[\mathbf{BEDOT\text{-}B\text{-}(NO_2)_2}]_3^{++}$, of the external rings. With examination of only the torsion angle changes as the compounds are

converted from the neutral to the dicationic state, we predict the bipolaron extends over 5 rings.

To further strengthen the argument for this bipolaron structure, the inter-ring bond distances were examined. The decrease in inter-ring bond lengths between neutral and dicationic species correlates to an increase in ring-to-ring π-overlap. In **Table 2.3**, the differences in inter-ring bond lengths

Table 2.3 Percent Change in Bond Lengths Between Rings (z=2 - z=0)

	A	B	C	D
[BEDOT-B]	-5.2	-5.2	--	--
[BEDOT-B-F_2]	-5.5	-5.5	--	--
[BEDOT-B-$(CN)_2$]	-5.3	-5.3	--	--
[BEDOT-B-$(NO_2)_2$]	-0.6	-2.1	--	--
$[BEDOT\text{-}B]_2$	-2.3	-3.8	-4.9	--
$[BEDOT\text{-}B\text{-}F_2]_2$	-2.5	-3.6	-5.1	--
$[BEDOT\text{-}B\text{-}(CN)_2]_2$	-2.6	-3.2	-5.2	--
$[BEDOT\text{-}B\text{-}(NO_2)_2]_2$	-3.8/-1.4	-4.0/-4.9	-4.9	--
$[BEDOT\text{-}B]_3$	-0.6	-1.1	-3.4	-5.3
$[BEDOT\text{-}B\text{-}F_2]_3$	-0.5	-0.6	-3.3	-5.3
$[BEDOT\text{-}B\text{-}(CN)_2]_3$	-0.8	-0.5	-3.4	-5.3
$[BEDOT\text{-}B\text{-}(NO_2)_2]_5$	-0.7	+0.2	-3.3	-4.9

identified in **Figure 2.12** as a function percent change in bond length. For reference, the percent change in length for a single sp^2 sp^2 bond (as in the central bond in butadiene (1.48Å)) going to a double sp^2-sp^2 bond (as in ethylene (1.34Å)) is 9.5 % (net change divided by neutral bond length). For **[BEDOT-B]**, **[BEDOT-B-F_2]**, and **[BEDOT-B-$(CN)_2$]**, the decrease in bond length was symmetrical to the center, and all had approximately the same reduction, -0.08Å. The nitro monomer, **[BEDOT-B-$(NO_2)_2$]**, was unsymmetrical, with a net shortening approximately half that of the other monomers, -0.04Å. Compounds **[BEDOT-B]**, **[BEDOT-B-F_2]**, and **[BEDOT-B-$(CN)_2$]**, all exhibited symmetrical bond contractions with the greatest reduction at the center of the molecule and decreasing contraction toward the termini. **[BEDOT-B-$(NO_2)_2$]** appears to concentrate the dicationic charge over four rings to one side of the molecule. Three of the bonds had similar contractions of approximately -0.06Å, and the other two bonds showed insignificant bond shortening. These results suggest that the bipolaron extends over 5 rings including 4 **EDOT** rings.

The electronic band gaps of the neutral compounds were estimated by two methods. The first method involved calculating the Highest Occupied Molecular Orbital (HOMO) to Lowest Unoccupied Molecular Orbital (LUMO) gap, and the second method was calculated for a ground state to first excited state triplet energy gap.

To determine the energy difference between the HOMO and LUMO orbitals in the neutral state, the energy of each π-electron for all compounds

was calculated, as well as the predicted energies for the π*-orbitals. By measuring the difference in the highest energy π-electron and its corresponding π*-orbital, the HOMO-LUMO gap is determined for each compound. The energies were compared as a function of inverse molecular weight, and extrapolated to infinite molecular weight to yield the calculated polymer HOMO-LUMO gap found in **Table 2.4**. In the HOMO-LUMO transition calculations, the band gap was determined to be between 6.6 and 6.9 eV. These values were very high compared with the spectroscopically determined band gaps of the polymers for **BEDOT-B** and **BEDOT-B-F_2**, which were 1.8 eV[12] and 1.9eV[36] respectively. These band gap calculations were normalized by simple subtraction to agree with the literature value of 1.8 eV. The energies calculated do not follow any trend.

Table 2.4 Results of Band Gap Calculations by Method

Compound	HOMO-LUMO (eV)	HOMO-LUMO[a]	S_0 to T_1 (eV)	S_0 to T_1[a] (eV)	Measured (eV)
BEDOT-B	6.59	1.80	2.67	1.80	1.80
BEDOT-B-F_2	6.93	2.14	2.78	1.90	1.85
BEDOT-B-$(CN)_2$	6.56	1.77	2.71	1.84	N/A[c]
BEDOT-B-$(NO_2)_2$	6.60	1.80	3.00	2.13	N/A[c]

[a] The calculated values were normalized to the value for poly(2-1)
[b] Spectroscopically determined
[c] Monomer does not polymerize electrochemically

The second method was a ground-triplet (S_0-T_1) transition, the results of which are found in **Table 2.4**. In this method, the neutral ground state structures were calculated as a triplet (unpaired spin) state. The energy of each π electron for all compounds was calculated. By measuring the difference in the highest energy π-electron and the first lower π-electron, the HOMO-(HOMO-1) gap is determined for each compound. The energies were compared as a function of inverse molecular weight, and extrapolated to infinite molecular weight to yield the calculated polymer S_0 to T_1 gap found in **Table 2.4**. After the values were normalized to the published value for poly(**BEDOT-B**),[92] a rational trend is found. The predicted (1.9 eV) and spectroscopically determined (1.85-1.9 eV) band gaps of poly(**BEDOT-B-F_2**) are in good agreement. The predicted band gaps for poly(**BEDOT-B-$(CN)_2$**) and poly(**BEDOT-B-$(NO_2)_2$**) are within reason by empirical estimation, but they could not be compared with spectroscopically determined values since the monomers do not electrochemically polymerize.

2.3 Conclusions

Five unique extended conjugation monomers with pendant electron withdrawing groups have been synthesized and analyzed. Fluoro, cyano, and nitro groups were used to probe the effect on the electronic properties of the monomers and polymers. Within this study, we have determined that cyano and nitro groups are too sterically demanding for use in a bis(EDOT)benzene

monomers and torque the rings out of plane to such a great extent that the monomers fail to polymerize

We have also determined that there is an electrostatic interaction between fluorine and sulfur in this system that decreases the inter-ring torsion angle to 3° Although computational results predict a larger torsion angle of 44°, the rotational barrier calculation shows <0.5 kcal/mol difference in energy of the two angles This result lead to other questions that are explored in the next three chapters

- What are the effects of varying the number of pendant fluorines on poly(BEDOT-B-F_x)?
- What other electrostatic interactions are found in poly(BEDOT-B) derivatives?
- What are the effects of incorporating other electron accepting groups such as pyridine into poly(BEDOT-B) derivatives?

With the aid of computational methods, we can predict the band gap of a polymer Although, we were only able to compare the results for two of the four monomers studied, we were able to predict based upon the rotational energy barrier that the remaining compounds would not polymerize Within this system, the band gap can be predicted using the ground state-triplet state calculations

2.4 Synthesis

2.4.1 General Procedures

All chemicals were purchased from Aldrich and used as received unless otherwise stated. *n*-Butyl lithium (2.5 M in hexanes) was purchased from Acros Chemical. Zinc chloride was obtained from Aldrich Chemical and dried before use over P_2O_5 under vacuum for two days. 3,4-Ethylenedioxythiophene (EDOT) was donated by AG Bayer and distilled under vacuum, purged with argon, and stored at -20 °C until used. THF, acetonitrile, acetic anhydride, chromium trioxide, phosphorous pentachloride, silver oxide, and methylene chloride were purchased from Fisher Scientific. 1,4-Dibromo-2,5-difluorobenzene was purchased from PCR and used as received. Tetra-*n*-butyl ammonium perchlorate (TBAP) was synthesized by the addition of perchloric acid to aqueous tetra-*n*-butyl ammonium bromide, the precipitate was collected and was recrystallized from ethanol. 1,4-Bis[2-(3,4-ethylenedioxy)thienyl]benzene (**BEDOT-B 2-1**) was prepared as previously reported [12]

Cyclic voltammetry was carried out using an EG&G Princeton Applied Research Model 273 potentiostat/galvanostat employing a platinum button working electrode (0.005 cm^2), a platinum plate counter electrode, and Ag/Ag^+ reference electrode or Ag^o wire quasi-reference electrode calibrated to ferrocene.

Elemental analyses was performed by Robertson Microlit Laboratories, Inc of Madison, New Jersey. All HRMS analyses were performed at the University of Florida. All ^{1}H-NMR spectra were obtained on a Varian Gemini-300 NMR spectrometer at 300 MHz with tetramethylsilane (TMS) or solvent as internal standard. All ^{13}C-NMR spectra were obtained on a Varian Gemini-300 NMR spectrometer at 75 MHz with TMS or solvent as internal standard. All ^{19}F-NMR spectra were obtained on a Varian VXR-300 NMR at 282 MHz with CCl_3F as internal standard.

2,4,2',4'-Bis[2-(3,4-ethylenedioxy)thienyl]-2',5'-difluorobenzene (BEDOT-B-F$_2$, 2-2)

n-Butyl lithium (14.1 mL, 35.2 mmol) was slowly added by syringe to a stirred solution of EDOT (5.00 g, 35.2 mmol) in THF (50 mL) at -78 °C under argon. The resulting yellow solution was stirred for an hour and cannula-transferred over 15 minutes to a stirring solution of $ZnCl_2$ (4.79 g, 35.2 mmol) in THF (50 mL) at room temperature. The mixture was stirred under argon for 1 h. The resulting EDOT-ZnCl complex was slowly added by cannula to a solution of 1,4-dibromo-2,5-difluorobenzene (2.39 g, 8.79 mmol) and $Pd(PPh_3)_4$ (200 mg, 0.2 mmol) in THF (20 mL). The bright yellow solution was stirred at 50 °C under argon for 96 h, and a precipitate formed after 48 h. The mixture was cooled to ambient temperature and quenched with water (200 mL). The THF was removed under reduced pressure, and the solid was collected by suction filtration and dried under vacuum. The crude solid was crystallized from toluene to yield tan crystals [mp 242-243 °C, 85%]. Anal. calcd. for

$C_{16}H_{12}F_2O_4S_2$: C, 54.82; H, 3.07; F, 9.63; O, 16.23; S, 16.26; found: C, 54.61; H, 3.14; F, 9.43; S, 16.33. ^1H NMR ($CDCl_3$, TMS) δ 4.25-4.36 (m, 8H), 6.46 (s, 2H), 7.79-7.85 (dd, J = 10.2 and 9.3, 2H). ^{19}F NMR ($CDCl_3$, CCl_3F) δ (-111.4-(-111.5)(t, J_{H-F} = 7.3 Hz). FAB-HRMS calcd for $C_{16}H_{12}F_2O_4S_2$: 394.0145; found: 394.0153.

2,4,3,2,5-Dibromoterephthalic Acid (2-3)

A solution of chromium trioxide (44.5 g) in acetic anhydride (350 mL) was added drop wise to a chilled (0 °C) solution of 2,5-dibromoxylene (20 g) in acetic anhydride (160 mL), over a period of 2 hours. The temperature was maintained at 0-10 °C for 4 h once the addition was complete. The reaction mixture was then precipitated into water and the solid was collected by suction filtration. The solid was washed with water (~2 L), and was added to a suspension of sodium hydroxide (45.5 g in 500 mL of water) and silver oxide (35.2 g, 4 eq). The mixture was heated to 60 °C for 2 h. The reaction mixture was filtered and then acidified to pH 1. The off-white solid was collected by suction filtration and recrystallized from water to yield white crystals [mp 318-21 °C, lit. 318-21°C,[88] 50%]. Anal. calcd. for $C_8H_4Br_2O_4$: C, 29.66; H, 1.24; Br, 49.33; O, 19.76; found: C, 29.96; H, 1.17; Br, 49.52. ^1H NMR (DMSO) δ 8.15 (s, 2H), 13.97 (b, 2H). ^{13}C NMR (DMSO, TMS) δ 118.9, 135.0, 137.0, 165.6. HRMS calcd for $C_8H_4Br_2O_4$: 321.8476; found: 321.8497.

2,4,4',1,4-Dibromo-2,5-dicyanobenzene (**2-4**)

A flask equipped with a short path distillation head was charged with compound **2-3** (5.00 g, 15.4 mmol), *p*-toluenesulfonamide (5.8 g, 34 mmol) and phosphorous pentachloride (14.1 g, 67.8 mmol), and was heated until all solids had melted. After an initial exotherm had subsided, the reaction mixture was heated to 200 °C and phosphorus oxychloride was distilled off. The cooled reaction mixture was dissolved in pyridine (100 mL) with mild heating (~50 °C), then was added to water (1 L). The solid was collected by suction filtration and was stirred in sodium bicarbonate (5% aq., 1 L) for 2 h. The solid was collected by suction filtration and was air dried overnight. The solid was recrystallized from toluene to yield a tan solid [mp 265-68 °C, 41%]. ^{1}H NMR (DMSO, TMS) δ 8.60 (s, 2H). ^{13}C NMR (DMSO) δ 115.3, 120.1, 124.1, 138.3. HRMS calcd for $C_8H_2Br_2N_2$ 283.8585; found: 283.8579.

2,4,5,1,4-Bis[2-(3,4-ethylenedioxy)thuenyl]-2,5-dicyanobenzene (**BEDOT-B-(CN)$_2$**, **2-5**)

Under an argon purge, **2-4** (1.4 g, 4.9 mmol), 2-trimethylstannyl-3,4-ethylenedioxythiophene (3.0 g, 9.8 mmol), and $Pd(PPh_3)_4$ (0.050 g) were combined and anhydrous toluene (30 mL) was added. The reaction mixture was heated to 90 °C for 72 h with stirring. The solvent was removed under reduced pressure to yield an orange solid. The solid was washed successively with THF, chloroform, and toluene to yield a bright yellow solid [mp 325-30 °C, 62%]. Anal. calcd for $C_{28}H_{12}N_2O_4S_2$: C, 58.81; H, 2.96; N, 6.86;

O, 15 67, S, 15 70, found. C, 57 69, H, 2 92, N, 6 81 ^{1}H NMR (DMSO) δ 4.29-4.34 (m, 8H), 6 97 (s, 2H), 8.21 (s, 2H) HRMS calcd for $C_{26}H_{12}N_2O_4S_2$ 408 0239, found 408 0234

2,4,6,1,4-Bis[[2-(3,4-ethylenedioxy)thienyl]-5,5'-di(trimethylsilyl)] 2,5-dicyanobenzene (BEDOT-B-(CN)$_2$-TMS$_2$, 2-6)

Under an argon purge, **2-4** (0 40 g, 1 4 mmol), 2-trimethylstannyl-3,4-ethylenedioxy-5-trimethylsilylthiophene (1 0 g, 2 8 mmol), and $Pd(PPh_3)_4$ (0 025 g) were combined and anhydrous toluene (20 mL) was added The reaction mixture was heated to 90 °C for 24 h. Pentane was added to the cooled reaction mixture to yield a yellow precipitate The solid was collected by suction filtration and purified by column chromatography using $CHCl_3$ as eluent on neutral alumina to yield a bright yellow solid [mp 217-20 °C, 90%] Anal. calcd for $C_{26}H_{28}N_2O_4S_2Si_2$ C, 56.49, H, 5 11, N, 5 07, O, 11.58, S, 11 60, Si, 10 16, found C, 55 63 H, 5 16, N, 4 83 ^{1}H NMR ($CDCl_3$, TMS) δ 0 33 (s, 18H), 4 36 (s, 8H), 8 15 (s, 2H) HRMS calcd for $C_{28}H_{28}N_2O_4S_2Si_2$ 552.1029, found 552 1018

2,4,7,1,4-Bis[2-(3,4 ethylenedioxy)thienyl] 2,5 dinitrobenzene (BEDOT-B-(NO$_2$)$_2$, 2-7)

Under an argon purge, 1,4-dibromo-2,5-dinitrobenzene (3 74 g, 11 5 mmol), 2 trimethylstannyl-3,4-ethylenedioxythiophene (7 00 g, 23 0 mmol), and $Pd(P^tPh_3)_4$ (0.10 g) were combined and anhydrous toluene (100 mL) was added The reaction mixture was heated to 90 °C for 24 h with stirring.

Pentane was added to the cooled reaction mixture, and the solid was collected by suction filtration The solid was washed with chloroform and was recrystallized from acetonitrile to yield a bright orange crystalline solid [mp 265-68 °C, 13 6%] Anal calcd for $C_{18}H_{12}N_2O_6S_2$ C 48 21, H, 2 70, N, 6 25, O, 28 54, S, 14 30, found C, 48 15, H, 2 68, N, 6 26, S, 14 28 ^{1}H NMR (DMSO) δ 4 20 (s, 8H), 6 94 (s, 2H), 8 09 (s, 2H) ^{13}C NMR (DMSO, TMS) δ 64 2, 64 7, 102 7, 108 0, 125 1, 127 7, 140 4, 141 3, 149 1 HRMS calcd for $C_{18}H_{12}N_2O_6S_2$ 448 0035, found 448 0039

2,4,7 1,4-Bis[2-(3,4-ethylenedioxy)thienyl]-2-nitrobenzene (BEDOT-B-NO_2, 2-8)

Under an argon purge, 1,4-dibromo-2-nitrobenzene (2 0 g, 7 1 mmol), 2-tributylstannyl-3,4-ethylenedioxythiophene (6 8 g, 16 mmol), and $Pd(PPh_3)_4$ (0 10 g) were combined and anhydrous DMF (50 mL) was added The reaction mixture was heated to 100 °C for 18 h with stirring. The reaction was quenched with water (500 mL). After 4 h, the solid was collected by suction filtration The solid was dissolved in acetone and carbon treated until the solution was pale orange, then, the solvent was evaporated and the solid was recrystallized from ethanol to yield yellow-orange crystals. [mp 148-49 °C, 84%] Anal calcd. for $C_{18}H_{13}N_1O_6S_2$ C, 53 59, H, 3 25, N, 3 47, O, 23 80, S, 15 89, found C, 53 53, H, 3 37, N, 3 38, S, 15 54 ^{1}H NMR (d6 acetone) δ 4 17-4 22 (m, 4H), 4 30-4 45 (m, 4H), 6 60 (s, 1H), 6 61 (s, 1H), 7 54-7 57 (d, J_{H-H}= 8 2 Hz, 1H) , 7 90-7 93 (dd, J_{H-H}= 1 99 Hz, J_{H-H}= 8 2 Hz, 1H) , 8 24 (d, J_{H-H}= 1 8 Hz, 1H) HRMS calcd for $C_{18}H_{13}N_1O_6S_2$ 4403 0184, found 403 0206

2.5 Computational Methods

A series of compounds were studied using computational chemical methods (**Figure 2.12**). The GAMESS program was used for molecular orbital geometry optimizations for the neutral and dicationic states using a restricted Hartree-Fock (RHF) self-consistent field (SCF) The SCF restricted open-shell Hartree-Fock (ROHF) approximation was used for open shell molecules in the triplet states.

Rotational barrier calculations at the AM1 level were implemented within GAUSSIAN92 In this calculation, the thienyl rings of the two EDOT moieties were held stationary, and the internal benzene ring was rotated at 10° or 20° intervals. The energies were normalized to the lowest energy conformation for each molecule studied The result was then halved to reflect to rotation of only one EDOT All frequencies for the optimized structures, calculated within GAMESS, were found to be positive ensuring that the global minimum had been reached

2.5 X-ray Experimental

The crystal data, data collection, and refinement parameters for the structures are listed below Data was collected with a Siemens SMART CCD area detector, using graphite monochromatized Mo Kα radiation (λ = 0.71073 Å) Intensities were also corrected for Lorentz and polarization effects and for

absorption. The structures were solved by direct methods using SHELXS[88] and refined on F^2, using all data, by full-matrix least-squares procedures with SHELXL-96[89]. Hydrogen atoms were included in calculated positions with isotropic displacement parameters 1.3 times the isotropic equivalent of their carrier carbons. The functions minimized were $\Sigma w(F_o^2 - F_c^2)$, with $w = [\sigma^2(F_o^2) + (aP)^2 + bP]^{-1}$, where $P = [\max(F_0)^2 + 2F_c^2]/3$. In all cases, final difference Fourier syntheses showed no unusual features. Tables of final atom coordinates and bonding geometry are given in Appendices I and II.

Crystal data for **BEDOT-B-F$_2$** at 120°C: $C_{18}H_{12}F_2O_4S_2$, Mr = 394.4, lemon needle, 0.81 x 0.09 x 0.09 mm, monoclinic, space group $P2_1/c$, a = 4.197(3), b = 10.025(5), c = 18.635(10) Å, β = 90.85(5)°, V = 780.6(8) Å^3, F(000) = 404, Z = 2, D_c = 1.678 g cm^{-3}, μ(Mo-Kα) = 3.87 cm^{-1}, $2\theta_{max}$ = 50°, 118 parameters, GooF = 0.84, wR2 = 0.3208 for all 1356 data, (a = 0.1476, b = 0), R1 = 0.1167 for 406 data with $F_o > 4\sigma(F_o)$.

Crystal data for **BEDOT-B-(CN)$_2$-TMS$_2$** at -115°C: $C_{26}H_{28}N_2O_4S_2Si_2$, Mr = 552.8, yellow block, 0.72 x 0.48 x 0.14 mm, triclinic, space group $P\bar{1}$, a = 8.6796(9), b = 9.2257(10), c = 10.3161(10) Å, α = 64.009(1), β = 73.116(1), γ = 68.3720(1)°, V = 682.0(1) Å^3, F(000) = 290, Z = 1, D_c = 1.346 g cm^{-3}, μ(Mo-Kα) = 3.18 cm^{-1}, $2\theta_{max}$ = 53°, 163 parameters, GooF = 1.20, wR2 = 0.1777 for all 2624 data, (a = 0.0762, b = 1.02), R1 = 0.0.642 for 2154 data with $F_o > 4\sigma(F_o)$.

Crystal data for **BEDOT-B-NO$_2$** at 133°C: $C_{18}H_{13}NO_6S_2$, Mr = 403.4, orange plate, 0.55 x 0.50 x 0.05 mm, orthorhombic, space group $P2_12_12_1$, a =

7.5073(1), b = 8.9627(1), c = 24.5106(4) Å, V = 1649.21(4) Å^3, F(000) = 832, Z = 4, D_c = 1.625 g cm^{-3}, μ(Mo-Kα) = 3.62 cm^{-1}, $2\theta_{max}$ = 50°, 244 parameters, GooF = 1.14, wR2 = 0.1490 for all 2877 data, (a = 0.086, b = 0.09), R1 = 0.0612 for 2721 data with $F_o > 4\sigma(F_o)$

CHAPTER 3
FLUORINATED 1,4-BIS[2-(3,4-ETHYLENEDIOXYTHIENYL)]BENZENES

3.1 Motivation

As an extension to the work in the previous chapter, a more in-depth study into fine tuning the electronic properties of bis(EDOT)benzenes is presented here. As introduced in Chapters 1 and 2, high gap, low oxidation potential materials are needed for anodically coloring materials for use in high contrast dual polymer electrochromic devices.[78] Fluorine is classified as a weak electron withdrawing group.[100] The electronic properties of poly(BEDOT-B)s can be incremental tuned by increasing the number of fluorines on the four available sites of the central benzene should produce a range of high gap, low oxidation potential polymers. By varying the number of fluorines (including 0, 1, 2, and 4), the electronic and optical properties of the monomers and subsequent polymers have been investigated. In addition to synthesis of the monomers and polymers, electroanalytical techniques have been used to elucidate the monomer oxidation/polymerization and polymer electrochemical reduction/oxidation (redox) properties. Spectroscopic techniques have been utilized to determine the band gap and the electrochromic switching of the resultant polymers.

3.2 Results and Discussion

The fluorinated analogues shown in **Figure 3.1** were synthesized by Negishi-style Pd catalyzed aryl cross-coupling reaction in good yields. The monofluoro derivative, 1,4-bis[2-(3,4-ethylenedioxy)thienyl]-2-fluorobenzene (**BEDOT-B-F$_1$, 3-1**), is reported here to be synthesized in 50% yield, although it is likely that the yield can be increased by optimizing the reaction.

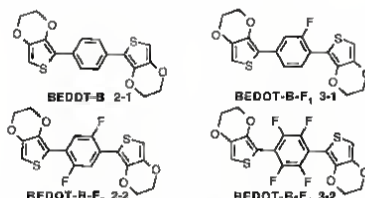

Figure 3.1 Fluorinated Bis(EDOT)Benzenes

The difluoro compound (**BEDOT-B-F$_2$, 2-2**) was synthesized and discussed in Chapter 2. The tetrafluoro analogue, 1,4-bis[2-(3,4-ethylenedioxy)thienyl]-2,3,5,6-tetrafluorobenzene (**BEDOT-B-F$_4$, 3-2**), was synthesized in good yields but isolation and purification was found to be difficult since it is highly soluble in solvents and solvent mixtures typically used in the work-up of a Negishi coupling reaction. To overcome this problem, the reaction mixture was extracted with diethyl ether, and with the addition of pentane, the

product precipitated out of solution. **BEDOT-B-F_4** was also synthesized by a Stille-type aryl cross-coupling in 54% yield. The lower yield was unexpected since electron withdrawing groups generally increase the rate and yields of the Stille reaction.[101] The work-up and isolation of the product from the Stille reaction is more facile, although special care needs to be given when handling highly toxic organotin reagents. **BEDOT-B-F_4** was most easily purified by sublimation.

One obvious omission from the series above is the trifluoro derivative of bis(EDOT)benzene. Several routes were attempted to produce the monomer include direct hydrodefluorination of **BEDOT-B-F_4** (**Figure 3.2**), and the synthesis of the 1,4-dibromo-2,3,5-trifluorobenzene (**Figure 3.3**). In the literature, both $LiAlH_4$[102,103] and Raney Ni[104] have been used to replace fluorine with hydrogen. In a reaction of **BEDOT-B-F_4** with $LiAlH_4$ in refluxing THF (~65 °C), no product was detected by ^{19}F NMR. The same reactants in refluxing diglyme (~160 °C) showed 10% of the trifluoro product after 48h by ^{19}F NMR. **BEDOT-B-F_4** has a single fluorine peak at δ = -140 Hz vs. CCl_3F, while the trifluoro product has three peaks at -139.5, -139.9 and -140.2 Hz. After an additional 48h, the same product ratio remained. All attempts at separation of the two compounds by recrystallization and chromatography failed. None of the fluorines were removed in reactions with Raney Ni in EtOH or dioxane.

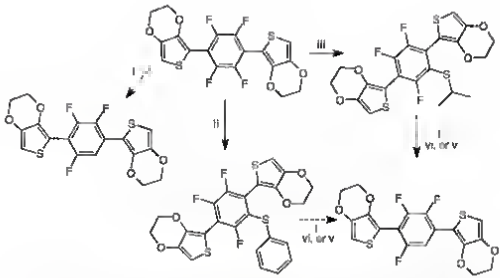

Figure 3.2. Attempted Syntheses of **BEDOT-B-F$_3$** by Hydrodefluorination: i) $LiAlH_4$/diglyme, ii) NaH, thiobenzene, iii) NaH isopropylthiol, vi) Raney Ni/EtOH, v) $NiBr_2/LiAlH_4$

With the failure of the Raney Ni reactions and separation of the products from $LiAlH_4$ reactions, a stepwise defluorination was designed. First, **BEDOT-B-F$_4$** was reacted with a thiol *via* nucleophilic aromatic substitution to produce the thioether, which was purified to eliminate any contamination of the tetrafluoro starting material. Both the phenylthioether and isopropylthioether analogues were synthesized in greater than 90 % yield as outlined in **Figure 3.2**. Attempts to remove the thioether with Raney Ni/EtOH, Raney Ni/dioxane, Raney Ni/THF, and Raney Ni/THF/EtOH were unsuccessful. In the literature,[105] $NiBr_2/LiAlH_4$ has been used on a variety of substrates to cleave the C-S bond, including hindered diarylsulfides. Use of $NiBr_2/LiAlH_4$ did desulfurize the product, but unfortunately both of the

thiophene rings were desulfurized and the diphenylsulfide was left intact as identified by ^{1}H NMR.

Due to the aforementioned problems with hydrodefluorination, the fluorination of 1,4-dibromo-2,5-difluorobenzene was attempted (**Figure 3.3**)

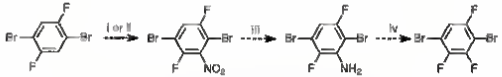

Figure 3.3 Attempted Synthesis of 1,4-Dibromo-2,3,5-trifluorobenzene
i) HNO_3 (97%)/H_2SO_4 (97%), ii) NO_2BF_4/sulfolane,
iii) $SnCl_4$/EtOH, iv) (a) $NaNO_2/H^+$ (b) $NaBF_4$/NaF

via a diazonium salt. 1,4-Dibromo-2,5-difluorobenzene was first nitrated using fuming nitric and sulfuric acid at 30 °C. This reaction only produced a small amount (<10% by ^{1}H NMR) of the 1,4-dibromo-3,5-difluoro-2-nitrobenzene. All attempts to increase the yield of the nitration by heating produced complex product mixtures (by GC) including the dinitro analogue (identified by ^{1}H NMR) which may be explosive. In deactivated rings, NO_2BF_4 in tetramethylene sulfone (sulfolane) can used in Friedel-Crafts type reaction to produce a nitrated ring.[106] The NO_2BF_4 in sulfolane produced a small amount (~20%) of 1,4-dibromo-3,5-fluoro-2-nitrobenzene (determined by ^{1}H NMR). Even with multiple distillations and extractions, the product was contaminated with sulfolane. Since pure intermediate could not be isolated, work on this route was discontinued.

To determine if the addition of fluorines to BEDOT-B in **BEDOT-B-F_4** would dramatically increase the benzene-EDOT torsion angle, the structure was determined by single crystal X-ray crystallography **Figure 3.4** shows a perspective view and atom labeling of **BEDOT-B-F_4**. The plane of the

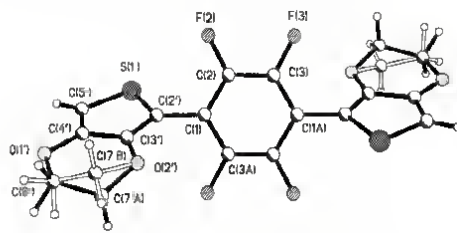

Figure 3 4 Perspective View and Atom Labeling of the X-ray Structure of **BEDOT-B-F_4**

thiophene ring of the EDOT group is twisted out of the plane of the attached benzene ring at an angle of 56 1°. In **BEDOT-B-F_4**, the torsion angle is 3 4°, with the thienyl sulfur pulled toward the fluorine, and the interior EDOT oxygen (O(2')) interacts with hydrogen, its nearest neighbor In **BEDOT-B-F_6** the interior EDOT oxygen (O(2')) has fluorine as a nearest neighbor, therefore the increased torsion angle is due to repulsion of the additional fluorines with the oxygens of the **EDOT**'s. If we examine the effective van der Waals radii of fluorine (1 50 Å), and hydrogen (1 20 Å), the fluorine is 0 3 Å larger

than hydrogen.[107] While there is only a small steric increase, there is also a change in electrostatic interactions in the molecule. In the case of **BEDOT-B-F_2**, the EDOT oxygen (O(2')), empirically possessing a partial negative charge, is interacting with a hydrogen with no effective charge. In contrast, the **BEDOT-B-F_4** EDOT oxygen (O(2')) is interacting with a fluorine (F(3')), empirically possessing a partial negative charge. The two electrostatically repel each other and force the rings out of the same plane. This in itself is not detrimental to the goal of high gap, low oxidation potential polymers. As the central ring is twisted out of plane, the π-overlap with the rest of the chain is diminished. This, in effect, reduces the conjugation length of the polymer and one would expect the inter-band transition to be driven to higher energy. As long as the barrier to planarity is low (as discussed in Chapter 2) the oxidation potential should not be increased out of the useful range (maximum potential of ~ 1V vs. Ag/Ag^+).

From the x-ray structures, we find that the **BEDOT-B-F_2** is planar while **BEDOT-B-F_4** is not planar in the solid state. In this case, we may have a unique probe to determine the conformation of these structures in solution, ^1H NMR. Examination of the ^1H NMR splitting of ethane bridge of EDOT, reveals an interesting correlation with the X-ray structures. **BEDOT-B-F_2** is planar due to the electrostatic interaction between the electropositive sulfur of EDOT and the electronegative fluorine. If we examine the ^1H NMR spectrum for the EDOT bridge (**Figure 3.5 (a)**), we see that there is a complex

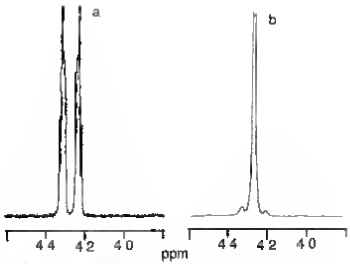

Figure 3.5 ^{1}H NMR Spectra of the EDOT Bridges of **BEDOT-B-F$_2$** (a) and **BEDOT-B-F$_4$** (b)

A,A',B B' spitting, with a peak to peak splitting of 0 084 ppm. In **BEDOT-B-F$_4$**, the EDOT bridge appears to be a singlet, but upon closer inspection there is a peak to peak splitting of 0 007 ppm. The larger peak to peak splitting of **BEDOT-B-F$_2$** is due to the interaction of one of the EDOT oxygens with the hydrogen attached to benzene, thus changing the shift of the adjacent methylene. In EDOT, the ethane bridge is observed as a singlet due to symmetry. In **BEDOT-B-F$_4$**, the EDOT is forced out of plane due to the electrostatic repulsion of the electronegative EDOT oxygen and pendant fluorine. With the EDOT forced out of plane, there is less interaction with the oxygen closest to the phenyl ring and therefore a decrease in the peak to peak separation. This difference in peak to peak separations of the EDOT bridge (in $CDCl_3$) suggests that the compounds have similar configurations in

the solid state as in solution. This peak to peak separation is discussed in more detail in Chapter 4 as it relates to steric interactions of other substituted bis(EDOT)benzenes

The monomers were polymerized by electrochemical oxidation/deposition methods and the redox properties of the resultant polymers were subsequently examined. The results of the electrochemical and spectroscopic analyses are found in **Table 3.1** with the values for the nonfluorinated analogue (**BEDOT-B**) for comparison.[12] The monomers were electrochemically polymerized using repeated scan polymerization with a standard three-electrode cell.

Table 3.1 Electrochemical Results of Fluorinated Monomers

Monomer	$E_{p,m}$	$E_{o,p}$	$E_{p,p}$	$E_{1/2}$	E_g
BEDOT-B[12]	0.61	-	-	0.23	1.8
BEDOT-B-F$_1$	0.69	-0.25	0.28	-0.06	1.9
BEDOT-B-F$_2$	0.91	0.51/-0.09	0.68/0.00	0.61/-0.03	1.9
BEDOT-B-F$_4$	0.61	-0.10	-0.68	-0.45	1.5

A more detailed description of the techniques used is found in Chapter 2.2. **Figure 3.6** shows the repeated potential scan polymerization for **BEDOT-B-F$_1$**. The onset for monomer oxidation ($E_{onset,m}$) is found at 0.61 V with a peak monomer oxidation potential ($E_{p,m}$) at 0.69 V

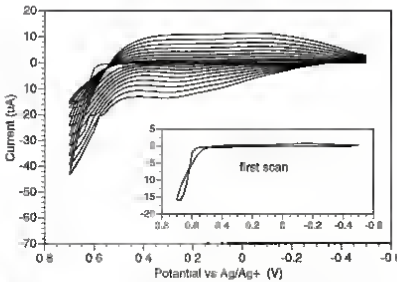

Figure 3 6 Repeated Potential Scan Electrochemical Polymerization of (10 mM) **BEDOT-B-F_1** (on a Pt Button in 0 1 M TBAP/CH_3CN at a Scan Rate of 100 mV/s)

On the reverse scan, the polymer exhibits a broad reduction from 0 55 V, with the fully reduced polymer formed around -0 4 V. In the second and subsequent anodic scans, the first feature is polymer oxidization, ca -0.2 V as indicated by the increased current response, then more monomer is oxidized/deposited on the electrode as polymer

Figure 3.7 shows the cyclic voltammetry of poly(**BEDOT-B-F_1**) in monomer-free electrolyte solution (0 1 M TBAP/CH_3CN) as the scan rate is increased from 100 to 1000mV/s in order to determine if the polymer is wall-adhered to the electrode surface Note that In **Figure 3.7**, the anodic and cathodic polymer redox processes increase linearly with increasing scan rate, this is indicative of a wall adhered polymer film The redox processes for

poly(**BEDOT-B-F$_1$**) include an oxidation peak at 0.28 V and a reduction peak at -0 25 V, thus giving a polymer redox half potential ($E_{1/2}$) of 0 V With an $E_{1/2}$ in this range, the polymer should be stable in the oxidized and reduced forms,

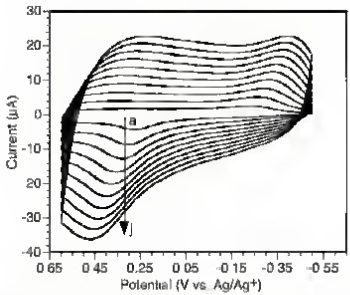

Figure 3 7 Cyclic Voltammetric Scan Rate Dependence of Poly(**BEDOT-B-F$_1$**) (on a Pt Button in 0 1 M TBAP/CH_3CN at Scan Rates of (a) 100 (b) 200 (c) 300 (d) 400 (e) 500 (f) 600 (g) 700 (h) 800 (i) 900 (j) 1000 mV/s)

leading to long term stability in a device It is important to note that the scan rates used in the above experiment are fast compared with the usual rates of 10 to 300 mV/s. The slower scan rates show no shift in redox potentials and as the rates become large, there is only a minimal shift in redox features suggesting a fast influx of charge compensating ions. The relevance of this

becomes evident if the polymers are to be used in electrochromic devices The rate of the redox processes is directly related to the switching speed

Figure 3.8 shows the repeated potential scan electrochemical polymerization of **BEDOT-B-F_4** The $E_{onset,ox}$ is ~0 4 V with a peak at 0 61 V Upon examination of the $E_{p,ox}$ of the related monomers, we find that **BEDOT-B-F_3** is only slightly higher than **BEDOT-B** and with the addition of one more fluorine as in **BEDOT-B-F_2**, the $E_{p,ox}$ increases to 0 91 V In the case of **BEDOT-B-F_4** we find that the $E_{p,ox}$ is the same as **BEDOT-B** (0 61V)

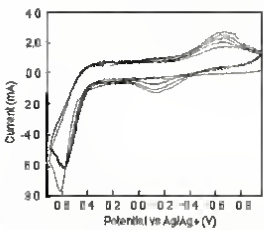

Figure 3.8 Repeated Potential Scan Electrochemical Polymerization of (10 mM) **BEDOT-B-F_4** (on a Pt Button in 0 1 M $TBAP/CH_2Cl_2$ at a Scan Rate of 100 mV/s)

Figure 3 9 shows the cyclic voltammetry of poly(**BEDOT-B-F_4**) at various scan rates. The redox processes for poly(**BEDOT-B-F_4**) include an oxidation peak at -0 10 V and a reduction peak at -0 68 V, thus giving a polymer redox half potential ($E_{1/2}$) of 0 V -0 45 V which is the lowest of the series

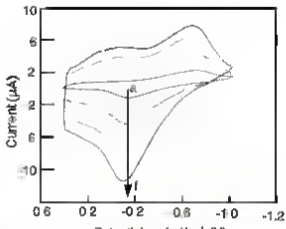

Figure 3 9 Cyclic Voltammetric Scan Rate Dependence of Poly(**BEDOT-B-F_4**) (on a Pt Button in 0 1 M TBAP/CH_2Cl_2 at Scan Rates of (a) 50 (b) 100 (c) 150 (d) 200 (e) 250 (f) 300 mV/s)

One way to explain the apparent discrepancy of the low oxidation potential of **BEDOT-B-F_4** is to examine the nature of electron withdrawing by fluorine The σ constant derived from the Hammett equation for fluorine is reported as 0 15 in the *para*-position and 0.34 in the *meta*-position The positive value of σ indicates that it is an electron withdrawing group If this value is reduced to its components of resonance and field effects (from the Taft equation), we see that while fluorine is a strong field effect withdrawing group (σ_I = 0 50, where NO_2 has a value of 0 65) it also has moderate resonance donation (σ_R = -0.31, where -OMe has a value of -0 42).[106] With each additional fluorine, the field effect is diminished due to a finite electron density of the σ-bonds on the benzene ring, while the resonance donation is additive and increases electron density in the delocalized π bonds The net result is an overall increase in the electron density of the π-cloud, which is

the determining factor in the oxidation potential of conjugated monomers and band gap of conjugated polymers

The polymer band gaps were determined by spectroscopy of thin polymer films electrochemically deposited onto ITO glass slides As shown in **Figure 3 10**, **BEDOT-B** has a narrow π–π^* peak that when extrapolated to

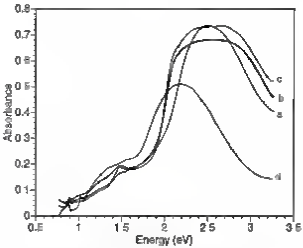

Figure 3 10 UV-Vis Spectra of Neutral Polymers of **BEDOT-B** (a), **BEDOT-B-F1** (b), **BEDOT-B-F2** (c), and **BEDOT-B-F4** (d)

background absorbance yields a band gap of 1 8 eV Poly(**BEDOT-B-F$_1$**) and poly(**BEDOT-B-F$_2$**) show very similar behavior and both have a band gap of 1 9 eV **BEDOT-B-F$_4$** shows a marked shift in both the λ_{max} and onset, to yield a band gap of 1.5 eV The visible color changes are the same for poly(**BEDOT-B**), poly(**BEDOT-B-F$_1$**), and poly(**BEDOT-B-F$_2$**), they all switch between red in the neutral state and blue/black in the doped state as expected for polymers with band gaps of ~2 eV On the other hand, **BEDOT-B-F$_4$** switches from blue

to very transmissive blue in the doped state, as found with poly(EDOT) which also exhibits a lower gap A spectroelectrochemical analysis was performed on poly(**BEDOT-B-F_4**) to determine the energy of the bipolarons. A set of spectra for poly(**BEDOT-B-F_4**) equilibrated at potentials between 0 0 and 1 2 V are shown in **Figure 3-11** The onset of the π–π^* band of electrochemically neutral polymer (a) can be extrapolated to the background absorbance to yield a band gap of 1.5 eV as stated previously As the polymer is electrochemically oxidized, the π–π^* band decreases in intensity and a lower energy band develops The bipolaron 2 band is visible in the figure, but the bipolaron 1 band is red shifted into the infrared The deposited film of poly(**BEDOT-B-F_4**) was found to have fully reversible electrochemical doping from -1 0 to 1 4 V vs Ag/Ag^+ by spectroscopy

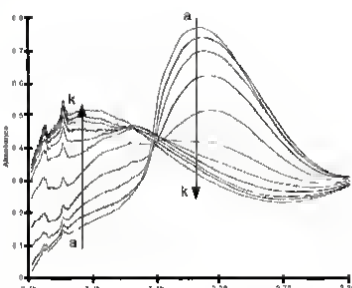

Figure 3 11 Spectroelectrochemical Analysis of Poly(**BEDOT-B-F_4**) (on a ITO in 0 1 M TBAP/CH_3CN at (a) -1 0 (b) -0 3 (c) -0 2 (d) -0 1 (e) 0 0 (f) 0 1 (g) 0 2 (h) 0 3 (I) 0 4 (j) 0 5 (k) 1 0 V)

3.3 Conclusions

A total of three fluorine containing monomers have synthesized and analyzed. By electrochemical analysis, monomers with one or two fluorines in direct conjugation with the polymer backbone had increased monomer and polymer oxidation potentials by as much as 300 mV. The band gap of both **BEDOT-B-F$_1$** and **BEDOT-B-F$_2$** also increased but only slightly (0.1 eV). The tetrafluoro analogue was shown to have much lower monomer and polymer oxidation potentials compared to the unsubstituted **BEDOT-B** or the other fluorinated analogues. The band gap of poly(**BEDOT-B-F$_4$**) was decreased by 0.3 eV compared with **BEDOT-B** and by 0.4 eV compared with **BEDOT-B-F$_1$** and **BEDOT-B-F$_2$**, significantly altering the electrochromic properties.

3.4 Synthesis

3.4.1 General Procedures

All chemicals were purchased from Aldrich and used as received unless otherwise stated. *n*-Butyl lithium (2.5 M in hexanes) was purchased from Acros Chemical. Zinc chloride was obtained from Aldrich Chemical and dried before use over P_2O_5 under vacuum for two days. 3,4-Ethylenedioxythiophene (EDOT) was donated by AG Bayer and distilled under vacuum, purged with argon and cooled to -20 °C until used. 1,4-

dibromo-2,3,5,6-tetrafluorobenzene and 1,4-dibromo-2-fluorobenzene which was purchased from Aldrich

Elemental analyses was performed by Robertson Microlit Laboratories, Inc of Madison, New Jersey All HRMS analysis was done at University of Florida All ^1H NMR spectra were obtained on a Varian Gemini-300 NMR spectrometer at 300 MHz NMR with tetramethylsilane or solvent as internal standard All ^{13}C NMR spectra were obtained on a Varian Gemini-300 NMR spectrometer at 75 MHz with tetramethylsilane or solvent as internal standard. All ^{19}F NMR spectra were obtained on a Varian Gemini-300 NMR spectrometer at 282 MHz with CCl_3F as internal standard

Cyclic voltammetry was carried out using an EG&G Princeton Applied Research Model 273 potentiostat/galvanostat employing a platinum button working electrode (0 005 cm^2), a platinum plate counter electrode, and a Ag/Ag^+ reference electrode The monomer concentration was 10 mM in each case, and the electrolyte was 0.1 M TBAP in CH_3CN or CH_2Cl_2. Acetonitrile (CH_3CN) and CH_2Cl_2 were purchased from Fisher Scientific and distilled before use from CaH_2

3.4.2 1,4-Bis[2-(3,4-ethylenedioxy)thienyl] 2 fluorobenzene. (BEDOT-B-F_1, 3-1)

n-Butyl lithium (12.0 mL, 29 9 mmol) was slowly added to a stirred solution of EDOT (4 25 g, 29 9 mmol) in THF (50 mL) at –78 °C under argon. The resulting yellow solution was stirred for an hour, then $ZnCl_2$ (4 07 g, 29 9 mmol) in THF (50 mL) was added by syringe at 0 °C over a 15 min. period.

The mixture was stirred under argon for 1h. A solution of 1,4–dibromo–2-fluorobenzene (2.39 g, 8 8 mmol) and $Pd(PPh_3)_4$ (192 mg, 0.2 mmol) in THF (20 mL) was added to the reaction mixture. The bright yellow solution was stirred at 50 °C under argon for 96h. It was then cooled to ambient temperature and quenched by pouring the mixture into HCl (1M) (200 mL). The THF was removed under vacuum, and the solid was collected by suction filtration and dried under vacuum. The crude solid was crystallized from acetonitrile to yield a tan crystals [mp 173-75 °C, 50%]. Anal. calcd for $C_{18}H_{12}F_2O_4S_2$: C, 57 44, H, 3 48, F, 5 05, O, 17 00; S, 17 03. Found: C, 57.30, H, 3.32, F, 5.37, S, 17.03. ^1H NMR ($CDCl_3$, TMS) δ 4 23-4.32 (m, 8H), 6 31 (s, 1H), 6.40 (s, 1H) 7 42-7 45 (dd, J_{H-F}= 8.5 Hz and J_{H-H}=1 7 Hz, 1H), 7.52-7.57 (dd, J_{H-F}= 13.5 Hz and J_{H-H}=1 7 Hz, 1H), 7 79-7 85 (t, J_{H-F}= 8 5 Hz, 1H). ^{19}F NMR ($CDCl_3$, CCl_3F) δ (-114)(s). HRMS: calcd for $C_{18}H_{12}F_2O_4S_2$: 376.0239, found: 376 0234.

3.4.3 1,4–Bis[2–(3,4–ethylenedioxy)thienyl]–2,3,5,6–tetrafluorobenzene (BEDOT–B–F_4, 3-2)

The synthesis was carried out as in 2.4 2 (**BEDOT-B-F_2, 2-2**) with the following *n*-butyl lithium (14.1 mL, 35 2 mmol), EDOT (5 0 mL, 35.2 mmol), $ZnCl_2$ (4 79 g, 35 2 mmol), 1,4–dibromo–2,3,5,5–tetrafluorobenzene (3 61 g, 11 7 mmol), and $Pd(PPh_3)_4$ (0.10 g). After four days, aqueous HCl (1M, 150 mL) was added to the reaction mixture, and the organic solvents were removed under reduced pressure. Diethyl ether (200 mL) was added to the dark mixture and was filtered. The organic layer was separated and combined with pentane (400 mL). The crude solid was crystallized from ether/pentane to yield a white

solid [mp 211-13 °C, 79%]. Anal. calcd for $C_{18}H_{10}F_4O_4S_2$: C, 50.23; H, 2.34; F, 17.66; O, 14.87; S, 14.90. Found: C, 50.05; H, 2.30; F, 18.12; S, 14.75. ^1H NMR ($CDCl_3$, TMS) δ 4.27-4.38 (m, 8H), 6.41 (s, 2H). ^{13}C NMR ($CDCl_3$, TMS) δ 65.4, 65.8, 98.0, 98.0, 100.0, 110.5, 138.0, 142.3. ^{19}F NMR ($CDCl_3$, CCl_3F) δ (-140.0)(s). HRMS: calcd for $C_{18}H_{10}F_4O_4S_2$: 429.9957, found: 429.9937.

3,4,4',1,4-Bis[2-(3,4-ethylenedioxy)thienyll-2,3,5,6-tetrafluorobenzene (BEDOT-B-F_4, 3-2)

Compound **BEDOT-B-F_4** was also synthesized by a Stille coupling as follows. In a round bottom flask equipped with a reflux column, a magnetic stir bar, and a gas adapter, 1,4-dibromo-2,3,5,6-tetrafluorobenzene (5.00 g, 16.2 mmol), (3,4-ethylenedioxy)thiophene-2-(tri-*n*-butyl)tin (15.4 g, 35.7 mmol), bis(triphenyl phosphine)-palladium (II) chloride (200 mg), and toluene (200 mL) were combine under an argon atmosphere and was heated at 100 °C for 18h. The toluene was removed by distillation at reduced pressure. The remaining oil was dissolved in acetone and precipitated in water. The solid was rinsed with hexane and was sublimed at 225 °C @ 1 torr to yield a white solid [mp 212-213 °C, 54 %]. ^1H NMR ($CDCl_3$, TMS) δ 4.27-4.38 (m, 8H), 6.41 (s, 2H).

3.5 X-ray Crystal Structure

The crystal data, data collection and refinement parameters for the structures are listed below. Data were collected with a Siemens SMART CCD

area detector, using graphite monochromatized Mo Kα radiation (λ = 0·71073 Å) Intensities were also corrected for Lorentz and polarization effects and for absorption The structures were solved by direct methods using SHELXS, and refined on F^2, using all data, by full-matrix least-squares procedures with SHELXL-96. Hydrogen atoms were included in calculated positions with isotropic displacement parameters 1.3 times the isotropic equivalent of their carrier carbons In all cases final difference Fourier syntheses showed no unusual features Tables of final atom coordinates and bonding geometry are given Appendices A and B

Crystal data for **BEDOT-B-F_4** at -120°C $C_{18}H_{10}F_4O_4S_2$, Mr = 430 4, colorless block, 0 58 x 0 52 x 0 23 mm triclinic, space group P-1, a = 6 4041(3), *b* = 7 8965(4), *c* = 9 5785(5) Å, α = 105 744(2), β = 93 430(2), γ = 110 299(2)°, V = 430 85(4) $Å^3$, F(000) = 218, Z = 1, D_C = 1.659 g cm^{-3}, μ(Mo-Kα) = 3 74 cm^{-1}, $2\theta_{max}$ = 53°, 137 parameters, GooF = 1 07, wR2 = 0 1649 for all 1657 data, (a = 0 0812, b = 0 13), R1 = 0.0588 for 1304 data with $F_O > 4\sigma(F_O)$

CHAPTER 4
SULFUR TO OXYGEN INTERACTIONS IN
1,4-BIS[2-(3,4-ETHYLENEDIOXY)THIENYL]BENZENES

4.1 Motivation

In order for a conjugated polymer to stabilize charge carriers, the backbone must easily attain a planar conformation across a number of double bonds. Previously, Marynick and Reynolds[66] calculated the optimized geometry for a series of bis(2-thienyl)benzenes at the PRDDO level and found that the unsubstituted analog had a calculated torsion angle of 24.3°, while the 2,5-dimethoxy substituted compound had a calculated angle of 40°. Additional MNDO calculations determined the barriers to planarity for both molecules to be 3-4 kcal/mol.

BEDOT-B has an EDOT to phenyl ring torsion angle of 27.5° as determined by x-ray crystal structure.[12] In analogy to the calculations carried out on the 2-thienyl derivative, we expected that, with 2,5 disubstitution on the benzene ring by the more sterically demanding alkoxy group, the torsion angle would be increased. As described in the previous chapter, the attraction between the electronegative fluorines on the central ring and the electropositive sulfur of EDOT reduced the torsion angle of the monomer in some instances to a planar structure. This led to the study of series of alkoxy

substituted BEDOT-B's to determine if a similar interaction is present between the electronegative oxygens of the alkoxy groups and the electropositive sulfur of the EDOT

4.2 Results and Discussion

The synthesis of the dibromodisubstituted benzenes required for the production of the monomers is detailed in Section 4-4. In general, most were made by simple etherification reactions with the exception of the diacyloxy compound which was synthesized by the reaction of dibromohydroquinone with acetic anhydride. All of these intermediates were fully characterized. The monomers, shown in **Figure 4.1**, were synthesized in good yields.

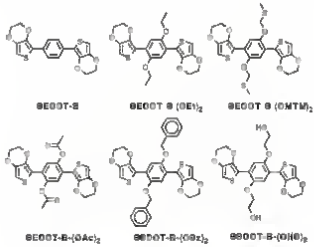

Figure 4.1: Dialkoxy BEDOT-B Monomers

1,4-Bis[2-(3,4-ethylenedioxy)thienyl] 2,5 diethoxybenzene (**BEDOT-B-(OEt)$_2$**) and 1,4-bis[2-(3,4-ethylenedioxy)thienyl] 2,5 di(methylthiomethoxy)benzene (**BEDOT-B-(OMTM)$_2$**) were synthesized by Negishi coupling in 87% and 96% yields, respectively 1,4-Bis[2-(3,4-ethylenedioxy)thienyl]-2,5-diacyloxybenzene (**BEDOT-B-(OAc)$_2$**) and 1,4-bis[2 (3 4-ethylenedioxy)thienyl]-2,5-dibenzyloxybenzene (**BEDOT-B-(OBz)$_2$**) were synthesized by Stille coupling in 68% and 72% yields respectively Note that these monomers could not be made in a Negishi coupling. In the case of **BEDOT-B-(OAc)$_2$**, the carbonyl of the acyloxy group reacts with the organozinc intermediates of the Negishi reaction In the Negishi reaction, an excess of butyl lithium is typically used to deprotonate EDOT and then the organolithium adduct is transmetalated to form the organozinc compound **BEDOT-B-(OBz)$_2$** could not be formed by this route since the excess butyl lithium deprotonates the benzylic sites and leads to side reactions 1,4-Bis[2-(3 4-ethylenedioxy)thienyl] 2,5-di(2-hydroxyethoxy) benzene (**BEDOT-B-(OHE)$_2$**) was not made directly, but the alcohol was protected as a tetrahydropyran (THP) group prior to the coupling step The Negishi coupling reaction to form 1,4-bis[2-(3,4-ethylenedioxy)thienyl]-2,5-di(ethoxy 2-tetrahydropyranylether) benzene (**BEDOT-B-(OHE-THP)$_2$**) proceeded in a 65% yield and the compound was deprotected in 76% yield using AmberLite® ion exchange resin in methanol

To determine the EDOT to phenyl torsion angle for the compounds shown above, the solid state structures were determined by single crystal x-ray crystallography and the results are shown in **Table 4.1**

Table 4.1: *Calculated* Charge Difference of S and O and **X-ray Results**

BEDOT-B Sidechain	*Hückel Charge O*	*Hückel Charge S*	*Δ Hückel Charges*	**Torsion Angle**	**S to O Distance**
H	*0.118**	*1.174*	*1.056**	**27.5**	**N.A.**
w/ THF	*N.A.*	*N.A.*	*N.A.*	**5.5**	**2.654**
w/o THF	*-0.231*	*1.239*	*1.470*	**6.0**	**2.638**
	-0.225	*1.249*	*1.474*	**4.3**	**2.696**
	-0.039	*1.121*	*1.099*	**31.4**	**2.902**
	-0.240	*1.251*	*1.491*	**52.1**	**3.114**
	-0.243	*1.239*	*1.482*	**11.1**	**2.678**

* calculated charge of hydrogen

HyperChem[36] was used to calculate the Hückel charges residing on the sulfur of the EDOT and oxygen of the pendant group in the **BEDOT-B**'s in this chapter. The ground state structures were calculated at the AM1 level and then the thiophene and benzene rings were restricted to a planar geometry across all three rings. The Hückel charges were calculated for all atoms but only the EDOT sulfur and pendant group oxygen are reported. As seen in **Table 4.1**, sulfur is always more electropositive than oxygen leading to an

electrostatic interaction. The extent of this interaction will be controlled by the charge difference.

Figure 4.2 shows a perspective view and atom labeling of **BEDOT-B-(OEt)$_2$**. The plane of the thiophene ring of the EDOT group is nearly planar with the central benzene ring at an angle of 6.0°. The small torsion angle can be explained by an electrostatic attraction of the electropositive sulfur (S) and the electronegative oxygen on the ring (O3). The difference in calculated

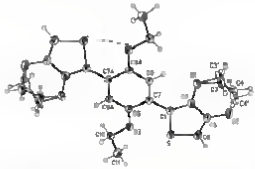

Figure 4.2. Perspective View and Atom Labeling of the X-ray structure of **BEDOT-B-(OEt)$_2$**

charge of (S) and (O3) in **BEDOT-B-(OEt)$_2$** was found to be 1.47. In addition to the charges and torsion angles, it is also important determine what, if any, interactions there are by examining the distance between the sulfur and the oxygen. The van der Waals radii for sulfur is 1.80 Å and for oxygen is 1.50 Å, therefore the van der Waals distance is 3.3 Å [108]. In **BEDOT-B-(OEt)$_2$**, the crystal structure shows a shorter sulfur to oxygen distance of 2.64 Å as illustrated by the dotted line in **Figure 4.2**.

Figure 4.3 shows a perspective view and atom labeling of the x-ray structure of **BEDOT-B-(OEt)$_2$** with tetrahydrofuran (THF) trapped in the crystal

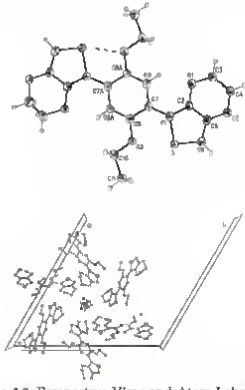

Figure 4.3 Perspective View and Atom Labeling of the X-ray structure and Crystal Packing of **BEDOT-B-(OEt)$_2$•THF Solvate**

lattice, making it **BEDOT-B-(OEt)$_2$•THF Solvate**. For each THF in the crystal there are three **BEDOT-B-(OEt)$_2$** molecules. This solvate crystal has a highly unusual space group of R-3 [109] where the THF molecules form a three-fold axis and the center of inversion. The torsion angle is 5.5° and the S-O distance is 2.65 Å and both values are comparable to the unsolvated crystal structure. Thus shows that the crystal packing has little effect on the torsion angles in S-O distance in **BEDOT-B-(OEt)$_2$**.

Figure 4.4 shows a perspective view and atom labeling of the x-ray structure of **BEDOT-B-(OHE)$_2$**. The torsion angle is 11.1° and the S-O distance is 2.68 Å. The difference in calculated charge of (S) and (O3) in

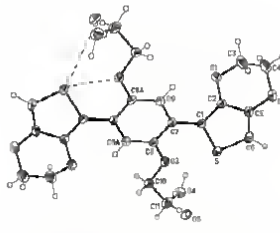

Figure 4.4. Perspective View and Atom Labeling of the X-ray Structure of **BEDOT-B-(OHE)$_2$**

BEDOT-B-(OHE)$_2$ was found to be 1.48, the same as **BEOOT-B-(OEt)$_2$**, but the torsion angle is ~5° higher. Close inspection of the crystal structure explains the increased torsion angle while having the same electrostatic potential. The alcohol functionality, shown as O4 and O5 due to equal population in two positions throughout the crystal, are bent back toward the thienyl S at a distance of 3.54 and 3.73 Å, respectively. This through-space interaction decreases the electrostatic attraction between S and O3, thus slightly increasing the torsion angle.

Figure 4.5 shows a perspective view and atom labeling of the x-ray structure of **BEDOT-B-(OMTM)$_1$**. The torsion angle is 4.3° and the S-O distance is 2.70 Å. The difference in the calculated charge between the thienyl (S) and -OMTM (O3) in **BEDOT-B-(OMTM)$_2$** was found to be 1.47. The values are essentially the same as **BEDOT-B (OEt)$_2$** and suggests that the electrostatic interaction in the two molecules are identical and the sulfur of the MTM group does not affect the monomers torsion angle or length of conjugation

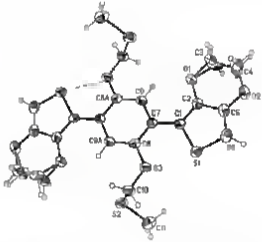

Figure 4.5 Perspective View and Atom Labeling of the X-ray structure of **BEDOT-B-(OMTM)$_2$**

Figure 4.6 shows a perspective view and atom labeling of the x-ray structure of **BEDOT-B-(OBz)$_2$**, the largest molecule of the series. The torsion angle is found to be a high 52.1° and the S-O distance is a long 3.11Å compared with the previous monomers. Note that the S-O distance is still within the van der Waals distance of 3.3Å. The difference in calculated charge of (S) and (O3) in **BEDOT-B-(OBz)$_2$** was found to be 1.49 which is essentially the same as

the previous monomers. The large torsion angle can be attributed to a lattice effects only found in **BEDOT-B-(OBz)$_2$**. In this structure, the long axis (shown as a solid line) of the molecule is along the benzyloxy groups. This causes the benzylic hydrogens the interact with the π-clouds of benzyl groups of adjacent molecules (**Figure 4.7**). In addition, the thienyl rings of EDOT form stacks. These two lattice effects are responsible for forcing the EDOT's out of plane

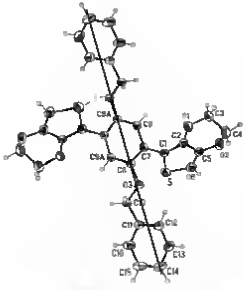

Figure 4.6 Perspective View and Atom Labeling of the X-ray structure of **BEDOT-B-(OBz)$_2$**

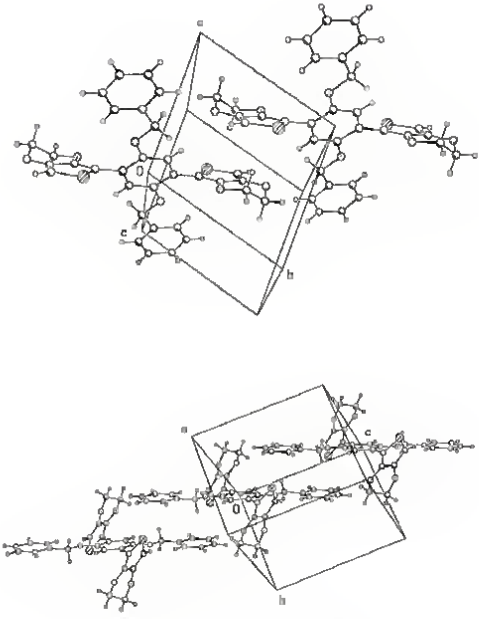

Figure 4.7 Crystal Packing Structures of **BEDOT-B-(OBz)$_2$**

Figure 4.8 shows a perspective view and atom labeling of the x-ray structure of **BEDOT-B-(OAc)$_2$**. The torsion angle is 34.1° and the S-O distance is 2.90 Å, somewhat longer than the previous monomers. The difference in calculated charge of the thienyl (S) and acyloxy (O3) in **BEDOT-B-(OAc)$_2$** was found to be a low 1.10. The S-O distance is at the borderline of the van der Waals radii and the difference in charge is the same as **BEDOT-B**. This result led to the conclusion that there is little or no electrostatic interaction between the S and O3 and that this is the cause of the increased torsion angle. Note that the carbonyl oxygen (O4) is above or below the plane of the central benzene and is 4.07 Å away from S.

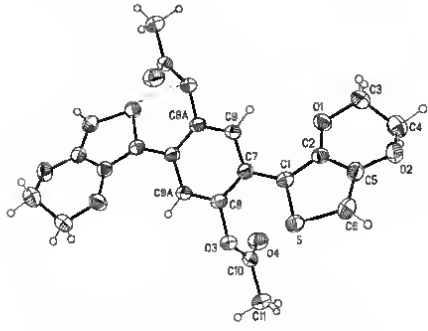

Figure 4.8 Perspective View and Atom Labeling of the X ray structure of **BEDOT-B-(OAc)$_2$**

A compilation of the x-ray results in conjunction with the calculated charges was shown in **Table 4.1**. **BEDOT-B** and **BEDOT-B-(OAc)$_2$** have a calculated charge difference of ~1.0 and they also have torsion angles of greater than 25°. **BEDOT-B-(OEt)$_2$**, **BEDOT-B-(OHE)$_2$**,and **BEDOT-B-(OMTM)$_2$** have a calculated charge difference of ~1.5 and they have torsion angles of less than 15°. The exception to this trend is **BEDOT-B-(OBz)$_2$** with a calculated charge difference of ~1.5 and a torsion angle of greater than 50°. This is likely due to intermolecular interactions in the solid state. This study shows that the torsion angle of the monomer can be predicted in many cases by computational chemistry. This can be helpful in determining if a prospective molecule has a large torsion angle or high barrier to planarity which could increase the monomer and subsequent polymer oxidation potentials. We can also use the attractive electrostatic interaction between S-O to increase the extent of conjugation in BEDOT-B's which would lower the redox properties. It might also be possible to use this attractive electrostatic interaction to decrease switching times and increase lifetime of a device since the polymer is already in a planar conformation. little or no molecular motion of the polymer is necessary to form planar bipolarons.

As introduced in Chapter 3.2, ^{1}H NMR and provide a useful probe to determine the conformation of these structures in solution. Examination of the splitting in the ethane bridge of EDOT correlates with the x-ray analyses. **BEDOT-B-F$_2$** is planar due to the electrostatic interaction between the electropositive sulfur of EDOT and the electronegative fluorine. Examination

the ^{1}H NMR spectrum for the EDOT bridge (**Figure 3 5**) shows complex A,A' B,B' splitting, with a peak to peak splitting of 0 084 ppm. The solution ^{1}H NMR of the EDOT bridge portion of the spectra of EDOT, **BEDOT-B**, **BEDOT-B-(OAc)$_2$**, and **BEDOT-B-(OBz)$_2$** in $CDCl_3$ are shown in **Figure 4.9**. In **BEDOT-B**, there is a 0 093 ppm splitting and an x-ray determined torsion angle of 27.5°.[12] The torsion angle of **BEDOT-B** determined by x-ray is not a good indication of the solution state of the molecule since there are not any electrostatic intramolecular attractions as found in **BEDOT-B-F$_2$**. **BEDOT-B** also exhibits a low barrier to rotation (**Figure 2.12**). EDOT has no splitting

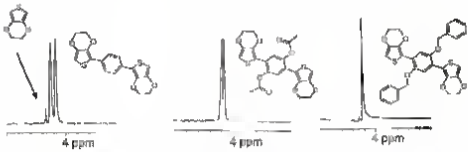

Figure 4 9 ^{1}H NMR of the EDOT bridge of Selected **BEDOT-B** s

since it is symmetrical. **BEDOT-B-(OAc)$_2$** (31 4° torsion angle) has a 0 028 ppm splitting while **BEDOT-B-(OBz)$_2$** (52.1° torsion angle) has a no visible splitting. Graphical examination of the peak to peak splitting versus the x-ray determined torsion angles for all monomers contained within this work shows a good correlation as shown in **Figure 4 10**

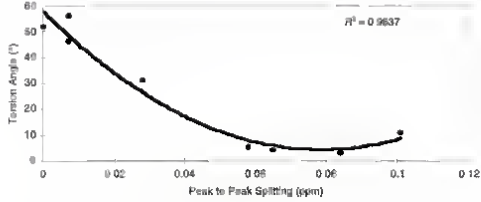

Figure 4.10 Peak to Peak ^{1}H NMR Splitting of the EDOT Bridge vs the X-ray-Determined Torsion Angles

Within experimental error, all of the monomers manifest the same behavior Note that **BEDOT-B-NO$_2$** was excluded since it is not symmetrical and has two set of peaks, one for each EDOT With computational, x-ray, and NMR analysis of the monomers, it is evident that the solid and solution states are similar due in part to the electrostatic attraction of the thienyl sulfur and the oxygen of the alkoxy substituents Likewise the torsion angles of new monomers in this series can be predicted by a combination of computational and NMR analysis

To determine how, and to what extent torsion angle differences affect the redox properties of the monomers and resultant polymers, all monomers were electrochemically polymerized using repeated scan polymerization **Figure 4.11** shows the repeated potential scan polymerization for **BEDOT-B-(OEt)$_2$**. The onset of monomer oxidation ($E_{onset,m}$) begins at 0 4 V with a peak

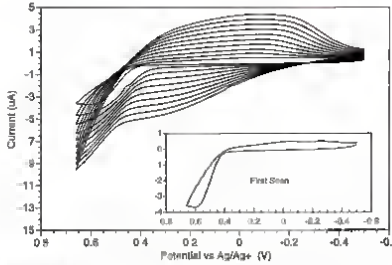

Figure 4.11: Repeated Potential Scan Electrochemical Polymerization of (10 mM) **BEDOT-B-(OEt)$_2$** (on a Pt button in 0.1 M TBAP/CH_3CN at a scan rate of 100 mV/s)

monomer oxidation potential ($E_{p,m}$) at 0.61 V. On the reverse scan, the polymer exhibits a broad reduction from 0.5 V, with the fully reduced polymer formed around -0.4 V. In the second and subsequent anodic scans, the first feature is polymer oxidization, ca. -0.0 V as indicated by the increased current response, then more monomer is oxidized/deposited on the electrode as polymer.

Figure 4.12 shows the cyclic voltammetry of poly(**BEDOT-B-(OEt)$_2$**) in monomer-free electrolyte solution (0.1 M TBAP/CH_3CN) as the scan rate is increased from 100 to 1000mV/s in order to determine if the polymer is well adhered to the electrode surface. It is important to note that the scan rates used in the above experiment are very fast compared with the usual rates of 10 to 300 mV/s. The slower scan rates show no shift in redox potentials and

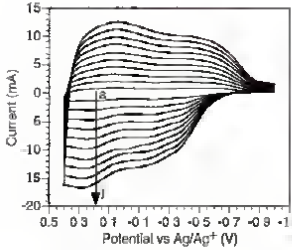

Figure 4.12. Cyclic Voltammetric Scan Rate Dependence of Poly(**BEDOT-B-(OEt)$_2$**) (on a Pt button in 0.1 M $TBAT/CH_3CN$ at a scan rates of (a) 100 (b) 200 (c) 300 (d) 400 (e) 500 (f) 600 (g) 700 (h) 800 (i) 900 (j) 1000 mV/s)

as the rates become large, there is only a minimal shift in redox features suggesting a fast influx of charge compensating ions. The relevance of this becomes evident if the polymers are to be used in electrochromic devices. The rate of redox processes is directly related to the switching speed. These polymers are expected to have switching speeds of <1 s suggested by the scan rate dependence work. The redox processes for poly(**BEDOT-B-(OEt)$_2$**) include two oxidation waves at -0.2 and 0.25 V and two reduction waves at 0.15 and -0.5 V, thus giving polymer redox half potentials ($E_{1/2}$) of -0.35 and 0.20 V at 100 mV/s.

Figure 4.13 shows the repeated potential scan electrochemical polymerization of **BEDOT-B-(OMTM)$_2$**. The $E_{onset,m}$ is –0.45 V with a peak at 0.51 V.

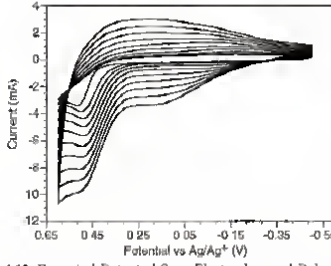

Figure 4.13 Repeated Potential Scan Electrochemical Polymerization of (10 mM) **BEDOT-B-(OMTM)$_2$** (on a Pt button in 0.1 M TBAP/CH_3CN at a scan rate of 100 mV/s)

Figure 4.14 shows the cyclic voltammetry of poly(**BEDOT-B-(OMTM)$_2$**) in monomer-free electrolyte solution (0.1 M TBAP/CH_3CN) as the scan rate is

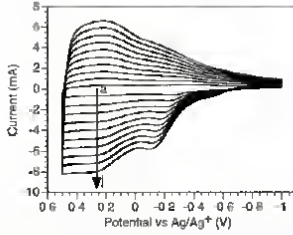

Figure 4.14 Cyclic Voltammetric Scan Rate Dependence of Poly(**BEDOT-B-(OMTM)$_2$**) (on a Pt button in 0.1 M TBAP/CH_3CN at a scan rates of (a) 100 (b) 200 (c) 300 (d) 400 (e) 500 (f) 600 (g) 700 (h) 800 (i) 900 (j) 1000 mV/s)

increased from 100 to 1000mV/s The redox processes for poly(**BEDOT-B-(OMTM)$_2$**) include an oxidation wave at 0 2 and a reduction wave at 0 3 V, thus giving polymer redox half potential ($E_{1/2}$) of 0 25 V at 100 mV/s.

Figure 4.15 shows the repeated potential scan electrochemical polymerization of **BEOOT-B-(OBz)$_2$** The $E_{onset,ox}$ is ~0 4 V with a peak at 0 46 V

Figure 4.16 shows the cyclic voltammetry of poly(**BEDOT-B-(OBz)$_2$**) in monomer-free electrolyte solution (0 1 M TBAP/CH_3CN) as the scan rate is increased from 100 to 1000mV/s The redox processes for poly(**BEOOT-B-(OBz)$_2$**) include an oxidation wave at -0 25 and a reduction wave at -0 45 V, thus giving polymer redox half potential ($E_{1/2}$) of -0 35 V at 100 mV/s

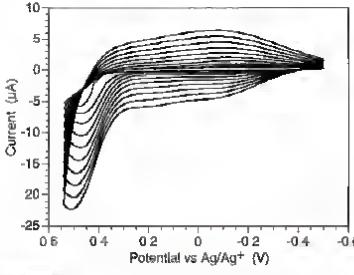

Figure 4.15 Repeated Potential Scan Electrochemical Polymerization of (10 mM) **BEOOT-B-(OBz)$_2$** (on a Pt button in 0.1 M TBAP/CH_3CN at a scan rate of 100 mV/s)

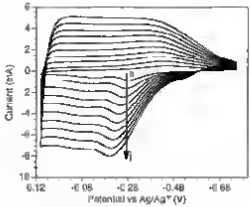

Figure 4.16 Cyclic Voltammetric Scan Rate Dependence of Poly(**BEDOT-B-(OBz)$_2$**) (on a Pt button in 0.1 M TBAP/CH_3CN at a scan rates of (a) 100 (b) 200 (c) 300 (d) 400 (e) 500 (f) 600 (g) 700 (h) 800 (i) 900 (j) 1000 mV/s)

increased from 100 to 1000mV/s. The redox processes for poly(**BEDOT-B-(OBz)$_2$**) include an oxidation wave at -0.25 and a reduction wave at -0.45 V, thus giving polymer redox half potential ($E_{1/2}$) of -0.35 V at 100 mV/s.

Figure 4.17 shows the repeated potential scan electrochemical polymerization of **BEDOT-B-(OHE)$_2$**. The $E_{monomer}$ is ~0.3 V with a peak at 0.45 V

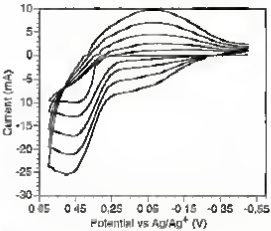

Figure 4.17 Repeated Potential Scan Electrochemical Polymerization of (10 mM) **BEDOT-B-(OHE)$_2$** (on a Pt button in 0.1 M TBAP/CH_3CN at a scan rate of 100 mV/s)

Figure 4.18 shows the cyclic voltammetry of poly(**BEDOT-B-(OHE)$_2$**) in monomer-free electrolyte solution (0.1 M TBAP/CH_3CN) as the scan rate is increased from 200 to 500mV/s. The redox processes for poly(**BEDOT-B-(OHE)$_2$**) include an oxidation wave at 0.25 and a reduction wave at 0.15 V, thus giving polymer redox half potential ($E_{1/2}$) of 0.2 V at 100 mV/s.

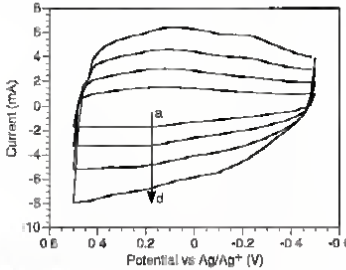

Figure 4.18: Cyclic Voltammetric Scan Rate Dependence of Poly(**BEDOT-B-(OHE)$_2$**) (on a Pt button in 0.1 M TBAP/CH3CN at a scan rates of (a) 200 (b) 300 (c) 400 (d) 500 mV/s)

Figure 4.19 shows the repeated potential scan electrochemical polymerization of **BEDOT-B-(OAc)$_2$**. The E_{onset} is ~0.6 V with a peak at 0.75 V.

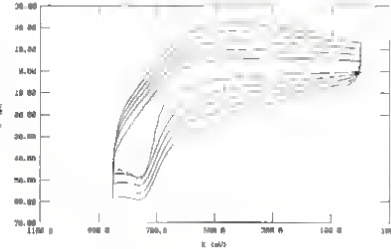

Figure 4.19 Repeated Potential Scan Electrochemical Polymerization of (10 mM) **BEDOT-B-(OAc)$_2$** on a Pt button in 0.1 M TBAP/CH_3CN at a scan rate of 100 mV/s

Figure 4.20 shows the cyclic voltammetry of poly(**BEDOT-B-(OAc)$_2$**) in monomer-free electrolyte solution (0.1 M TBAP/CH_3CN) as the scan rate is

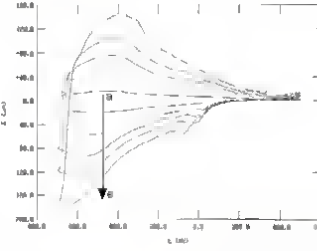

Figure 4.20 Cyclic Voltammetric Scan Rate Dependence of Poly(**BEDOT-B-(OAc)$_2$**) (on a Pt button in 0.1 M TBAP/CH_3CN at a scan rates of (a) 100 (b) 300 (c) 500 (d) 700 (e) 1000 mV/s)

increased from 100 to 1000mV/s The redox processes for poly(**BEDOT-B-(OAc)$_2$**) include an oxidation wave at 0 53 and a reduction wave at 0 46 V, thus giving polymer redox half potential ($E_{1/2}$) of 49 V at 100 mV/s With all of the data presented above summarized on **Table 4.2**, we are able find a few trends First, all the new monomers with the exception of **BEDOT-B-(OAc)$_2$** have approximately the same (within 150 mV) $E_{p,m}$ with an average of 0 5 V

Table 4 2 Electrochemical Results of Dialkoxy Monomers

Monomer	$E_{p,m}$	$E_{c,p}$	$E_{a,p}$	$E_{1/2}$
BEDOT-B[12]	0.61	-	-	0.23
BEDOT-B-(OEt)$_2$	0 59	0.15/-0.50	-0 20/0.25	0.20/-0 35
BEDOT-B-(OMTM)$_2$	0.51	0 20	0.30	0.25
BEDOT-B-(OAc)$_2$	0 75	0 46	0.53	0 49
BEDOT-B-(OBz)$_2$	0 48	-0 45	-0.25	-0 35
BEDOT-B-(OHE)$_2$	0 45	0 15	0.25	0.20

all potentials are determined at 100mV/s

As such, all polymers effectively can be viewed as low oxidation potential polymers. This suggests that the electron density of the monomers are

similar and that **BEDOT-B-(OBz)$_2$** has a low barrier to planarity **BEDOT-B-(OAc)$_2$** has a $E_{p,m}$ ~250 mV higher than exhibited by the other monomers and 140 mV higher than **BEDOT-B** The higher oxidation potential is due to the change in electron density of the central benzene ring The oxygens of the other monomers are electron donors, the oxygen bonded to the phenyl ring in the acyloxy group has less electron density by resonance due to the proximity of the carbonyl, therefore the acetyloxy group is less of an electron donor than the other groups. The broad redox peaks made it difficult to assign $E_{1/2}$ of the polymers As an aside, all of the electropolymerized films were electrochromic, switching from a red neutral state to a blue oxidized state, and there was no noticeable shift in band gap (1.8 eV for all) across the series

4.3 Conclusions

A series of electropolymerizable monomers was synthesized to help elucidate the effect of intramolecular interactions in alkoxy substituted bis(EDOT) benzenes The monomers were analyzed by x-ray diffraction to determine the solid state torsion angle, and by NMR to indicate that the same structure is maintained in solution The monomers were induced to be coplanar due to the electrostatic attraction of the electropositive EDOT sulfur and the electronegative alkoxy oxygen, except where electronic constraints limited the interaction

By electrochemical methods, all of the monomers electro oxidatively polymerized to form electroactive, electrochromic films This also showed that there is little or no steric effect of the alkoxy groups limiting the electropolymerization or electroactive switching of the monomers and resultant polymers

4.4 Synthesis

4.4.1 General Procedures

n-Butyl lithium (2.5 M in hexanes), dimethylsulfoxide (DMSO) and $Pd(PPh_3)_4$ were obtained from Aldrich and used as received. 3,4–Ethylenedioxythiophene (EDOT) was donated by AG Bayer and distilled under vacuum, purged with argon and frozen until used. Anhydrous THF and $ZnCl_2$ in ether were obtained from Aldrich Chemical Tetra–*n*–butyl ammonium perchlorate (TBAP) was synthesized by the addition of perchloric acid to aqueous tetra–*n*–butyl ammonium bromide, the precipitate was collected and was recrystallized from ethanol

All ^1H NMR spectra were obtained on a Varian Gemini 300 NMR spectrometer at 300 MHz with tetramethylsilane or solvent as internal standard All ^{13}C NMR spectra were obtained on a Varian Gemini-300 NMR spectrometer at 75 MHz with tetramethylsilane or solvent as internal standard Elemental analysis was performed by Robertson Microlit

Laboratories, Inc. of Madison, New Jersey. All HRMS analysis was done at the University of Florida.

Cyclic voltammetry was carried out using an EG&G Princeton Applied Research Model 273 potentiostat/galvanostat employing a platinum button working electrode (0.005 cm^2), a platinum plate counter electrode, and a Ag/Ag^+ reference electrode. The monomer concentration was 10 mM in each case, and the electrolyte was 0.1 M TBAP in CH_3CN or CH_2Cl_2. CH_3CN and CH_2Cl_2 were purchased from Fisher Scientific and distilled before use from CaH_2.

4.4.2. 1,4-Dibromo-2,5-diethoxybenzene (4-1)

DMSO (90 mL), 2,5-dibromohydroquinone[111] (10 g, 0.037 mol), potassium hydroxide (3.8 g, 0.095 mol), and iodoethane (12.8 g, 0.082 mol) were combine and stirred at room temperature for 24 h. The reaction mixture was added to water (900 mL) and stirred for 1 h. The supernant was decanted, water (900 mL) was added, and the mixture was stirred for 1 h. The solid was collected by suction filtration. The solid was recrystallized from ethanol/water to yield an off-white solid [mp 138-9 °C, 45%]. Anal. calcd. for $C_{10}H_{12}O_2Br_2$: C, 37.07; H, 3.73; O, 9.88; Br, 49.32. Found: C, 36.77; H, 3.58; Br 49.27. ^1H NMR ($CDCl_3$, TMS) δ 1.39-1.43 (t, 6H), 3.97-4.04 (q, 4H), 7.06 (s, 2H). ^{13}C NMR ($CDCl_3$, TMS) δ 14.7, 65.9, 111.1, 118.6, 149.9. HRMS: calcd. for $C_{10}H_{12}O_2Br_2$: 321.9204, found 321.9209.

4.4.3 1,4-Bis[2-(3,4-ethylenedioxy)thienyl]-2,5-diethoxybenzene (BEDOT-B-(OEt)$_2$, 4-2)

The synthesis was carried out as for **BEDOT-B F$_2$** (2.4.2) with the following: n-butyl lithium (19.8 mL, 0.049 mol), EDOT (7.0 g, 0.049 mol), $ZnCl_2$ (6.73 g, 0.049 mol), **4-1** (4.0 g, 0.017 mol), and $Pd(PPh_3)_4$ (0.100 g). The crude solid was recrystallized from THF at -10 °C to yield tan crystals [mp 211-13 °C, 87%]. Anal. calcd for $C_{22}H_{22}O_6S_2$: C, 59.18; H, 4.97; O, 21.50; S, 14.36. Found: C, 59.02; H, 4.83; S, 14.02. ^{1}H NMR ($CDCl_3$, TMS): δ 1.46-1.51 (t, 6H), 4.07-4.14 (q, 4H), 4.20-4.31 (m, 8H), 6.35 (s, 2H), 7.69 (s, 2H). HRMS: calcd for $C_{22}H_{22}O_6S_4$: 446.0858, found: 446.0933.

4.4.4 1,4-Dibromo-2,5-di(methylthiomethoxy)benzene (4-3)

Hexamethylphosphoramide (HMPA, 200 mL) was used to dissolve 1,4-dibromohydroquinone (33.03 g, 0.123 mol). Sodium hydride (6.21 g, 0.259 mol) was added in small portions at ambient temperature. After stirring for one hour, chloromethyl methyl sulfide (25 g, 0.259 mol) was added in one addition, and the reaction mixture was stirred at ambient temperature. After four hours, the green-brown reaction mixture was precipitated into water and was refrigerated overnight. The solid was collected by suction filtration and dried in a vacuum desiccator for 24 h. The crude solid was recrystallized from 2-propanol to yield tan needles [mp 121-25 °C, 81%]. Anal. calcd for

$C_{12}H_{12}Br_2O_2S_2$: C, 30.95; H, 3.12; Br, 41.17; O, 8.24; S, 16.52. Found: C, 31.18; H, 3.02. ^1H NMR ($CDCl_3$, TMS) δ 2.28 (s, 6H), 5.17 (s, 4H), 7.20 (s, 2H). HRMS calcd for $C_{16}H_{12}Br_2O_2S_2 + H^+$: 386.8724, found: 386.8732.

4,4,5,1,4-Bis[2-(3,4-ethylenedioxy)thienyl]-2,5-di(methylthiomethoxy)benzene ([**BEDOT-B-(OMTM)$_2$**, **4-4**)

The synthesis was carried out as for **BEDOT-B-F$_2$** (2.4.2) with the following: n-butyl lithium (42.4 mL, 0.106 mol), EDOT (15.0 mL, 0.106 mol), $ZnCl_2$ (14.45 g, 0.106 mol), **4-3** (10.29 g, 0.265 mol), and $Pd(PPh_3)_4$ (0.100 g). The crude solid was crystallized from cyclohexane (1 g/1.5 L) to yield a yellow solid [mp 163-65 °C, 96% crude]. Anal. calcd for $C_{28}H_{32}O_6S_6$: C, 51.75; H, 4.34; O, 18.80; S, 25.11. Found: C, 51.96; H, 4.29. ^1H NMR ($CDCl_3$, TMS) δ 2.30 (s, 6H), 4.25-4.34 (m, 8H), 5.17 (s, 4H), 6.40 (s, 2H), 7.77 (s, 2H). HRMS: calcd for $C_{28}H_{32}O_6S_6$: 510.0299, found: 510.0256.

4,4,6,1,4-Dibenzyloxy-2,5-dibromobenzene (**4-5**)

The synthesis was carried out as in **4-3** with the following: DMSO (90 mL), 2,5-dibromoquinone (10 g, 0.037 mol), potassium hydroxide (3.8 g, 0.095 mol), and benzylbromide (14.1 g, 0.082 mol). The solid was recrystallized from ethanol to yield an off-white crystalline powder [mp 162-64 °C, 55%]. Anal. calcd for $C_{20}H_{16}O_2Br_2$: C, 53.60; H, 3.60; O, 7.14; Br, 35.66. Found: C, 53.57; H, 3.46. ^1H NMR ($CDCl_3$, TMS) δ 5.09 (s, 4H), 7.20 (s, 2H), 7.31-7.49 (m, 10H). ^{13}C NMR ($CDCl_3$, TMS) δ 71.9, 111.5, 119.2, 127.2, 128.1, 128.6, 136.1, 150.0. HRMS calcd for $C_{20}H_{16}O_2Br_2$: 445.9517, found: 445.9539.

4,4,7,1,4-Bis[2-(3,4-ethylenedioxylthienyl]-2,5-dibenzyloxybenzene ((**BEDOT-B-(OBz)$_2$**, **4-6**)

The synthesis was carried out as for **BEDOT-B-CN$_2$** (2.4.5) with the following: **4-5** (2.80 g), 2-trimethylstannyl 3,4 ethylenedioxythiophene (3.84 g), $Pd(PPh_3)_4$ (0.100 g), and toluene (55 mL). The solid was recrystallized from acetone/ethanol (1:1) to yield a yellow crystalline powder [mp: 171-73 °C; 72%]. Anal. calcd. for $C_{32}H_{26}O_6S_2$: C, 67.35; H, 4.59; O, 16.82; S, 11.24. Found: C, 67.17; H, 4.58; S 11.13. ^{1}H NMR ($CDCl_3$, TMS) δ 4.22 (s, 8H), 5.17 (s, 4H), 6.35 (s, 2H), 7.27 (s, 2H), 7.34-7.52 (m, 10H). HRMS: calcd for $C_{32}H_{26}O_6S_2$: 570.1171, found: 570.1169.

4,4,8,1,4-Dibromo-2,5-di(ethoxy-2-tetrahydropyranylether) benzene (**4-7**)

DMF (100 mL), 2,5-dibromohydroquinone (5 g, 0.019 mol), potassium carbonate (16.3 g, 0.093 mol), sodium iodide (0.10 g), and 2-chloroethanol tetrahydropyranal ether (9.2 g, 0.056 mol) were combined and heated at 90 °C for 24 h. The reaction mixture was added to water (400 mL), and the solid was collected by suction filtration. The solid was recrystallized from ethanol to yield an off-white crystalline powder [mp: 97-99 °C; 45%]. Anal. calcd. for $C_{20}H_{28}O_6Br_2$: C, 45.82; H, 5.38; O, 18.31; Br, 30.48. Found: C, 45.81; H, 5.19; Br, 30.62. ^{1}H NMR ($CDCl_3$, TMS) δ 1.48-1.86 (b, 12H), 3.47-3.537 (m, 4H), 3.76-3.92 (m, 4H), 4.12-4.15 (m, 4H), 4.75-4.77 (t, 2H), 7.16 (s, 2H). ^{13}C NMR ($CDCl_3$, TMS) δ 19.1, 25.3, 30.3, 61.8, 65.5, 69.8, 98.7, 111.2, 119.0, 150.2. HRMS: calcd for $C_{20}H_{28}O_6Br_2$: 522.0253, found: 522.0206.

4,4,9,1,4-Bis[2-(3,4-ethylenedioxy)thienyl]-2,5-di(ethoxy-2-tetrahydropyranyl ether)benzene (4-8)

The synthesis was carried out as for **BEDOT-B-F_2** (2.4.2) with the following. n-butyl lithium (28.14 mL, 0.070 mol), EDOT (10.0 mL, 0.070 mol), $ZnCl_2$ (9.59 g, 0.070 mol), **4-6** (6.49 g, 0.023 mol), and $Pd(PPh_3)_4$ (0.200 g). The crude solid was recrystallized from acetone/water to yield yellow crystals [mp 132-45 °C, 65%]. ^1H NMR (acetone, TMS) δ 1.4-1.8 (m, 12H), 3.4-3.47 (m, 4H), 3.81-3.87 (dd, 4H), 4.05-4.09 (dd, 4H), 4.22-4.37 (m, 8H), 6.47 (s, 2H), 7.85 (s, 2H). ^{13}C NMR (acetone, TMS) δ 19.9, 26.3, 31.3, 62.0, 70.0, 99.4, 100.3, 113.5, 114.3, 122.0, 139.9, 142.3, 149.7. HRMS calcd for $C_{32}H_{38}O_{10}S_2$ 646.1906; found 646.1874.

4,4,10,1,4-Bis[2-(3,4-ethylenedioxy)thienyl] -2,5-di(ethoxy-2-hydroxy)benzene ((**BEDOT-B-(OHE)$_2$**, **4-9**)

Methanol (100mL), Amberlite (2.0 g) and **4-8** (1.0 g) were combined and refluxed for 1h. The resulting solution was filtered, then the solvent was removed. The resulting powder was recrystallized from ethanol to yield a yellow crystalline powder [184-185 °C, 76%]. Anal. calcd for $C_{22}H_{22}O_8S_2$: C, 55.22, H, 4.63, O, 26.75, S, 13.40. Found: C, 55.07, H, 4.67, S, 12.89. ^1H NMR ($CDCl_3$, TMS) δ 3.63 (s, 2H), 3.84 (s, 4H), 4.02 (s, 4H), 4.14 (s, 4H), 4.26 (s, 4H), 6.34 (s, 2H), 7.69 (s, 2H). HRMS calcd for $C_{22}H_{22}O_8S_2$ 478.0756, found 478.0681.

4.4.11 1,4-Diacyloxy-2,5-dibromobenzene (4-10)

The 2,5-Dibromohydroquinone (5.0 g, 0.0187 mol) was combined with acetic anhydride (20 mL) and pyridine catalyst (1 drop). The reaction mixture was stirred for 5h at room temperature. The solid was collected by suction filtration, was washed with water, then dried under vacuum for 24 h. The solid was recrystallized twice from methanol/water to yield white needles [mp 164-65 °C, 86%]. Anal. calcd. for $C_{10}H_8Br_2O_4$: C, 34.12; H, 2.29; Br, 45.41; O, 18.18. Found: C, 34.17; H, 2.19. ^{1}H NMR (acetone-d6, TMS) δ 2.33 (s, 6H), 7.65 (s, 2H). HRMS calcd for $C_{10}H_8Br_2O_4$: 349.8789, found: 349.8701.

4.4.12 1,4-Bis[2-(3,4-ethylenedioxy)thienyl]-2,5-diacyloxybenzene ((BEDOT-B-(OAc)$_2$, 4-11)

The synthesis was carried out as in 2.4.5 with the following: **4-10** (9.5 g, 0.0270 mol), 2-tributylstanyl-3,4-ethylenedioxythiophene (31.73 g, 0.0552 mol), $Pd(PPh_3)_4$ (0.100 g), and toluene (100 mL). The solid was recrystallized from acetonitrile/water to yield a tan solid [mp 288-90 °C, 68%]. Anal. calcd. for $C_{22}H_{18}O_8S_2$: C, 55.69; H, 3.82; O, 26.97; S, 13.51. Found: C, 55.41; H, 3.66; S, 13.26. ^{1}H NMR ($CDCl_3$, TMS) δ 2.28 (s, 6H), 4.15-4.21 (m, 8H), 6.33 (s, 2H), 7.62 (s, 2H). HRMS calcd for $C_{22}H_{18}O_8S_2$: 474.0443, found: 474.0449.

4.5 X-ray Experimental

Data were collected at 173 K on a Siemens SMART PLATFORM equipped with A CCD area detector and a graphite monochromator utilizing

MoK_α radiation (λ = 0.71073 Å) A hemisphere of data (1381 frames) was collected using the ω-scan method (0.3° frame width) The first 50 frames were remeasured at the end of data collection to monitor instrument and crystal stability (maximum correction on I was < 1 %) Psi scan absorption corrections were applied based on the entire data set.

The structure was solved by the Direct Methods in *SHELXL-97*,[99] and refined using full-matrix least squares. The non-H atoms were treated anisotropically, whereas the hydrogen atoms were calculated in ideal positions and were riding on their respective carbon atoms

Experimental for **BEDOT-B-(OEt)$_2$** Cell parameters were refined using 8192 reflections A total of 155 parameters were refined in the final cycle of refinement using 2009 reflections with $I > 2\sigma(I)$ to yield R_1 and wR_2 of 3.44% and 9.33% , respectively Refinement was done using F^2

Experimental for **BEDOT-B-(OEt)$_2$•THF Solvate** Cell parameters were refined using 8192 reflections A total of 137 parameters were refined in the final cycle of refinement using 2309 reflections with $I > 2\sigma(I)$ to yield R_1 and wR_2 of 3.52% and 9.22% , respectively Refinement was done using F^2

Experimental for **BEDOT-B-(OHE)$_2$** Cell parameters were refined using 3872 reflections. A total of 157 parameters were refined in the final cycle of refinement using 1758 reflections with $I > 2\sigma(I)$ to yield R_1 and wR_2 of 4.48% and 9.65% , respectively Refinement was done using F^2

Experimental for **BEDOT-B-(OMTM)$_2$** Cell parameters were refined using 6305 reflections A total of 165 parameters were refined in the final

cycle of refinement using 1972 reflections with $I > 2\sigma(I)$ to yield R_1 and wR_2 of 4 05% and 8 77% , respectively Refinement was done using F^2

Experimental for **BEDOT-B-(OBz)$_2$** Cell parameters were refined using up to 8192 reflections. A total of 151 parameters were refined in the final cycle of refinement using 2744 reflections with $I > 2s(I)$ to yield R1 and wR2 of 3.79% and 10.27% , respectively Refinement was done using F2

Experimental for **BEDOT-B-(OAc)$_2$** Cell parameters were refined using 4658 reflections A total of 145 parameters were refined in the final cycle of refinement using 1944 reflections with $I > 2\sigma(I)$ to yield R_1 and wR_2 of 5 17% and 14.72% , respectively Refinement was done using F^2

Table 4.3 Crystal Data and Structure Refinement for **BEDOT-B-(OEt)$_2$**

Empirical formula	$C_{22}H_{22}O_6S_2$	
Formula weight	446.52	
Temperature	173(2) K	
Wavelength	0.71073 Å	
Crystal system	Orthorhombic	
Space group	Pbca	
Unit cell dimensions	a = 12.0267(2) Å	α = 90°
	b = 11.3835(2) Å	β = 90°
	c = 14.5357(2) Å	γ = 90°
Volume, Z	1990.02(6) Å^3, 4	
Density (calculated)	1.490 Mg/m^3	
Absorption coefficient	0.307 mm^{-1}	
F(000)	936	
Crystal size	0.26 x 0.19 x 0.19 mm	
Theta range for data collection	2.80 to 27.50°	
Limiting indices	-16≤h≤14, -11≤k≤15, -19≤l≤18	
Reflections collected	30066	
Independent reflections	2292 [R(int) = 0.0265]	
Absorption correction	Empirical	
Min. and Max. Transmission	0.797 and 0.956	
Refinement method	Full-matrix least-squares on F^2	
Data / restraints / parameters	2292 / 7 / 155	
Goodness-of-fit on F^2	1.062	
Final R indices [I>2sigma(I)]	R1 = 0.0344, wR2 = 0.0933 [2009]	
R indices (all data)	R1 = 0.0403, wR2 = 0.0976	
Largest diff. peak and hole	0.341 and -0.371 e Å^{-3}	

Table 4.4 Crystal Data and Structure Refinement for **BEDOT-B-$(OEt)_2$•THF Solvate**

Empirical formula	$C_{20.33}H_{24.67}O_{6.33}S_2$	
Formula weight	470 55	
Temperature	173(2) K	
Wavelength	0 71073 Å	
Crystal system	Trigonal	
Space group	R -3	
Unit cell dimensions	a = 29.3123(1) Å	α = 90°
	b = 29.3123(1) Å	β = 90°
	c = 6.8706(1) Å	γ = 120°
Volume, Z	5112 40(7) Å^3, 9	
Density (calculated)	1.376 Mg/m^3	
Absorption coefficient	0 283 mm^{-1}	
F(000)	2466	
Crystal size	0.30 x 0.27 x 0.27 mm	
Theta range for data collection	1.39 to 27 5°	
Limiting indices	-38≤h≤34, -38≤k≤35, -8≤l≤8	
Reflections collected	30066	
Independent reflections	2597 [R(int) = 0 0240]	
Absorption correction	Semi-empirical from psi-scans	
Max and min transmission	0 947 and 0 764	
Refinement method	Full-matrix least-squares on F^2	
Data / restraints / parameters	2597 / 0 / 137	
Goodness-of-fit on F^2	1.060	
Final R indices [I>2sigma(I)]	R1 = 0 0352, wR2 = 0 0922 [2309]	
R indices (all data)	R1 = 0 0403, wR2 = 0 0961	
Extinction coefficient	not measured	
Largest diff peak and hole	0 46 and -0 31 e.Å^{-3}	

Table 4 5: Crystal Data and Structure Refinement for **BEDOT-B-(OHE)$_2$**

Empirical formula	$C_{24}H_{22}O_8S_2$	
Formula weight	478.52	
Temperature	173(2) K	
Wavelength	0 71073 Å	
Crystal system	Monoclinic	
Space group	P2(1)/c	
Unit cell dimensions	a = 4 4307(1) Å	α = 90°
	b = 17 9428(3) Å	β = 91 839(1)°
	c = 13 0420(2) Å	γ = 90°
Volume Z	1036.29(3) Å^3, 2	
Density (calculated)	1 534 Mg/m^3	
Absorption coefficient	0 307 mm^{-1}	
F(000)	500	
Crystal size	0 30 x 0 10 x 0 10 mm	
Theta range for data collection	1 93 to 27 49°	
Limiting indices	-5≤h≤5, -23≤k≤17, -16≤l≤16	
Reflections collected	7267	
Independent reflections	2371 [R(int) = 0 0444]	
Absorption correction	Empirical	
Max and min transmission	0 977 and 0.392	
Refinement method	Full-matrix least-squares on F^2	
Data / restraints / parameters	2371 / 1 / 157	
Goodness-of-fit on F^2	1 010	
Final R indices [I>2sigma(I)]	R1 = 0 0448, wR2 = 0 0965 [1758]	
R indices (all data)	R1 = 0 0650, wR2 = 0 1041	
Extinction coefficient	0 0043(12)	
Largest diff peak and hole	0 409 and -0 324 e Å^{-3}	

Table 4.6 Crystal Data and Structure Refinement for **BEDOT-B-(OMTM)$_2$**

Empirical formula	$C_{22}H_{22}O_6S_4$	
Formula weight	510 64	
Temperature	173(2) K	
Wavelength	0 71073 Å	
Crystal system	Orthorhombic	
Space group	Pbca	
Unit cell dimensions	a = 16 8864(3) Å	α = 90°
	b = 7 6906(2) Å	β = 90°
	c = 17.3427(4) Å	γ = 90°
Volume, Z	2252 24(9) Å^3, 4	
Density (calculated)	1·506 Mg/m^3	
Absorption coefficient	0 460 mm^{-1}	
F(000)	1064	
Crystal size	0.30 x 0.14 x 0.07 mm	
Theta range for data collection	2.35 to 27.50°	
Limiting indices	-21≤h≤16, -9≤k≤9, -17≤l≤22	
Reflections collected	15701	
Independent reflections	2578 [R(int) = 0.0429]	
Absorption correction	Empirical	
Min and Max Transmission	0 812 and 0 977	
Refinement method	Full-matrix least-squares on F^2	
Data / restraints / parameters	2578 / 7 / 165	
Goodness-of-fit on F^2	1 083	
Final R indices [I>2sigma(I)]	R1 = 0 0405 wR2 = 0 0877 [1972]	
R indices (all data)	R1 = 0 0613 wR2 = 0 0980	
Extinction coefficient	0 0008(5)	
Largest diff peak and hole	0 369 and -0 304 e Å^{-3}	

Table 4.7 Crystal Data and Structure Refinement for **BEDOT-B-(OBz)$_2$**

Empirical formula	$C_{32}H_{28}O_6S_2$
Formula weight	570.65
Temperature	173(2) K
Wavelength	0.71073 Å
Crystal system	Triclinic
Space group	P-1
Unit cell dimensions	a = 7.7833(5) Å α = 92.359(1)°
	b = 8.6750(6) Å β = 106.884(1)°
	c = 10.5342(7) Å γ = 104.449(1)°
Volume, Z	654.11(8) Å^3, 1
Density (calculated)	1.449 Mg/m^3
Absorption coefficient	0.251 mm^{-1}
F(000)	298
Crystal size	0.24 x 0.24 x 0.30 mm
Theta range for data collection	2.04 to 27.50°
Limiting indices	-9≤h≤10, -9≤k≤11, -13≤l≤13
Reflections collected	4333
Independent reflections	2903 [R(int) = 0.0255]
Absorption correction	Integration
Max. and min. transmission	0.9546 and 0.9055
Refinement method	Full-matrix least-squares on F^2
Data / restraints / parameters	2903 / 0 / 181
Goodness-of-fit on F^2	1.106
Final R indices [I>2sigma(I)]	R1 = 0.0379, wR2 = 0.1027 [2744]
R indices (all data)	R1 = 0.0400, wR2 = 0.1057
Largest diff. peak and hole	0.609 and -0.207 e Å^{-3}

Table 4.8 Crystal Data and Structure Refinement for **BEDOT-B-(OAc)$_2$**

Empirical formula	$C_{22}H_{18}O_6S_2$	
Formula weight	474.48	
Temperature	173(2) K	
Wavelength	0.71073 Å	
Crystal system	Monoclinic	
Space group	P2(1)/c	
Unit cell dimensions	a = 7.8320(1) Å	α = 90°
	b = 16.6889(3) Å	β = 106.594(1)°
	c = 8.1551(1) Å	γ = 90°
Volume, Z	1021.54(3) Å^3, 2	
Density (calculated)	1.543 Mg/m^3	
Absorption coefficient	0.311 mm^{-1}	
F(000)	492	
Crystal size	0.38 x 0.21 x 0.07 mm	
Theta range for data collection	2.44 to 27.49°	
Limiting indices	-7≤h≤10, -21≤k≤21, -10≤l≤7	
Reflections collected	6988	
Independent reflections	2332 [R(int) = 0.0257]	
Absorption correction	None	
Refinement method	Full-matrix least-squares on F^2	
Data / restraints / parameters	2332 / 0 / 145	
Goodness-of-fit on F^2	1.042	
Final R indices [I>2sigma(I)]	R1 = 0.0517, wR2 = 0.1472 [1944]	
R indices (all data)	R1 = 0.0624, wR2 = 0.1564	
Largest diff. peak and hole	0.628 and -0.692 e Å^{-3}	

CHAPTER 5
BIS(EDOT) PYRIDINES N-DOPING AND ACID SENSITIVITY

5.1 Motivation

Over the past 25 years, research in conductive polymers has had to overcome many daunting obstacles, including insolubility, instability in air, bioincompatibility, and limited variations of electronic properties. One of the latest challenges is n-doping, the formation of negative charge-carriers on the conjugated polymer backbone. Up to this chapter, the polymers discussed in this dissertation have been p doped, where electrons were removed from the π-orbitals. In n-doping, electrons are added to the π-cloud. One of the main problems associated with n-doping is that the potentials required to reduce the polymers to their n-doped state are sufficiently cathodic to reduce oxygen and water if they are not rigorously removed from the system.

In the recent literature, several examples of n-doping have been reported. Poly(bithiophene) and poly(1,2-bis(2 thienyl)ethylene) exhibit irreversible n-doping, attributed to ion assisted reduction of double bonds by water.[111] Some of the more stable n-dopable polymers are ladder polymers based on BBL [poly(benzimidazole-benzophenanthroline)] (**Figure 5.1**) which

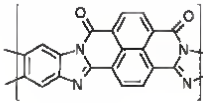

Figure 5.1 n-Dopable Polymers

reversibly reduces at -1.2 V vs. SCE. A different ladder polymer based on fused benzenes is a stable n doping polymer at -0.9 vs. SCE.[112]

One approach to produce n-dopable systems is to use low gap polymers. The electrochemical gap between the onset potential of the polymer oxidation and reduction is the band gap and is equivalent to the HOMO-LUMO based electronic band gap discussed earlier (Chapter 1). If the band gap is small then it is likely that both p-doping and n-doping can be accessible and sufficiently stable in a single polymer. One of these low gap polymers is based on cyclopenta[2,1-b;4,3-b']dithiophen-4-(cyano-nonafluorobutylsulfonyl) methylidene (CNFBS) (**Figure 5.1**) which n dopes at -0.6 V vs. Ag/Ag^+.[113] The dicyano analog of CNFBS is also a low gap polymer with a reduction potential of -0.6 V vs. SCE, but the monomer is poorly soluble.[114] Poly(isothianaphthene) (PITN) is another low band gap polymer which has also been used for n-doping.[115]

One theory, proposed in a paper by de Leeuw,[116] suggests that nitrogen–containing poly(heterocycles) induce stability in n-doped systems, one such example is poly(pyridine), which has a reduction potential of -1.9 V vs. SCE.

Another example of this is seen in polyquinoxalines (**Figure 5.1**) which reversibly n-dope at -1.8 vs. Ag/Ag^{+}.[117] In related research, polyquinoxalines were quaternized, thus producing polymers with resident positive charge to help stabilized the n-doped state.[118] Polyheterocycles such as poly(4,4'-dialkyl-2,2'-bithiazole-5,5-diyl)s[119] and copoly(thiophene-quinoxaline)[120] have been found to be n-dopable as determined by electrochemistry and spectroelectrochemistry.

Based on the theory that nitrogen containing heterocycles induce stability in n-doped systems, a series of pyridine-containing extended conjugation monomers based on the bis(EDOT) family were synthesized. In addition to the possibility of n-doping, the pyridine moiety can be quaternized with acid. Conjugated polymers containing pyridine should therefore be useful as pH sensitive switches. This chapter describes the synthesis and electrochemical polymerization of 2,5-bis(2-[3,4-ethylenedioxythienyl])pyridine, a pyridine-containing extended conjugation monomer. The electronic and optical properties are examined in the n-doped and quaternized states.

5.2 Results and Discussion

2,6-Bis[2-(3,4-ethylenedioxythienyl)]pyridine (**5-2**) and 3,5-bis[2-(3,4-ethylenedioxythienyl)]pyridine (**5-3**) shown in **Figure 5.2** were synthesized using a Negishi-type aryl cross coupling reaction[88] in 57% and 42% yields, respectively. The *meta* isomers were chosen with the expectation of

obtaining low oxidation potential, high gap polymers The resultant polymers would have an effective conjugation length of four rings (Pyr-EDOT-EDOT-Pyr) due to cross conjugation of the *meta*- linkages. Pyridine was also selected due to its electron accepting ability to produce a "push-pull" polymer system as discussed in Chapter 1.5. The monomers were found to be electroinactive below 1.5 V vs Ag/Ag^+ in CH_3CN or CH_2Cl_2

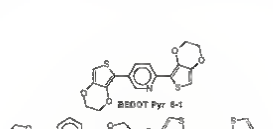

Figure 5.2 Monomers Based on Bis(EDOT)Pyridines

The thiophene analogue, 3,5-bis(2-thienyl)pyridine, was poorly electroactive, but the 2,6-bis(2-thienyl)pyridine was shown to produce smooth films [121] A possible reason for the poor electroactivity is that the electron accepting ability of the pyridine in conjunction with the restriction of delocalization to only two rings drives the oxidation potential higher than 1.5 V vs. Ag/Ag^+. The remaining isomer, 2,5-bis[2-(3,4-ethylenedioxythienyl)]pyridine (**BEDOT-Pyr, 5-1**) was synthesized in a 93% yield **BEDOT-Pyr** was electrochemically polymerized using repeated scan and potentiostatic deposition with a standard three-electrode cell from a 10 mM/0.1 M TBAP/CH_3CN/CH_2Cl_2 (1:1) or 7.5 mM/0.1 M TBAP/ CH_3CN solution to yield poly{2,5-bis[2-(3,4-

ethylenedioxythienyl)]pyridine} (poly(**BEDOT-Pyr**)) As seen in **Figure 5.3**, the onset for monomer oxidation occurs at 0.55 V with a peak at 0.65 V

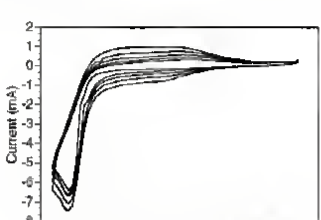

Figure 5.3 Repeated Potential Scan Electrochemical Polymerization of (10mM) **BEDOT-Pyr** (on a Pt Button in 0.1 M TBAP/CH_3CN/CH_2Cl_2 (1:1) at a Scan Rate of 100 mV/s)

The electrochemistry shown in **Figure 5.3** was performed in 1:1 CH_3CN/CH_2Cl_2 solution due to the limited solubility of BEDOT-Pyr in CH_3CN (maximum of 7.5 mM) To study the optical properties and n-doping electrochemistry, the polymer was deposited potentiostatically from a 7.5 mM CH_3CN solution since CH_2Cl_2 is not stable to the reduction potentials within the experiment.[122] The $E_{p,a}$ is very close to that of **BEDOT-B** (0.61 V vs Ag/Ag^+)[12], but it does exhibit a higher $E_{1/2}$ by >250 mV Thus indicates that there is good conjugation, but there is an effect of the electron-accepting pyridine **Figure 5.3** shows the cyclic voltammetry of poly(**BEDOT-Pyr**) in monomer-free electrolyte solution (0.1 M TBAP/CH_3CN/CH_2Cl_2) as the scan

rate is increased from 100 to 500 mV/s Note that in **Figure 5.4**, the anodic and cathodic polymer redox processes increase linearly with increasing scan rate, indicative of a well-adhered polymer film The redox processes for poly(**BEDOT-Pyr**) include broad oxidation and reduction peaks centered at 0 55 V and 0.37, respectively, resulting in an $E_{1/2}$ of 0 49 V Compared with other bis(EDOT) polymers, the $E_{1/2}$ is high, this is due to the electron accepting ability of the pyridine

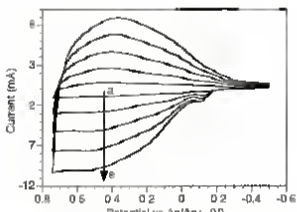

Figure 5.4 Cyclic Voltammetric Scan Rate Dependence of Poly(**BEDOT-Pyr**) (on a Pt Button in 0 1 M TBAP/CH_3CN at a Scan Rates of (a) 100 (b) 200 (c) 300 (d) 400 (e) 500 mV/s)

Questionable reports of extremely low band gaps have appeared in the recent literature, with values derived from what appears to be bipolaron bands or shoulders on the π–π^* band [72] To validate our results and eliminate possible error, the band gap of poly(**BEDOT-Pyr**) was determined by comparison of three different films deposited at different thicknesses. The UV-Vis-NIR spectra were obtained for poly(**BEDOT-Pyr**) deposited potentiostatically at 15, 25, and 35 mC on ITO glass (**Figure 5 5**) These films

were electrochemically reduced at -1 0 V. The electrochemical reduction was performed to insure that the polymer was fully reduced to its neutral state The identification of the band edge of three films of increasing thickness shows that, although the slope of the onset changes, all three samples can be extrapolated to the background absorbance to yield a band gap of 1 9 eV

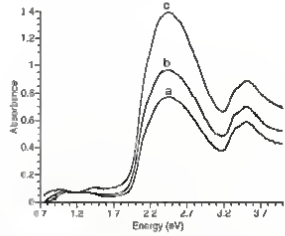

Figure 5.5 UV-VIS-NIR Spectra of Poly(**BEDOT-Pyr**) (deposited as a function of charge passed from 7 5 mM **BEDOT-Pyr** in 0.1 M TBAP/CH_3CN onto ITO glass (a) 15 (b) 20 (c) 25 mC)

Note that, even with increasing film thickness, the absorbance below 1 9 eV does not change significantly relative to the absorbance increase observed in the π-π^* band This property is desirable in optical applications due to the high absorbance contrast between different wavelengths

Figure 5.6 is a combination of two experiments to show the full range of electrochemical processes possible in poly(**BEDOT-Pyr**) In these experiments, a single film is deposited onto a Pt button electrode from a 7.5 mM **BEDOT-Pyr**/0 1 M TBAP solution of CH_3CN in a dry box. The film was

cycled between -1 0 V to +0 7 V five times, and the fifth cycle (shown below) was recorded to show the oxidative doping and de-doping of the polymer (**Figure 5.5** a) at 100 mV/s. The film was then cycled between -1 0 V to -2 4 V five times, with the fifth cycled was recorded to show the reductive doping and de-doping of the polymer (**Figure 5 6** b) at 100 mV/s.

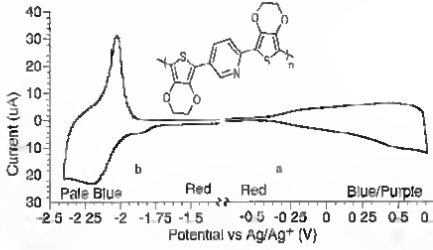

Figure 5.6 Anodic (a) and Cathodic (b) Electrochemistry of Poly(**BEDOT-Pyr**)

Note that it is inadvisable to repeatedly cycle from p-doped to n-doped states due to the formation of pre-peaks that increase with each subsequent scan. These pre peaks, which may be due to trapped charge carriers, can be misinterpreted as redox peaks if separate oxidation and reduction experiments are not performed On the right side of the figure, the broad oxidation (p-doping) is shown On the left side, the sharp single peak for reduction (n-doping) of the polymer is shown The electrochemical band gap,

which is measured from the onset of the reduction and oxidation peaks is roughly 1 8 eV, which is consistent with the optical band gap

The appearance of reduction peaks by electrochemical methods does not prove that the polymer is n-doping The polymer must form lower energy bands that correspond to charge carriers A definitive method for the determination of the formation of charge carriers is to observe them by UV-Vis-NIR spectroscopy, but unfortunately, creation of an airless spectroelectrochemical cell has not been completed by the publication of this work. However, electrochromic behavior has been observed in the dry box, the film changes colors from pale blue (reduced, -2 2 V) to red (neutral, -0.5 V) to blue/purple (oxidized, +0.75 V) This color change is indicative of the formation of charge carriers in conjugated polymers

One of the unique properties of poly(**BEDOT-Pyr**) is that it contains sites that can be quaternized These quaternized sites are in direct conjugation of the backbone, therefore can affect on the electronic properties as the polymer is acidified To determine the effect of pH on poly(**BEDOT-Pyr**) the UV-Vis-NIR spectrum was obtained for one film as a function of pH. Aqueous buffer solutions of various pH were prepared To determine if the films were stable to aqueous solution, the UV-Vis-NIR spectrum was obtained for a film in monomer-free 0 1 M TBAP/CH_3CN solution and in a Na_2HPO_4/citric acid pH7 buffer solution. There is no change in the π–π^* band (λ_{max} 510 nm) As seen in **Figure 5.7**, the λ_{max} is only slightly effected until pH2, where there is a sharp 70 nm red shift through pH1 Thus change is

apparent if the λ_{max} is plotted as a function of pH, as seen in **Figure 5.8**. The λ_{max} is constant until the film is exposed to a pH2 buffer solution at which time it begins to red shift. By pH1, the λ_{max} has shifted by 70 nm and is constant with decreasing pH. The evident quaternization of the film at around pH2 is higher that that of pyridine in solution at ~ pH5.

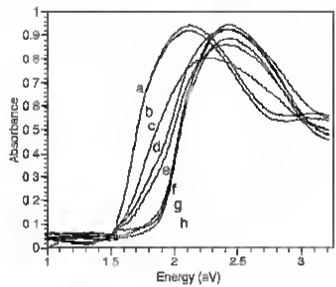

Figure 5.7 UV-Vis-NIR Spectra of **BEDOT-Pyr** as a Function of pH
(a) 0.5 (b) 1 (c) 1.5 (d) 2 (e) 3 (f) 5 (g) 6 (h) 7

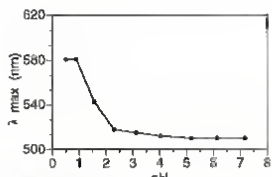

Figure 5.8: Poly(BEDOT-Pyr) λ_{max} as a Function of pH

This is supported by the literature,[123] in which a set of thiophene and furan substituted pyridines show a marked decrease in basicity. We attribute this to the need for the EDOT to be twisted out of plane as the polymer is protonated.

In addition to the above result, the electroactivity is dramatically reduced upon acidification of the film. This is due to the increased oxidation potential of the now positively charged polymer. The film changes from a red to a indigo/blue with exposure to acid. The films can be reversibly switched between the acidified and neutral state by exposure to 1 M HCl followed by rinsing with deionized water.

5.3 Conclusions

Three unique extended conjugation monomers containing pyridine have been synthesized and analyzed. Of the three monomers, one was found to be electroactive and form electrochromic films. Poly(**BEDOT-Pyr**) was shown to be a p- and n- doping polymer with color changes at each transition. Poly(**BEDOT-Pyr**) can be quaternized with acid and the resulting films exhibit a 70 nm red shift in the λ_{max} having potential as an acid sensing switch.

5.4 Synthesis

5.4.1 General Procedures

All chemicals were purchased from Aldrich unless otherwise stated. *n*-Butyl lithium (2.5 M in hexanes) was purchased from Acros Chemical. 3,4-

Ethylenedioxythiophene (EDOT) was donated by AG Bayer and distilled under vacuum, purged with argon, and stored at -20 °C until used. Tetra–*n*–butyl ammonium perchlorate (TBAP) was synthesized by the addition of perchloric acid to aqueous tetra–*n*–butyl ammonium bromide, the precipitate was collected and was recrystallized from ethanol.

Elemental analysis was performed by Robertson Microlit Laboratories, Inc of Madison, New Jersey. All HRMS analysis was done at University of Florida. ^{1}H NMR spectra were obtained on a Varian Gemini 300 NMR spectrometer at 300 MHz NMR with tetramethylsilane or solvent as internal standard.

Cyclic voltammetry was carried out using an EG&G Princeton Applied Research Model 273 potentiostat/galvanostat employing a platinum button working electrode (0.005 cm^2), a platinum plate counter electrode, and a Ag/Ag^+ reference electrode. The monomer concentration was 2 to 7.5 mM in each case, and the electrolyte was 0.1 M TBAP in CH_3CN or CH_2Cl_2. Acetonitrile (CH_3CN) and CH_2Cl_2 were purchased from Fisher Scientific and distilled before use from CaH_2.

5,4,2 2,5-Bis[2-(3,4-ethylenedioxythienyl)]pyridine (BEDOT-Pyr, 5-1)

n-Butyl lithium (14.1 mL, 35.2 mmol) was slowly added by syringe to a stirred solution of EDOT (5.00 g, 35.2 mmol) in THF (50 mL) at -78 °C under argon. After 30 minutes, a $ZnCl_2$ solution (35.2 mL of 1.0M solution in diethyl ether) was cannula-transferred into the flask. A white precipitate

formed, then dissolved as the reaction mixture was warmed to 0° C at which it was held for one hour A solution of 2,5-dibromopyridine (2.78 g, 8.79 mmol) and $Pd(PPh_3)_4$ (100 mg) in THF (20 mL) was added to the resulting EDOT-ZnCl complex The solution was stirred at 50 °C under argon for 3d The mixture was cooled to ambient temperature and quenched with water (500 mL) The THF was removed under reduced pressure, and the solid was collected by suction filtration and dried under vacuum. The crude solid was crystallized from THF/water to yield tan crystals [mp 189-190 °C, 93%] Anal calcd for $C_{17}H_{13}N_1S_2O_4$ C 56.81, H3.65, N 3 90, found C 56 90, H 3 72, N 3 85 ^{1}H-NMR (d6-Acetone) δ 4 33 -4 50 (m,8) 6.57 (s 1), 6.59 (s,1), 7 98-8 07 (q,2), 8 86 (d,1) FAB-HRMS Calc ($C_{17}H_{13}N_1S_2O_4$)+H 360 0364; found 360 0352

5,4,2 2,6-Bis[2-(3,4-ethylenedioxythienyl)]pyridine (5-2)

The synthesis was carried out as in the synthesis of **BEDOT-Pyr** with the following *n*-butyl lithium (14 1 mL, 35 2 mmol), EDOT (5 00 g, 35.2 mmol), $ZnCl_2$ (35.2 mL), 2,6-dibromopyridine (2.78 g, 8 79 mmol), $Pd(PPh_3)_4$ (100 mg), and THF (70 mL) The crude solid was crystallized from THF/water to yield tan crystals [mp 275-279 °C, 57%] Anal calcd for $C_{17}H_{13}N_1S_2O_4$ C 56 81, H3 65, N 3 90, found C 56 47, H 3 66, N 3 83 ^{1}H-NMR (d6-acetone) δ 4 33 -4 49 (m,8) 6.57 (s,1), 6.60 (s,1), 7 77-7 80 (t,3, J_{H-H} = 3 3 Hz) FAB-HRMS Calc ($C_{17}H_{13}N_1S_2O_4$)+H 360 0364, found 360 0362.

5,4,3,3,5-Bis[2-(3,4-ethylenedioxythienyl)]pyridine (5-3)

The synthesis was carried out as in the synthesis of **BEDOT-Pyr** with the following: *n*-butyl lithium (14.1 mL, 35.2 mmol), EDOT (5.00 g, 35.2 mmol), $ZnCl_2$ (35.2 mL), 3,5-dibromopyridine (2.78 g, 8.79 mmol), $Pd(PPh_3)_4$ (100 mg), and THF (70 mL). The crude solid was crystallized from THF to yield tan crystals [mp 273-275 °C, 42%]. Anal. calcd. for $C_{17}H_{13}N_1S_2O_4$: C, 56.81; H, 3.65; N, 3.90; found: C, 56.750; H, 3.67; N, 4.01. ^{1}H-NMR (d6-acetone): δ 4.35 -4.47 (m,8), 6.70 (s,1), 8.51-8.52 (t,1, J = 2.1 Hz), 8.95-8.96 (d,2, J_{H-H} = 1.8 Hz). FAB-HRMS Calc. ($C_{17}H_{13}N_1S_2O_4$)+H 360.0364, found 360.0366.

APPENDIX A
TABLES OF BOND LENGTHS AND ANGLES

Table A-1 Bond Lengths (Å) and Bond Angles (°) for **BEDOT-B-F_2, 2-2**

C(1)-C(3)#1	1.392(17)	C(1)-C(2)	1.414(16)	C(1)-C(2')	1.460(17)
C(2)-F(2)	1.347(13)	C(2)-C(3)	1.351(17)	C(3)-C(1)#1	1.392(17)
S(1')-C(5')	1.700(14)	S(1')-C(2')	1.730(12)	C(2')-C(3')	1.407(16)
C(3')-O(2')	1.360(14)	C(3')-C(4')	1.400(18)	C(4')-O(1')	1.376(15)
C(4')-C(5')	1.419(18)	O(1')-C(6')	1.416(16)	C(6')-C(7')	1.501(18)
C(7')-O(2')	1.444(16)				

C(3)#1-C(1)-C(2)	113.1(11)	C(3)#1-C(1)-C(2')	123.0(11)
C(2)-C(1)-C(2')	123.8(11)	F(2)-C(2)-C(3)	119.0(10)
F(2)-C(2)-C(1)	117.0(12)	C(3)-C(2)-C(1)	123.9(11)
C(2)-C(3)-C(1)#1	122.9(11)	C(5')-S(1')-C(2')	95.2(7)
C(3')-C(2')-C(1)	127.0(11)	C(3')-C(2')-S(1')	109.3(9)
C(1)-C(2')-S(1')	123.6(9)	O(2')-C(3')-C(4')	124.1(11)
O(2')-C(3')-C(2')	123.6(11)	C(4')-C(3')-C(2')	112.3(11)
O(1')-C(4')-C(3')	121.5(12)	O(1')-C(4')-C(5')	123.5(12)
C(3')-C(4')-C(5')	115.0(12)	C(4')-C(5')-S(1')	108.2(10)
C(4')-O(1')-C(6')	111.4(11)	O(1')-C(6')-C(7')	110.1(12)
O(2')-C(7')-C(6')	110.5(12)	C(3')-O(2')-C(7')	111.3(11)

Table A-2 Bond Lengths (Å) and Bond Angles (°) for **BEDOT-ß-$(CN)_2$-TMS_2, 2-6**

C(1)-C(3)#1	1.391(4)	C(1)-C(2)	1.418(4)	C(1)-C(2')	1.462(4)
C(2)-C(3)	1.392(4)	C(2)-C(21)	1.445(4)	C(3)-C(1)#1	1.391(4)
S(1')-C(2')	1.722(3)	S(1')-C(5')	1.728(3)	C(2')-C(3')	1.382(4)
C(3')-O(1')	1.363(4)	C(3')-C(4')	1.421(4)	C(4')-C(5')	1.360(4)
C(4')-O(2')	1.381(4)	C(5')-Si(1)	1.870(3)	O(1')-C(6')	1.449(4)
C(6')-C(7')	1.505(5)	C(7')-O(2')	1.435(4)	Si(1)-C(52)	1.853(4)
Si(1)-C(53)	1.855(4)	Si(1)-C(51)	1.860(4)	C(21)-N(21)	1.142(4)

C(3)#1-C(1)-C(2)	116.8(3)	C(3)#1-C(1)-C(2')	120.2(3)
C(2)-C(1)-C(2')	123.0(3)	C(3)-C(2)-C(1)	121.3(3)
C(3)-C(2)-C(21)	117.3(3)	C(1)-C(2)-C(21)	121.4(3)
C(1)#1-C(3)-C(2)	121.9(3)	C(2')-S(1')-C(5')	94.32(14)
C(3')-C(2')-C(1)	126.5(3)	C(3')-C(2')-S(1')	109.6(2)
C(1)-C(2')-S(1')	123.8(2)	O(1')-C(3')-C(2')	123.7(3)
O(1')-C(3')-C(4')	124.1(3)	C(2')-C(3')-C(4')	112.1(3)
C(5')-C(4')-O(2')	123.6(3)	C(5')-C(4')-C(3')	115.7(3)
O(2')-C(4')-C(3')	120.8(3)	C(4')-C(5')-S(1')	108.3(2)
C(4')-C(5')-Si(1)	129.2(2)	S(1')-C(5')-Si(1)	122.48(18)
C(3')-O(1')-C(6')	113.5(2)	O(1')-C(6')-C(7')	111.5(3)
O(2')-C(7')-C(6')	111.0(3)	C(4')-O(2')-C(7')	110.1(2)
C(52)-Si(1)-C(53)	110.58(18)	C(52)-Si(1)-C(51)	109.98(19)
C(53)-Si(1)-C(51)	112.11(18)	C(52)-Si(1)-C(5')	109.00(16)
C(53)-Si(1)-C(5')	108.89(16)	C(51)-Si(1)-C(5')	106.13(15)
N(21)-C(21)-C(2)	177.7(4)		

Symmetry transformations used to generate equivalent atoms #1 -x,-y,1-z

Table A-3 Bond Lengths (Å) and Bond Angles (°) for **BEDOT-ß-NO_2 2-8**

C(1)-C(6)	1.380(6)	C(1)-C(2)	1.412(5)	C(1)-C(2')	1.467(5)
C(2)-C(3)	1.377(5)	C(2)-N(1)	1.470(5)	C(3)-C(4)	1.388(5)
C(4)-C(5)	1.419(5)	C(4)-C(2')	1.471(5)	C(5)-C(6)	1.380(5)
S(1')-C(5')	1.711(5)	S(1')-C(2')	1.729(4)	C(2')-C(3')	1.354(6)
C(3')-O(2')	1.375(5)	C(3')-C(4')	1.434(5)	C(4')-C(5')	1.343(6)
C(4')-O(1')	1.360(5)	O(1')-C(6')	1.435(5)	C(6')-C(7')	1.510(6)
C(7')-O(2')	1.419(5)	S(1")-C(5")	1.702(5)	S(1")-C(2")	1.733(4)
C(2")-C(3")	1.364(6)	C(3")-O(2")	1.370(5)	C(3")-C(4")	1.428(6)
C(4")-C(5")	1.361(6)	C(4")-O(1")	1.364(5)	O(1")-C(6")	1.441(5)
C(6")-C(7")	1.489(7)	C(7")-O(2")	1.439(5)	N(1)-O(2)	1.221(4)
N(1)-O(1)	1.225(4)				

C(6)-C(1)-C(2)	115.4(3)	C(6)-C(1)-C(2')	120.7(3)
C(2)-C(1)-C(2')	123.9(3)	C(3)-C(2)-C(1)	122.5(3)
C(3)-C(2)-N(1)	116.4(3)	C(1)-C(2)-N(1)	121.1(3)
C(2)-C(3)-C(4)	121.3(4)	C(3)-C(4)-C(5)	117.0(3)
C(3)-C(4)-C(2')	121.2(3)	C(5)-C(4)-C(2")	121.8(3)
C(6)-C(5)-C(4)	120.4(4)	C(5)-C(6)-C(1)	123.4(4)
C(5')-S(1')-C(2')	92.57(19)	C(3')-C(2')-C(1)	129.4(3)
C(3')-C(2')-S(1')	109.5(3)	C(1)-C(2')-S(1')	120.8(3)
C(2')-C(3')-O(2')	124.8(4)	C(2')-C(3')-C(4')	114.2(4)
O(2')-C(3')-C(4')	120.9(3)	C(5')-C(4')-O(1')	125.0(4)
C(5')-C(4')-C(3')	111.7(4)	O(1')-C(4')-C(3')	123.2(4)
C(4')-C(5')-S(1')	112.0(3)	C(4')-O(1')-C(6')	113.6(3)
O(1')-C(6')-C(7')	111.1(3)	O(2')-C(7')-C(6')	110.8(4)
C(3')-O(2')-C(7')	111.1(3)	C(5")-S(1")-C(2")	92.9(2)
C(3')-C(2')-C(4)	130.8(4)	C(3")-C(2")-S(1")	109.7(3)
C(4)-C(2")-S(1")	119.4(3)	C(2")-C(3")-O(2')	124.6(4)

Table A-3 Bond Lengths (Å) and Bond Angles (°) for **BEDOT-B-NO_2 2-8** (continued)

C(2')-C(3')-C(4'')	113.5(4)	O(2'')-C(3'')-C(4')	121.9(3)
C(5'')-C(4'')-O(1'')	124.0(4)	C(5')-C(4'')-C(3')	112.4(4)
O(1'')-C(4')-C(3'')	123.7(4)	C(4'')-C(5'')-S(1'')	111.5(3)
C(4')-O(1'')-C(6'')	111.6(3)	O(1'')-C(6'')-C(7'')	111.5(4)
O(2'')-C(7'')-C(6'')	112.2(4)	C(3')-O(2'')-C(7'')	111.3(3)
O(2)-N(1)-O(1)	124.0(3)	O(2)-N(1)-C(2)	118.1(3)
O(1)-N(1)-C(2)	117.9(3)		

Table A-4 Bond Lengths (Å) and Bond Angles (°) for **BEDOT-B-F_4, 3-2.**

C(1)-C(3)#1	1.381(4)	C(1)-C(2)	1.394(4)	C(1)-C(2')	1.472(4)
C(2)-F(2)	1.337(4)	C(2)-C(3)	1.385(4)	C(3)-F(3)	1.339(4)
C(3)-C(1)#1	1.381(4)	S(1')-C(5')	1.708(4)	S(1')-C(2')	1.721(3)
C(2')-C(3')	1.351(4)	C(3')-O(2')	1.355(3)	C(3')-C(4')	1.424(4)
C(4')-C(5')	1.352(5)	C(4')-O(1')	1.368(4)	O(1')-C(6')	1.375(5)
C(6')-C(7'B)	1.423(8)	C(6')-C(7'A)	1.454(11)	O(2')-C(7'A)	1.410(8)
O(2')-C(7'B)	1.456(7)				

C(3)#1-C(1)-C(2)	117.0(2)	C(3)#1-C(1)-C(2')	120.8(3)
C(2)-C(1)-C(2')	122.2(3)	F(2)-C(2)-C(3)	118.2(3)
F(2)-C(2)-C(1)	120.8(2)	C(3)-C(2)-C(1)	121.0(3)
F(3)-C(3)-C(1)#1	120.2(2)	F(3)-C(3)-C(2)	117.7(3)
C(1)#1-C(3)-C(2)	122.0(3)	C(5')-S(1')-C(2')	91.97(15)
C(3')-C(2')-C(1)	126.7(2)	C(3')-C(2')-S(1')	111.0(2)
C(1)-C(2')-S(1')	122.3(2)	C(2')-C(3')-O(2')	124.6(2)
C(2')-C(3')-C(4')	113.0(3)	O(2')-C(3')-C(4')	122.4(3)
C(5')-C(4')-O(1')	124.9(3)	C(5')-C(4')-C(3')	112.4(3)
O(1')-C(4')-C(3')	122.7(3)	C(4')-C(5')-S(1')	111.7(2)
C(4')-O(1')-C(6')	114.0(2)	O(1')-C(6')-C(7'B)	120.4(5)
O(1')-C(6')-C(7'A)	122.6(4)	C(3')-O(2')-C(7'A)	114.4(4)
C(3')-O(2')-C(7'B)	112.3(4)	O(2')-C(7'A)-C(6')	116.2(8)
C(6')-C(7'B)-O(2')	115.2(6)		

Symmetry transformations used to generate equivalent atoms: #1 2-x, 1-y, 2-z

Table A-5 Bond Lengths (Å) and Bond Angles (°) for **BEDOT-B-(OEt)$_2$, 4-2**.

S-C6	1 710(2)	S-C1	1 742(2)	O1-C2	1 370(2)
O1-C3	1 444(2)	O1-C3	1 446(2)	C1-C2	1 390(2)
C1-C7	1 472(2)	O2-C5	1.373(2)	O2-C4	1 442(2)O2-
C4	1 444(2)	C2-C5	1 422(2)	O3-C8	1 364(2)
O3-C10	1 434(2)	C3-C4	1 495(3)	C3-H3A	0 9900
C3-H3B	0 9900	C3 -C4	1 494(3)	C3'-H3 A	0 9900
C3'-H3 B	0 9900	C4-H4A	0 9900	C4-H4B	0 9900
C4'-H4 A	0 9900	C4'-H4'B	0 9900	C5-C6	1 356(2)
C6-H6A	0 9500	C7-C9	1 405(2)	C7-C8	1 411(2)
C8-C9#1	1.385(2)	C9-C8#1	1.385(2)	C9-H9A	0 9500
C10-C11	1 511(2)	C10-H10A	0 9900	C10-H10B	0 9900
C11-H11A	0 9800	C11-H11B	0 9800	C11-H11C	0 9800

C6-S-C1	93.31(7)	C2-O1-C3	113 4(7)
C2-O1-C3	111 84(14)	C3 -O1-C3	26 1(6)
C2-C1-C7	128 36(13)	C2-C1-S	108 49(10)
C7-C1-S	123 10(11)	C5-O2-C4	111 67(12)
C5-O2-C4	108 7(4)	C4-O2-C4	35 1(5)
O1-C2-C1	124 25(13)	O1-C2-C5	121 89(13)
C1-C2-C5	113 87(13)	C8-O3-C10	120 01(11)
O1-C3-C4	111 4(2)	O1-C3-H3A	109 4
C4-C3-H3A	109 4	O1-C3-H3B	109 4
C4-C3-H3B	109 4	H3A-C3-H3B	108.0
O1-C3 -C4	108 0(6)	O1-C3 -H3 A	110.1
C4 -C3 -H3 A	110 1	O1-C3'-H3 B	110 1
C4 -C3 -H3 B	110 1	H3 A-C3 -H3 B	108.4

Table A-5 Bond Lengths (Å) and Bond Angles (°) for **BEDOT-B-(OEt)$_2$, 4-2**. (continued)

O2-C4-C3	109.5(2)	O2-C4-H4A	109.8
C3-C4-H4A	109.8	O2-C4-H4B	109.8
C3-C4-H4B	109.8	H4A-C4-H4B	108.2
O2-C4'-C3'	111.7(10)	O2-C4'-H4'A	109.3
C3'-C4'-H4'A	109.3	O2-C4'-H4'B	109.3
C3'-C4'-H4'B	109.3	H4'A-C4'-H4'B	107.9
C6-C5-O2	124.16(14)	C6-C5-C2	112.81(13)
O2-C5-C2	123.02(14)	C5-C6-S	111.52(12)
C5-C6-H6A	124.2	S-C6-H6A	124.2
C9-C7-C8	116.46(12)	C9-C7-C1	120.71(12)
C8-C7-C1	122.83(13)	O3-C8-C9#1	122.79(13)
O3-C8-C7	115.66(12)	C9#1-C8-C7	121.54(13)
C8#1-C9-C7	122.00(13)	C8#1-C9-H9A	119.0
C7-C9-H9A	119.0	O3-C10-C11	105.41(12)
O3-C10-H10A	110.7	C11-C10-H10A	110.7
O3-C10-H10B	110.7	C11-C10-H10B	110.7
H10A-C10-H10B	108.8	C10-C11-H11A	109.5
C10-C11-H11B	109.5	H11A-C11-H11B	109.5
C10-C11-H11C	109.5	H11A-C11-H11C	109.5
H11B-C11-H11C	109.5		

Symmetry transformations used to generate equivalent atoms:

#1 -x,-y,-z

Table A-6. Bond Lengths (Å) and Bond Angles (°) for **BEDOT-B-$(OEt)_2$•THF adduct 4-2•THF adduct.**

S-C6	1.710(1)	S-C1	1.748(1)	O1-C2	1.370(1)
O1-C3	1.442(2)	C1-C2	1.379(2)	C1-C7	1.468(2)
O2-C5	1.366(2)	O2-C4	1.420(2)	C2-C5	1.421(2)
C3-C4	1.495(2)	C3-H3A	0.9900	C3-H3B	0.9900
O3-C8	1.372(2)	O3-C10	1.428(2)	C4-H4A	0.9900
C4-H4B	0.9900	C5-C6	1.352(2)	C6-H6A	0.9500
C7-C9	1.403(2)	C7-C8	1.409(2)	C8-C9#1	1.383(2)
C9-C8#1	1.383(2)	C9-H9A	0.9500	C10-C11	1.510(2)
C10-H10A	0.9900	C10-H10B	0.9900	C11-H11A	0.9800
C11-H11B	0.9800	C11-H11C	0.9800		

C6-S-C1	93.03(7)	C2-O1-C3	112.5(1)
C2-C1-C7	127.5(1)	C2-C1-S	108.71(9)
C7-C1-S	123.8(1)	C5-O2-C4	112.3(1)
O1-C2-C1	124.5(1)	O1-C2-C5	121.8(1)
C1-C2-C5	113.7(1)	O1-C3-C4	111.3(1)
O1-C3-H3A	109.4	C4-C3-H3A	109.4
O1-C3-H3B	109.4	C4-C3-H3B	109.4
H3A-C3-H3B	108.0	C8-O3-C10	119.3(1)
O2-C4-C3	111.0(1)	O2-C4-H4A	109.4
C3-C4-H4A	109.4	O2-C4-H4B	109.4
C3-C4-H4B	109.4	H4A-C4-H4B	108.0
C6-C5-O2	124.0(1)	C6-C5-C2	113.2(1)
O2-C5-C2	122.8(1)	C5-C6-S	111.3(1)
C5-C6-H6A	124.4	S-C6-H6A	124.4
C9-C7-C8	116.6(1)	C9-C7-C1	120.5(1)

Table A-6 Bond Lengths (Å) and Bond Angles (°) for **BEDOT-B-$(OEt)_2$•THF adduct, 4-2•THF adduct** (continued)

C8-C7-C1	123 0(1)	O3-C8-C9#1	123 1(1)
O3-C8-C7	115 9(1)	C9#1-C8-C7	121 0(1)
C8#1-C9-C7	122.4(1)	C8#1-C9-H9A	118.8
C7-C9-H9A	118 8	O3-C10-C11	107 0(1)
O3-C10-H10A	110.3	C11-C10-H10A	110 3
O3-C10-H10B	110 3	C11-C10-H10B	110.3
H10A C10-H10B	108 6	C10-C11-H11A	109 5
C10-C11-H11B	109.5	H11A-C11-H11B	109 5
C10-C11-H11C	109 5	H11A-C11-H11C	109.5
H11B-C11-H11C	109 5		

Symmetry transformations used to generate equivalent atoms
#1 x+5/3,-y+1/3,-z+4/3

Table A-7 Bond Lengths (Å) and Bond Angles (°) for **BEDOT-B-(OBz)$_2$, 4-9**

S-C6	1.713(2)	S-C1	1.741(2)	O1-C2	1.375(3)
O1-C3	1 434(3)	C1-C2	1 380(3)	C1-C7	1 473(3)
O2-C5	1 374(3)	O2-C4	1 443(3)	C2-C5	1 425(3)
C3-C4	1 479(4)	C3 H3A	0 9900	C3-H3B	0 9900
O3-C8	1 375(2)	O3-C10	1 431(3)	O4-C11	1.311(3)
O4-H4	0 9825	O4-H11D	0 3865	C4-H4A	0 9900
C4-H4B	0 9900	O5-C11	1.320(3)	O5-H5	0 7779
O5-H11A	0 4200	C5-C6	1.353(3)	C6-H6A	0 9500
C7-C8	1 400(3)	C7-C9	1 408(3)	C8-C9#1	1 384(3)
C9-C8#1	1.384(3)	C9-H9A	0 9500	C10-C11	1 502(3)
C10-H10A	0 9900	C10-H10B	0 9900	C11-H11A	0 9600
C11-H11B	0 9599	C11-H11C	0 9600	C11-H11D	0 9599

C6-S-C1	93 31(11)	C2-O1-C3	112.5(2)
C2-C1-C7	127 8(2)	C2-C1-S	108 6(2)
C7-C1-S	123.5(2)	C5-O2-C4	112 4(2)
O1-C2-C1	124 6(2)	O1-C2-C5	121 4(2)
C1-C2-C5	114 0(2)	O1-C3-C4	112 7(2)
O1-C3-H3A	109 1	C4-C3-H3A	109 1
O1-C3-H3B	109 1	C4-C3-H3B	109 1
H3A C3-H3B	107 8	C8-O3-C10	119 2(2)
C11-O4-H4	102.6	C11-O4-H11D	21 0
H4-O4-H11D	93 8	O2-C4-C3	111 9(2)
O2-C4-H4A	109 2	C3-C4-H4A	109 2
O2-C4-H4B	109 2	C3-C4-H4B	109 2
H4A C4-H4B	107 9	C11-O5-H5	122 9

Table A-7 Bond Lengths (Å) and Bond Angles (°) for **BEDOT-B-(OBz)$_2$ 4-9** (continued)

C11-O5-H11A	25 8	H5-O5-H11A	97 1
C6-C5-O2	124.0(2)	C6-C5-C2	112.9(2)
O2-C5-C2	123 1(2)	C5-C6-S	111 2(2)
C5-C6-H6A	124 4	S-C6-H6A	124 4
C8-C7-C9	116.5(2)	C8-C7-C1	123 2(2)
C9-C7-C1	120.3(2)	O3-C8-C9#1	122 2(2)
O3-C8-C7	116.0(2)	C9#1-C8-C7	121 8(2)
C8#1-C9-C7	121.7(2)	C8#1-C9-H9A	119 1
C7-C9-H9A	119 1	O3-C10-C11	106 7(2)
O3-C10-H10A	110 4	C11-C10-H10A	110 4
O3-C10-H10B	110.4	C11-C10-H10B	110 4
H10A-C10-H10B	108 6	O4-C11-O5	100 0(3)
O4-C11-C10	114.8(2)	O5-C11-C10	119.3(2)
O4-C11-H11A	108.2	O5-C11-H11A	11 0
C10-C11-H11A	108.6	O4-C11-H11B	109 0
O5-C11-H11B	104.3	C10-C11-H11B	108 6
H11A-C11-H11B	107.5	O4-C11-H11C	106 5
O5-C11-H11C	108 0	C10-C11-H11C	107 5
H11A-C11-H11C	111.4	H11B-C11-H11C	4 0
O4-C11-H11D	8.3	O5-C11-H11D	107 3
C10-C11-H11D	107.2	H11A-C11-H11D	114 9
H11B-C11-H11D	110 0	H11C-C11-H11D	107 0

Symmetry transformations used to generate equivalent atoms #1 -x+1,-y+1,-z

Table A-5 Bond Lengths (Å) and Bond Angles (°) for **BEDOT-B-(OMTM)$_2$ 4-4**

S1-C6	1.716(2)	S1-C1	1 746(2)	S2-C10	1 796(2)
S2-C11	1 798(3)	O1-C2	1 371(2)	O1-C3	1 441(2)
O1-C3'	1 441(3)	C1-C2	1 383(3)	C1-C7	1 468(3)
O2-C5	1 373(3)	O2-C4	1 439(3)	O2-C4	1 443(2)
C2-C5	1 422(3)	C3-C4	1 492(5)	C3-H3A	0 9900
C3-H3B	0 9900	C3'-C4'	1 491(5)	C3'-H3' A	0 9900
C3'-H3' B	0.9900	O3-C8	1 383(2)	O3-C10	1 430(2)
C4-H4A	0 9900	C4-H4B	0.9900	C4'-H4' A	0.9900
C4'-H4' B	0 9900	C5-C6	1 345(3)	C6-H6	0 9598
C7-C9	1 398(3)	C7-C8	1 407(3)	C8-C9#1	1 376(3)
C9-C8#1	1 376(3)	C9-H9	0 9601	C10-H10A	0.9900
C10-H10B	0 9900	C11-H11A	0 9800	C11-H11B	0 9800
C11-H11C	0 9800				

C6-S1-C1	93 00(11)	C10-S2-C11	99.29(11)
C2-O1-C3	114.3(2)	C2-O1-C3	107 5(7)
C3-O1-C3	24 7(5)	C2-C1-C7	127 8(2)
C2-C1-S1	108 4(2)	C7-C1-S1	123 8(2)
C5-O2-C4	114.7(5)	C5-O2-C4	112 2(2)
C4-O2-C4	35 1(5)	O1-C2-C1	124.1(2)
O1-C2-C5	121.8(2)	C1-C2-C5	114 0(2)
O1-C3-C4	110 1(3)	O1-C3-H3A	109 6
C4-C3-H3A	109.6	O1-C3-H3B	109 6
C4-C3-H3B	109.6	H3A-C3-H3B	108.1
O1-C3'-C4'	119 8(8)	O1-C3'-H3' A	107 4
C4'-C3'-H3' A	107 4	O1-C3'-H3' B	107 4

Table A-5 Bond Lengths (Å) and Bond Angles (°) for **BEDOT-B-(OMTM)$_2$, 4-4** (continued)

C4 -C3 -H3 B	107 4	H3 A-C3 -H3 B	106 9
C8-O3-C10	118 4(2)	O2-C4-C3	113 6(3)
O2-C4-H4A	108 8	C3-C4-H4A	108.8
O2-C4-H4B	108 8	C3-C4-H4B	108 8
H4A-C4-H4B	107 7	O2-C4-C3	100.5(10)
O2-C4 -H4 A	111.7	C3 -C4 -H4 A	111 7
O2-C4 H4B	111 7	C3 -C4 H4 B	111 7
H4 A-C4 -H4 B	109 4	C6-C5-O2	124 4(2)
C6-C5-C2	113 0(2)	O2-C5-C2	122.5(2)
C5-C6-S1	111.5(2)	C5-C6-H6	124.2
S1-C6-H6	124 3	C9-C7-C8	116 0(2)
C9-C7-C1	120 0(2)	C8-C7-C1	123 9(2)
C9#1-C8-O3	122 8(2)	C9#1-C8-C7	121 1(2)
O3-C8-C7	116 1(2)	C8#1-C9-C7	122.9(2)
C8#1-C9-H9	118 7	C7-C9-H9	118.4
O3-C10-S2	114 7(2)	O3-C10-H10A	108 6
S2-C10-H10A	108 6	O3-C10-H10B	108.6
S2-C10-H10B	108 6	H10A-C10-H10B	107 6
S2-C11-H11A	109 5	S2-C11-H11B	109.5
H11A-C11 H11B	109 5	S2-C11-H11C	109.5
H11A-C11-H11C	109.5	H11B-C11-H11C	109 5

Symmetry transformations used to generate equivalent atoms: #1 -x,-y+2,-z

Table A-9 Bond Lengths (Å) and Bond Angles (°) for **BEDOT-B-(OHE)$_2$**, **4-6**

S-C6	1.718(2)	S-C1	1.7353(14)	O1-C2	1.364(2)
O1-C3	1.441(2)	C1-C2	1.367(2)	C1-C7	1.479(2)
O2-C5	1.370(2)	O2-C4	1.430(2)	C2-C5	1.432(2)
O3-C8	1.373(2)	O3-C10	1.428(2)	C3-C4	1.501(2)
C3-H3A	0.9900	C3-H3B	0.9900	C4-H4A	0.9900
C4-H4B	0.9900	C5-C6	1.356(2)	C6-H6	0.9500
C7-C9	1.402(2)	C7-C8	1.405(2)	C8-C9#1	1.390(2)
C9-C8#1	1.390(2)	C9-H9	0.9500	C10-C11	1.507(2)
C10-H10A	0.9900	C10-H10B	0.9900	C11-C12	1.384(2)
C11-C16	1.399(2)	C12-C13	1.396(2)	C12-H12	0.9500
C13-C14	1.383(2)	C13-H13	0.9500	C14-C15	1.389(3)
C14-H14	0.9500	C15-C16	1.389(2)	C15-H15	0.9500
C16-H16	0.9500				

C6-S-C1	92.87(7)	C2-O1-C3	112.78(11)
C2-C1-C7	127.45(12)	C2-C1-S	109.72(10)
C7-C1-S	122.69(10)	C5-O2-C4	111.29(11)
O1-C2-C1	123.60(12)	O1-C2-C5	122.88(12)
C1-C2-C5	113.49(13)	C8-O3-C10	117.54(10)
O1-C3-C4	112.31(13)	O1-C3-H3A	109.1
C4-C3-H3A	109.1	O1-C3-H3B	109.1
C4-C3-H3B	109.1	H3A-C3-H3B	107.9
O2-C4-C3	111.75(14)	O2-C4-H4A	109.3
C3-C4-H4A	109.3	O2-C4-H4B	109.3
C3-C4-H4B	109.3	H4A-C4-H4B	107.9
C6-C5-O2	124.86(13)	C6-C5-C2	112.76(13)

Table A-9 Bond Lengths (Å) and Bond Angles (°) for **BEDOT-B-(OHE)$_2$**, **4-6** (continued)

O2-C5-C2	122.38(13)	C5-C6-S	111 15(11)
C5-C6-H6	124 4	S-C6-H6	124 4
C9-C7-C8	118 70(12)	C9-C7-C1	119 26(12)
C8-C7-C1	122.02(12)	O3-C8-C9#1	123 89(12)
O3-C8-C7	115.70(12)	C9#1-C8-C7	120.36(12)
C8#1-C9-C7	120 93(12)	C8#1-C9-H9	119.5
C7-C9-H9	119.5	O3-C10-C11	108 69(11)
O3-C10-H10A	110.0	C11-C10-H10A	110.0
O3-C10-H10B	110 0	C11-C10-H10B	110 0
H10A-C10-H10B	108.3	C12-C11-C16	119.30(14)
C12-C11-C10	122.57(13)	C16-C11-C10	118 12(13)
C11-C12-C13	120 14(14)	C11-C12-H12	119 9
C13-C12-H12	119 9	C14-C13-C12	120.5(2)
C14-C13-H13	119 7	C12-C13-H13	119 7
C13-C14-C15	119 5(2)	C13-C14-H14	120 2
C15-C14-H14	120 2	C16-C15-C14	120.2(2)
C16-C15-H15	119 9	C14-C15-H15	119 9
C15-C16-C11	120 3(2)	C15-C16-H16	119 9
C11-C16-H16	119 9		

Symmetry transformations used to generate equivalent atoms: #1 -x,-y,-z

Table A-10 Bond Lengths (Å) and Bond Angles (°) for **BEDOT-B-(OAc)$_2$, 4-11**

S-C6	1.716(3)	S-C1	1 739(2)	O1-C2	1 363(3)
O1-C3	1 454(3)	C1-C2	1 382(3)	C1-C7	1 464(3)
O2-C5	1 369(3)	O2-C4	1 427(4)	C2-C5	1 424(3)
O3-C10	1 372(3)	O3-C8	1 403(3)	C3-C4	1 492(5)
C3-H3A	0 9900	C3-H3B	0.9900	O4-C10	1 196(3)
C4-H4A	0 9900	C4-H4B	0 9900	C5-C6	1 356(4)
C6-H6A	0.9900	C6-H6B	0 9900	C7-C8	1 400(3)
C7-C9	1 404(3)	C8-C9#1	1 380(3)	C9-C8#1	1 380(3)
C9-H9A	0 9500	C10-C11	1.493(3)	C11-H11A	0.9800

C11-H11B	0.9800	C11-H11C	0 9800
C6-S-C1	93 02(12)	C2-O1-C3	112.7(2)
C2-C1-C7	128 2(2)	C2-C1-S	109 4(2)
C7-C1-S	122 3(2)	C5-O2-C4	111 9(2)
O1-C2-C1	124 0(2)	O1-C2-C5	122 9(2)
C1-C2-C5	113 1(2)	C10-O3-C8	116 0(2)
O1-C3-C4	113.5(2)	O1-C3-H3A	108 9
C4-C3-H3A	108 9	O1-C3-H3B	108 9
C4-C3-H3B	108.9	H3A-C3-H3B	107 7
O2-C4-C3	111 8(2)	O2-C4-H4A	109 3
C3-C4-H4A	109 3	O2-C4-H4B	109.3
C3-C4-H4B	109 3	H4A-C4-H4B	107 9
C6-C5-O2	123 8(2)	C6-C5-C2	113 5(2)
O2-C5-C2	122.7(2)	C5-C6-S	111 0(2)
C5-C6-H6A	109 4	S-C6-H6A	109 4
C5-C6-H6B	109 4	S-C6-H6B	109 4

Table A-10 Bond Lengths (Å) and Bond Angles (°) for **BEDOT-B-(OAc)$_2$, 4-11** (continued)

H6A-C6-H6B	108.0	C8-C7-C9	116.1(2)
C8-C7-C1	123.8(2)	C9-C7-C1	120.2(2)
C9#1-C8-C7	123.0(2)	C9#1-C8-O3	117.3(2)
C7-C8-O3	119.6(2)	C8#1-C9-C7	120.9(2)
C8#1-C9-H9A	119.5	C7-C9-H9A	119.5
O4-C10-O3	122.0(2)	O4-C10-C11	127.3(2)
O3-C10-C11	110.7(2)	C10-C11-H11A	109.5
C10-C11-H11B	109.5	H11A-C11-H11B	109.5
C10-C11-H11C	109.5	H11A-C11-H11C	109.5
H11B-C11-H11C	109.5		

Symmetry transformations used to generate equivalent atoms: #1 -x,-y+1,-z

APPENDIX B
ATOM COORDINATES AND EQUIVALENT ISOTROPIC DISPLACEMENT PARAMETERS

Table B-1 Atomic Coordinates and Equivalent Isotropic Displacement Parameters (Å^2) for **BEDOT-B-F$_2$, 2-2.**

Atom	10^4 x	10^4 y	10^4 z	10^3 U_{eq}
C(1)	-3000(30)	6001(12)	343(7)	24(3)
C(2)	-3840(30)	6006(12)	-394(6)	24(3)
C(3)	-5780(40)	5094(12)	-709(6)	27(3)
S(1)	444(11)	8404(3)	251(2)	34(1)
C(2')	-890(30)	6986(11)	651(6)	21(3)
C(3')	140(40)	7015(12)	1403(6)	28(3)
C(4')	1970(30)	8151(12)	1563(7)	30(3)
C(5')	2490(40)	9016(13)	974(7)	35(4)
O(1')	3280(20)	8352(9)	2236(4)	39(3)
C(6')	1730(40)	7567(13)	2759(7)	40(4)
C(7')	1540(50)	6141(13)	2515(8)	50(5)
O(2')	-470(30)	6027(9)	1882(4)	36(3)
F(2)	-2720(20)	7022(7)	-792(4)	38(2)

Table B-2. Atomic Coordinates and Equivalent Isotropic Displacement Parameters ($Å^2$) for **BEDOT-B-$(CN)_2$-TMS_2, 2-6**.

Atom	10^4 x	10^4 y	10^4 z	10^3 U_{eq}
C(1)	675(4)	418(4)	3481(3)	33(1)
C(2)	1247(4)	810(4)	4412(3)	35(1)
C(3)	573(4)	402(4)	5885(3)	35(1)
S(1)	1583(1)	2788(1)	754(1)	37(1)
C(2')	1337(4)	840(4)	1925(3)	34(1)
C(3)	1779(4)	-195(4)	1153(3)	34(1)
C(4)	2342(4)	621(4)	-350(3)	35(1)
C(5)	2327(4)	2243(4)	-765(3)	35(1)
O(1')	1749(3)	-1829(3)	1779(2)	41(1)
C(6')	2169(4)	-2624(4)	734(4)	42(1)
C(7)	3470(5)	-1990(4)	520(4)	46(1)
O(2)	2865(3)	-217(3)	-1298(2)	43(1)
Si(1)	2916(1)	3760(1)	2622(1)	36(1)
C(51)	3178(5)	5504(5)	2333(4)	49(1)
C(52)	1190(5)	4570(5)	-3692(4)	53(1)
C(53)	4881(5)	2661(5)	-3527(4)	48(1)
C(21)	2571(5)	1621(5)	3876(4)	44(1)
N(21)	3592(5)	2288(5)	3486(4)	60(1)

Table B-3 Atomic Coordinates and Equivalent Isotropic Displacement Parameters (Å^2) for **BEDOT-B-NO$_2$ 2-8**.

Atom	10^4 x	10^4 y	10^4 z	10^3 U_{eq}
C(1)	-8402(5)	-2094(4)	-465(2)	24(1)
C(2)	-7717(5)	-670(4)	-595(1)	23(1)
C(3)	-7616(5)	468(4)	-218(2)	25(1)
C(4)	-8125(6)	252(4)	320(2)	25(1)
C(5)	-8738(5)	-1103(4)	465(2)	27(1)
C(6)	-8875(5)	-2297(5)	74(2)	27(1)
S(1)	-8275(2)	5125(1)	705(1)	33(1)
C(2)	-8691(5)	-3281(4)	-868(2)	25(1)
C(3)	-9439(5)	-3202(4)	-1369(2)	25(1)
C(4)	-9692(6)	-4622(4)	1628(2)	26(1)
C(5)	-9111(6)	-5748(5)	-1313(2)	33(1)
O(1)	-10443(4)	-4783(3)	-2129(1)	34(1)
C(6)	-10765(7)	-3393(5)	-2403(2)	35(1)
C(7)	-11360(6)	-2206(4)	-2005(2)	32(1)
O(2)	-10008(4)	-1909(3)	-1615(1)	31(1)
S(1')	-7029(2)	3141(1)	539(1)	37(1)
C(2')	-8026(6)	1469(4)	721(2)	29(1)

Table B-3 Atomic Coordinates and Equivalent Isotropic Displacement Parameters (Å^2) for **BEDOT-B-NO$_2$, 2-8** (continued)

Atom	10^4 x	10^4 y	10^4 z	10^3 U_{eq}
C(3')	-8529(5)	1520(5)	1256(2)	27(1)
C(4')	-8134(6)	2909(4)	1515(2)	31(1)
C(5')	-7317(7)	3888(5)	1172(2)	40(1)
O(1')	-8543(4)	3220(3)	2045(1)	37(1)
C(6")	-8970(7)	1885(5)	2346(2)	40(1)
C(7")	-10153(7)	879(5)	2026(2)	42(1)
O(2")	-9323(4)	368(3)	1531(1)	33(1)
N(1)	-6987(5)	-352(4)	-1139(1)	29(1)
O(1)	-6034(4)	-1299(3)	-1350(1)	35(1)
O(2)	-7316(4)	858(3)	-1344(1)	36(1)

Table B-4 Atomic Coordinates and Equivalent Isotropic Displacement Parameters (Å^2) for **BEDOT-B-F$_4$, 3-2**

Atom	10^4 x	10^4 y	10^4 z	10^3 U_{eq}
C(1)	8025(4)	4129(4)	8912(3)	27(1)
C(2)	8465(4)	3233(4)	9899(3)	30(1)
F(2)	7042(3)	1500(3)	9833(2)	44(1)
C(3)	10407(4)	4092(4)	10952(3)	32(1)
F(3)	10782(3)	3100(3)	11805(2)	42(1)
S(1)	3302(1)	2565(2)	8242(1)	51(1)
C(2')	5964(4)	3256(4)	7792(3)	31(1)
C(3')	5856(4)	2966(4)	6328(3)	30(1)
C(4')	3599(5)	2185(5)	5550(3)	43(1)
C(5')	2053(5)	1916(7)	6451(4)	60(1)
O(1')	3100(4)	1762(5)	4057(2)	67(1)
C(6')	4967(7)	2244(8)	3390(4)	65(1)
O(2')	7678(3)	3361(3)	5644(2)	36(1)
C(7 A)[a]	7216(14)	3460(30)	4216(9)	42(3)
C(7 B)[a]	7093(13)	2400(20)	4063(7)	42(2)

[a] Disordered, occupancy 50%

Table B-5 Atomic Coordinates and Equivalent Isotropic Displacement Parameters (Å^2) for **BEDOT-B-(OEt)$_2$**, **4-2**

Atom	10^4 x	10^4 y	10^4 z	10^3 U_{eq}
S	153(1)	3213(1)	1316(1)	30(1)
O1	1420(1)	492(1)	2545(1)	29(1)
C1	482(1)	1729(1)	1415(1)	23(1)
O2	1731(1)	2626(1)	3595(1)	35(1)
C2	1045(1)	1559(1)	2240(1)	23(1)
O3	-772(1)	2264(1)	-152(1)	31(1)
C3	2201(2)	615(3)	3295(2)	32(1)
C3'	1734(15)	493(13)	3503(4)	50(4)
C4	1792(2)	1471(2)	3997(1)	34(1)
C4'	2399(8)	1578(6)	3683(8)	44(4)
C5	1207(1)	2607(1)	2755(1)	26(1)
C6	774(1)	3568(1)	2337(1)	32(1)
C7	225(1)	859(1)	697(1)	22(1)
C8	-396(1)	1135(1)	-97(1)	23(1)
C9	612(1)	-302(1)	768(1)	23(1)
C10	-1395(1)	2639(1)	-940(1)	25(1)
C11	1682(2)	3910(1)	759(1)	36(1)

Table B-6 Atomic Coordinates and Equivalent Isotropic Displacement Parameters ($Å^2$) for **BEDOT-B-$(OEt)_2$•THF Solvate, 4-2•THF Solvate**

Atom	10^4 x	10^4 y	10^4 z	10^3 U_{eq}
S	6808(1)	1395(1)	7174(1)	35(1)
O1	7850(1)	2257(1)	11060(1)	31(1)
C1	7434(1)	1704(1)	8229(2)	27(1)
O2	6840(1)	2168(1)	11774(2)	44(1)
C2	7425(1)	1970(1)	9871(2)	26(1)
C3	7703(1)	2368(1)	12891(2)	41(1)
O3	7366(1)	1136(1)	4848(2)	41(1)
C4	7315(1)	2571(1)	12606(3)	48(1)
C5	6929(1)	1931(1)	10224(2)	32(1)
C6	6559(1)	1631(1)	8900(2)	39(1)
C7	7885(1)	1678(1)	7424(2)	28(1)
C8	7851(1)	1394(1)	5724(2)	30(1)
C9	8380(1)	1948(1)	8328(2)	31(1)
C10	7309(1)	873(1)	3039(2)	36(1)
C11	6755(1)	683(1)	2333(2)	40(1)

Table B-7 Atomic Coordinates and Equivalent Isotropic Displacement Parameters ($Å^2$) for **BEDOT-B-(OMTM)$_2$, 4-4**

Atom	10^4 x	10^4 y	10^4 z	10^3 U_{eq}
S1	-1754(1)	10027(1)	1678(1)	36(1)
S2	-1816(1)	13526(1)	-739(1)	42(1)
O1	-333(1)	6065(2)	1528(1)	37(1)
C1	-978(1)	8836(3)	1273(1)	28(1)
O2	-1430(1)	5719(2)	2793(1)	43(1)
C2	-893(1)	7306(3)	1684(1)	29(1)
C3	-195(2)	4860(6)	2150(2)	42(1)
C3	-504(10)	4579(12)	2006(5)	44(4)
O3	-1184(1)	12130(2)	566(1)	38(1)
C4	-964(2)	4300(4)	2493(2)	45(1)
C4'	-682(4)	4828(15)	2841(6)	42(4)
C5	1437(1)	7126(3)	2306(1)	33(1)
C6	-1929(1)	8491(3)	2376(1)	39(1)
C7	-497(1)	9449(3)	622(1)	28(1)
C8	-587(1)	11089(3)	274(1)	30(1)
C9	106(1)	8399(3)	325(1)	30(1)
C10	-1350(1)	13740(3)	186(1)	36(1)
C11	-2830(2)	13332(4)	-434(2)	49(1)

Table B-8 Atomic Coordinates and Equivalent Isotropic Displacement Parameters ($Å^2$) for **BEDOT-B-(OHE)$_2$**, **4-6**.

Atom	10^4x	10^4y	10^4z	10^3U_{eq}
S	3936(1)	3263(1)	3043(1)	33(1)
O1	1826(2)	4681(1)	-360(1)	29(1)
C1	2471(2)	3040(2)	1413(1)	24(1)
O2	4650(2)	7278(1)	1515(1)	33(1)
C2	2781(2)	4469(2)	900(1)	23(1)
O3	-156(1)	1164(1)	2437(1)	27(1)
C3	2601(3)	6219(2)	-732(2)	36(1)
C4	3229(3)	7542(2)	402(2)	38(1)
C5	4168(2)	5746(2)	1829(2)	26(1)
C6	4916(2)	5267(2)	3026(2)	32(1)
C7	1207(2)	1474(2)	709(1)	22(1)
C8	-99(2)	526(2)	1241(1)	23(1)
C9	1281(2)	928(2)	-540(1)	24(1)
C10	-1536(2)	283(2)	2975(1)	26(1)
C11	-1365(2)	1202(2)	4273(1)	25(1)
C12	-75(2)	2675(2)	4773(2)	32(1)
C13	24(2)	3473(2)	5981(2)	37(1)
C14	-1163(2)	2805(2)	6688(2)	37(1)
C15	-2443(2)	1317(2)	6199(2)	39(1)
C16	-2541(2)	513(2)	5001(2)	33(1)

Table B-9 Atomic Coordinates and Equivalent Isotropic Displacement Parameters (Å^2) for **BEDOT-B-(OBz)$_2$ 4-9**

Atom	10^4 x	10^4 y	10^4 z	10^3 U_{eq}
S	7092(2)	3388(1)	-2133(1)	38(1)
O1	3425(4)	2772(1)	398(1)	36(1)
C1	5602(5)	3540(1)	-932(2)	26(1)
O2	4046(4)	1545(1)	-1019(1)	43(1)
C2	4591(5)	2869(1)	-557(2)	28(1)
C3	1831(6)	2081(1)	487(2)	43(1)
O3	8410(4)	4814(1)	-1711(1)	35(1)
O4	12902(7)	4676(2)	-3143(3)	39(1)
C4	3490(6)	1444(1)	56(2)	45(1)
O5	8879(7)	4818(2)	-3883(2)	34(1)
C5	4958(5)	2258(1)	-1239(2)	33(1)
C6	6265(6)	2456(1)	-2121(2)	44(1)
C7	5352(5)	4283(1)	-463(2)	24(1)
C8	6724(5)	4920(1)	-856(2)	26(1)
C9	3592(5)	4387(1)	406(2)	27(1)
C10	9556(5)	5450(1)	-2236(2)	32(1)
C11	10729(5)	5172(1)	-3235(2	42(1)

Table B-10 Atomic Coordinates and Equivalent Isotropic Displacement Parameters (Å^2) for **BEDOT-B-(OAc)$_2$ 4-11**

Atom	10^4 x	10^4 y	10^4 z	10^3 U_{eq}
S	-3259(1)	3164(1)	-2382(1)	35(1)
O1	-2250(2)	4883(1)	-5177(2)	37(1)
C1	-2255(3)	4050(1)	-2745(3)	29(1)
O2	-4754(3)	3724(1)	-7186(2)	43(1)
C2	-2830(3)	4236(1)	-4467(3)	29(1)
O3	-21(2)	3355(1)	409(2)	31(1)
C3	-3223(5)	4995(2)	-6968(4)	49(1)
O4	2155(3)	3225(1)	-867(3)	42(1)
C4	-3703(5)	4228(2)	7929(4)	51(1)
C5	-4052(3)	3665(2)	-5448(3)	33(1)
C6	-4426(4)	3059(2)	-4499(3)	36(1)
C7	-1100(3)	4521(1)	-1350(3)	28(1)
C8	-3(3)	4186(1)	157(3)	29(1)
C9	-1067(3)	5360(1)	-1467(3)	30(1)
C10	1122(3)	2915(2)	-232(3)	32(1)
C11	854(4)	2039(2)	-27(4)	42(1)

REFERENCES

[1]Hoffmann, R. *Angew Chem Int Ed. Engl* **1987** *26*, 846

2Owen, J. Ionic Conductivity. In Comprehensive Polymer Science, Allen, G, Bevington, J C , Eds , Booth, C , Price, C , Volume Eds , Vol 2, Pergamon Press. Elmsfork, NY, 1989, Chapter 21

[3]Bloor, D Electrical Conductivity. In *Comprehensive Polymer Science*, Allen, G, Bevington, J C , Eds , Booth C , Price, C , Volume Eds , Vol 2, Pergamon Press Elmsfork, NY, 1989, Chapter 22

[4]Menon R , Yoon, C O , Moses, D , Heeger, A J Metal Insulator Transition in Doped Conductive Polymers in *Handbook of Conductive Polymers*, 2nd Ed Skotheim T A., Elsenbaumer, R. L , Reynolds, J R , Eds , Marcel Dekker New York, 1998 pp27-84

[5]Adams, D M *Inorganic Solids*, Wiley & Sons New York, 1974, Chapter 2

[6]Cox, P A *The Electronic Structure and Chemistry of Solids*, Oxford University Press New York, 1987, Chapter 1

[7]Vardeny, Z. V , Wei, X. Optical Probes of Photoexcitations in Conductive Polymers in *Handbook of Conductive Polymers*, 2nd Ed. Skotheim, T. A., Elsenbaumer, R. L., Reynolds, J. R , Eds., Marcel Dekker New York, 1998, pp 639-66

[8]Burroughes, J H., Bradley, D D C., Brown, A. R Marks, R. N , Mackay, K , Friend, R. H , Burn P L., Holmes, A B *Nature* **1990**, *347*, 539

[9]Tang, C. W , VanSlyke, S A. *Appl Phys Lett* **1987**, *51*, 913

[10]Chung, T C , Kaufman, J H , Heeger, A J , Wudl, F *Phys Rev* **1984** *30*, 702.

[11]Nowak M J , Rughooputh, S D D V , Holta, S ; Heeger, A. J *Macromolecules* **1987**, *20*, 965

[12]Sotzing, G A., Reynolds, J R., Steel, P J *Chem Mater* **1996**, *8*, 882

[13]Pei, Q., Zuccarello, G., Ahlskog, M., Inganäs, O. *Polymer* **1994**, *35*, 1347

[14]Nawa, K., Imae, I., Noma, N., Shirota, Y. *Macromolecules* **1995**, *28*, 723

[15]Tada, K., Hosoda, K., Hirohata, M., Hidayat, R., Kawai, T., Onoda, M., Teraguchi, M., Masuda, T., Zakhidov, A. A., Yoshino, K. *Synth. Met* **1997**, *85*, 1305

[16]Halls, J. J. M., Friend, R. H. *Synth. Met* **1997**, *85*, 1307

[17]Curran, S., Roth, S., Davey, A. P., Drury, A., Blau, W. *Synth. Met* **1996**, *83*, 239

[18]Ragimov, A. V., Mamedov, B. A., Gasanova, S. G. *Polym. Int* **1997**, *43*, 343

[19]Jonas, F., Morrison, J. T. *Synth. Met* **1997**, *85*, 1397

[20]Omastova, M., Kosina, S., Pionteck, J., Janke, A., Pavlinec, J. *Synth. Met* **1996**, *81*, 49

[21]Kaynak, A. *Mater. Res. Bull* **1996**, *31*, 845

[22]Kaynak, A., Unsworth, J., Clout, R., Mohan, A., Beard, G. E. *J. Appl. Polym. Sci* **1994**, *54*, 269

[23]Makela, T., Pienimaa, S., Taka, T., Jussila, S., Isotalo, H. *Synth. Met* **1997**, *85*, 1335

[24]Gofer, Y., Sarker, H., Killian, J. G., Poehler, T. O., Searson, P. C. *Appl. Phys. Lett* **1997**, *71*, 1582

[25]Sarker, H., Gofer, Y., Killian, J. G., Poehler, T. O., Searson, P. C. *Synth. Met* **1997**, *88*, 179

[26]Arbizzani, C., Catellani, M., Mastragostino, M., Mingazzini, C. *Electrochim. Acta* **1995**, *40*, 1871

[27]Meider, H., Springborg, M. *J. Phys. Chem. B* **1997**, *101*, 6949

[28]Rodriguez-Monge, L., Larson, S., *J. Phys. Chem* **1996**, *100*, 6298

[29]Corish, J., Hanratty, V. C. A., Morton-Blake, D. A., Benere, F. *Synth. Met* **1991**, *39*, 311

[30]Ito, T., Shirakawa, H., Ikeda, S. *J. Polym. Sci. Polym. Chem. Ed.* **1974**, *12*, 11

[31]Shirakawa, H., Louis, E. J., MacDiarmid, A. G., Chiang, C. K., Heeger, A. J. *J. Chem. Soc., Chem. Commun.* **1977**, 578.

[32]Chiang, C. K., Fincher, C. R., Park, Y. W., Heeger, A. J., Shirakawa, H., Louis, E. J., Gau, S. C., MacDiarmid, A. G. *Phys. Rev. Lett.* **1977**, *39*, 1098.

[33]Shirakawa, H. Synthesis of Polyacetylene in *Handbook of Conductive Polymers*, 2nd Ed. Skotheim, T. A., Elsenbaumer, R. L., Reynolds, J. R., Eds. Marcel Dekker: New York, 1998, pp 197-208.

[34]Schlüter, A.-D., Wegner, G. *Acta. Polym.* **1993**, *44*, 59.

[35]Huang, W. S., MacDiarmid, A. G., *Polymer* **1993**, *34*, 1833.

[36]Genies, E. M., Boyle, A., Lapkowski, M., Tsintavis, C. *Synth. Met.* **1990**, *36*, 139.

[37]Rabolt, J. F., Clarke, T. C., Kanazawa, K. K., Reynolds, J. R., Street, G. B. *J. Chem. Soc., Chem. Commun.* **1980**, 347.

[38]Shacklette, L. W., Elsenbaumer, R. L., Chance, R. R., Eckhardt, H., Frommer, J. E., Baughman, R. H. *J. Chem. Phys.* **1981**, *75*, 1919.

[39]Lux, F. *Polymer* **1994**, *35*, 2915.

[40]Gonzalez-Tejera, M. J., Carrillo, I., Hernandez-Fuentes, I. *Synth. Met.* **1995**, *73*, 135.

[41]Glenis, S., Benz, M., LeGoff, E., Schindler, J. L., Kannewurf, C. R., Kanatzidis, M. G. *J. Am. Chem. Soc.* **1993**, *115*, 12519.

[42]Vernitskaya, T. V., Efimov, O. N. *Usp. Khim.* **1997**, *66*, 489.

[43]Leclerc, M., Faid, K. *Adv. Mater.* **1997**, *9*, 1087.

[44]Higgins, S. J. *Chem. Soc. Rev.* **1997**, *26*, 247.

[45]Ohsawa, T., Kaneto, K., Yoshino, K. *Jpn. J. Appl. Phys.* **1984**, *23*, L663.

[46]Nessakh, B., Kotkowaski-Machnik, Z., Tedjar, F. *J. Electroanal. Chem.* **1990**, *269*, 263.

[47]Tourillon, G., Garnier, F. *J. Electroanal. Chem.* **1982**, *135*, 173.

[48]Diaz, A. F.; Kanazawa, K. K., Gardini, G. P. *J. Chem. Soc., Chem. Commun* **1979**, 635.

[49]Patil, A. O.; Heeger, A. J.; Wudl, F. *Chem. Rev.* **1988**, *88*, 183.

[50]Diaz, A. F.; Crowley, J.; Bargon, J.; Gardini, G. P.; Torrance, J. B. *J. Electroanal. Chem.* **1981**, *121*, 355.

[51]Kanazawa, K. K.; Diaz, A. F.; Giess, R. H.; Gill, W. D.; Kwak, J. F.; Logan, J. A.; Rabolt, J. F.; Street, G. B. *J. Chem. Soc., Chem. Commun.* **1979**, 854.

[52]Ruhe, J.; Ezquerra, T.; Wegner, G. *Synth. Met.* **1989**, *28*, C177.

[53]Ruhe, J.; Ezquerra, T.; Wegner, G. *Polym. Bull.* **1987**, *18*, 277.

[54]Korn-Youssoufi, H.; Garnier, F.; Srivastava, P.; Godillot, P.; Yassar, A. *J. Am. Chem. Soc.* **1997**, *119*, 7388.

[55]Imisides, M. D.; John, R.; Wallace, G. G. *CHEMTECH* **1996**, *26*, 19.

[56]Miller, G. G.; Elsenbaumer, R. L. *J. Chem. Soc., Chem. Commun.* **1986**, 1346.

[57]Hotta, S. Rughooputh, S. D. D. V.; Heeger, A. J.; Wudl, F. *Macromolecules* **1987**, *20*, 212.

[58]Yassar, A.; Roncali, J.; Garnier, F. *Macromolecules* **1989**, *22*, 80.

[59]Elsenbaumer, R. L.; Jen, K. Y.; Oboodi, R. *Synth. Met.* **1986**, *15*, 169.

[60]Leclerc, M.; Prud'homme, R. E. *Macromolecules* **1987**, *20*, 2153.

[61]Daoust, G.; Leclerc, M. *Macromolecules* **1991**, *24*, 455.

[62]Tanaka, S.; Sato, M. A.; Kaeriyama, K. *Synth. Met.* **1988**, *25*, 277.

[63]Leclerc, M.; Daoust, G. *Synth. Met.* **1991**, *41-43*, 529.

[64]Jonas, F.; Heywang, G.; Schmidtberg, W.; Heinze, J.; Dietrich, M. Method of Imparting Antistatic Properties to a Substrate by Coating the Substrate with a Novel Polythiophene. U. S. Patent 5,035,926, July 30, 1991.

[65]Kossmehl, G.; Chatzitheodorou, G. *Makromol. Chem., Rapid Commun.* **1983**, *4*, 639.

[66]Kossmehl, G.; Chatzitheodorou, G. *Makromol. Chem.* **1982**, *183*, 1711.

[67]Shi, L. H., Garnier, F., Roncali, J. *Macromolecules* **1992**, *25*, 6425

[68]Engelmann, G., Werner, J., Kossmehl, G., Welzel, H.-P., Tschuncky, P., Heinze, J. *Macromolecules* **1996**, *29*, 3370

[69]McCullough, R. D., Ewbank, P. C. Regioregular Head-to-Tail Coupled Poly(3-alkylthiophene) and its Derivatives in *Handbook of Conductive Polymers*, 2nd Ed. Skotheim, T. A., Elsenbaumer, R. L., Reynolds, J. R., Eds.; Marcel Dekker: New York, 1998, pp 225-58.

[70]McCullough, R. D., Lowe, R. D. *J. Chem. Soc., Chem. Commun.* **1992**, 70

[71]Chen, T.-A., Reike, R. D. *J. Am. Chem. Soc.* **1992**, *114*, 10087.

[72]Roncali, J. *Chem. Rev.* **1997**, *97*, 173

[73]Pelter, A., Jenkins, I., Jones, D. E. *Tetrahedron* **1997**, *53*, 10357.

[74]Zotti, G., Zecchin, S., Schiavon, G., Berlin, A., Pagani, G., Borgonovo, M., Lazzaroni, R. *Chem. Mater.* **1997**, *9*, 2876

[75]Hong, S. Y., Song, J. M. *J. Chem. Phys.* **1997**, *107*, 10607

[76]Reynolds, J. R., Katritzky, A. R., Soloducho, J., Belyakov, S., Sotzing, G. A., Pyo, M. *Macromolecules* **1994**, *27*, 7225

[77]Child, A. D., Sankaran, B., Larmat, F., Reynolds, J. R. *Macromolecules*, **1995**,*28*, 6571

[78]Sapp, S. A., Sotzing, G. A., Reddinger, J. L., Reynolds, J. R. *Adv. Mater.* **1996**, *8*, 808

[79]Sotzing, G. A., Reddinger, J. L., Katritzky, A. R., Soloducho, J., Musgrave, R., Reynolds, J. R. *Chem. Mater.* **1997**, *9*, 1578.

[80]Reynolds, J. R., Ruiz, J. P., Child, A. D., Nayak, K., Marynick, D. S. *Macromolecules* **1991**,*24*, 678

[81]Ruiz, J. P., Dharia, J. R., Reynolds, J. R., Buckley, L. J. *Macromolecules* **1992**, *25*, 849

[82]Reynolds, J. R., Child, A. D., Ruiz, J. P., Hong, S. Y., Marynick, D. S. *Macromolecules* **1993**, *26*, 2095

[83]Sotzing, G. A., Reynolds, J. R. *J. Chem. Soc., Chem. Commun* **1995**, 703.

[84]Sotzing, G. A., Thomas, C. A., Reynolds, J. R., Steel, P. J. *Macromolecules* **1998**, *31*, 3750.

[85]Reddinger, J. L., Sotzing, G. A., Reynolds, J. R. *J. Chem. Soc., Chem. Commun* **1996**, 1777.

[86]Irvin, D. J., Reynolds, J. R. *Polym. Adv. Technol.* **1998**, *9*, 260.

[87]Lamba, J. J. S., Tour, J. M. *J. Am. Chem. Soc.* **1994**, *116*, 11723.

[88]McIntyre, J. E., Ravens, D. A. S. *J. Chem. Soc.* **1961**, 4082.

[89]Nishimura, T. *Organic Syntheses*, Wiley & Sons: New York, 1963, Collect. Vol. IV, 713.

[90]Pearl, I. A. *Organic Syntheses*, Wiley & Sons: New York, 1963, Collect. Vol. IV, 972.

[91]Miller, C. S. *Organic Syntheses*; Wiley & Sons: New York, 1955, Collect. Vol. III, 646.

[92]Sotzing, G. A., Reynolds, J. R. *Adv. Mater.* **1997**, *9*, 795.

[93]Jackson, C. L., Calhane, D. E. *Am. Chem. J.* **1902**, *28*, 451.

[94]Abruña, H. *Coordination Chemistry Reviews* **1988**, *86*, 135.

[95]Schmidt, M. W., Baldridge, K. K., Boatz, J. A., Elbert, S. T., Gordon, M. S., Jensen, J. H., Koseki, S., Matsunaga, N., Nguyen, K. A., Su, S. J., Windus, T. L., Dupuis, M., Montgomery, J. A. *J. Comput. Chem.* **1993**, *14*, 1347.

[96]HyperChem, release 5.1 Pro for Windows, HyperCube Software, 1997.

[97]Hehre, W. J., Radom, L., Schleyer, P. R., Pople, J. A. *Ab Initio Molecular Orbital Theory*, Wiley, New York, **1986**, p80.

[98]Sheldrick, G. M. *Acta Crystallogr., Sect. A*, **1990**, *46*, 467.

[99]Sheldrick, G. M. *SHELXL-96*, University of Gottingen, Germany, 1996.

[100]March, J. Localized Chemical Bonding. In *Advanced Organic Chemistry*; Wiley & Sons: New York, 1985; pp 3-23.

[101]Stille, J. K. *Angew. Chem. Int. Ed. Engl.* **1986**, *25*, 508.

[102]Brown, H. C.; Krishnamurthy, S. *J. Org. Chem.* **1969**, *34*, 3918.

[103]Karabatsos, G. J.; Shone, R. L. *J. Org. Chem.* **1968**, *33*, 619.

[104]Buu-Hoi, N. P.; Xuong, N. D.; van Bac, N. *Bull. Soc. Chim. Fr.* **1963**, 2442.

[105]Luh, T. Y.; Ni, Z.-J. *Synthesis* **1990**, 89.

[106]Kuhn, S. J.; Olah, G. A. *J. Am. Chem. Soc.* **1961**, *83*, 4564.

[107]Huheey, J. E.; Keiter, E. A.; Keiter, R. L. Chemical Forces in *Inorganic Chemistry*, HarperCollins: New York, 1993, pp 290-317.

[108]Bondi, A. *J. Phys. Chem.* **1964**, *68*, 441.

[109]Abboud, K. A.; Irvin, D. J.; Reynolds, J. R. *Acta. Cryst.* **1998**, *accepted*.

[110]Irvin, J. A.; Reynolds, J. R. *Polymer* **1998**, *39*, 2339.

[111]Zotti, G.; Schiavon, G.; Zecchin, S. *Synth. Met.* **1995**, *72*, 275.

[112]Debad, J. D.; Bard, A. J. *J. Am. Chem. Soc.* **1998**, *120*, 2476.

[113]Perraris, J. P.; Henderson, C.; Torres, D.; Meeker, D. *Synth. Met.* **1995**, *72*, 147.

[114]Ferraris, J. P.; Lambert, T. L. *J. Chem. Soc., Chem. Commun.* **1991**, 1268.

[115]King, G.; Higgins, S. J. *J. Chem. Mater.* **1995**, *5*, 447.

[116]deLeeuw, D. M.; Simenon, M. M. J.; Brown, A. R.; Einerhand, R. E. F. *Synth. Met.* **1997**, *87*, 53.

[117]Yamamoto, T.; Sugiyama, K.; Kushida, T.; Inoue, T.; Kanbara, T. *J. Am. Chem. Soc.* **1996**, *118*, 3930.

[118]Kanbara, T.; Yamamoto, T. *Macromolecules* **1993**, *26*, 1975.

[119]Yamamoto, T.; Suganuma, H.; Maruyama, T.; Inoue, T.; Muramatsu, Y.; Arai, M.; Komarudin, D.; Ooba, N.; Tomaru, S.; Sasaki, S.; Kubota, K. *Chem. Mater.* **1997**, *9*, 1217.

[120]Kanbara, T.; Miyazaki, Y.; Yamamoto, T. *J. Polym. Sci., Polym. Chem. Ed.* **1995**, *33*, 999.

[121]Mitsuhara, T., Tanaka, S., Kaeriyama, K. *Makromol. Chem.* **1988**, *189*, 1755.

[122]Sawyer, D. T., Sobkowiak, A., Roberts, J. L. Jr. Solvents and Electrolytes. In *Electrochemistry for Chemist*, 2nd ed., Wiley & Sons: New York, 1995, pp299-341.

[123]Jones, R. A., Civcir, P. U. *Tetra.* **1997**, *53*, 11529.

BIOGRAPHICAL SKETCH

David James Irvin was born on August 9, 1967, in Bozeman, MT. He graduated from San Marcos High School (San Marcos, TX) in 1986 after meeting his future wife, Jennifer. In the spring of 1988, he began his undergraduate education at Southwest Texas State University in San Marcos, TX. Under the guidance of Professor Patrick E. Cassidy from the spring of 1989, David conducted undergraduate research in the field of high temperature polymers, working on the synthesis of new fluorinated poly(imide-amide)s. David married Jennifer in the spring of 1991. In the summer of 1991, he was awarded the Nippon Steel Chemical Summer Research Fellowship which included three months of research in Kitakyushu, Japan. He obtained his B.S. (chemistry, minor in math) in December 1991, and in order to complete his research, he continued his studies at SWTSU, where he was granted an M.S. in Chemistry in August 1993. In the fall of 1993, he began graduate studies at the University of Florida under the guidance of Professor John R. Reynolds. David was the recipient of the Research and Development Laboratories Summer Graduate Research Fellowship, for which he worked at Wright-Patterson Airforce Base in Dayton, OH, during the summer of 1996. He completed his Ph.D. in the fall of 1998.

I certify that I have read this study and that in my opinion it conforms to acceptable standards of scholarly presentation and is fully adequate, in scope and quality, as a dissertation for the degree of Doctor of Philosophy

John R Reynolds, Chairman
Professor of Chemistry

I certify that I have read this study and that in my opinion it conforms to acceptable standards of scholarly presentation and is fully adequate, in scope and quality, as a dissertation for the degree of Doctor of Philosophy

Kenneth B Wagener
Professor of Chemistry

I certify that I have read this study and that in my opinion it conforms to acceptable standards of scholarly presentation and is fully adequate, in scope and quality, as a dissertation for the degree of Doctor of Philosophy

Randolph S Duran
Associate Professor of Chemistry

I certify that I have read this study and that in my opinion it conforms to acceptable standards of scholarly presentation and is fully adequate, in scope and quality, as a dissertation for the degree of Doctor of Philosophy

Lisa A McElwee-White
Professor of Chemistry

I certify that I have read this study and that in my opinion it conforms to acceptable standards of scholarly presentation and is fully adequate, in scope and quality, as a dissertation for the degree of Doctor of Philosophy

Mark W. Meisel
Professor of Physics

This dissertation was submitted to the Graduate Faculty of the Department of Chemistry in the College of Liberal Arts and Sciences and to the Graduate School and was accepted as partial fulfillment of the requirements for the degree of Doctor of Philosophy

December, 1998

Dean, Graduate School